ABSTRACT

Title of Document: **EXPERIMENTAL ANALYSIS AND ANALYTICAL MODELING OF SYNTHETIC JET-CROSS FLOW INTERACTIONS**

Sandra Ugrina, Doctor of Philosophy, 2007

Directed By: Professor Alison Flatau
Department of Aerospace Engineering

Synthetic jet actuators are light, compact fluidic devices that have demonstrated efficient energy transfer capabilities important in preventing or delaying flow separation. The unique operational mechanism of these actuators suggests they could be used to induce significant load distribution changes at lower angles of attack, where the flow is fully attached. This research was motivated by an interest to study the design challenges and performance aspects of these control systems needed to maneuver unmanned/micro aerial vehicles without the need of utilizing conventional control surfaces.

Axisymmetric, 32-mm diameter synthetic jet actuators, based on piezoelectric composite technology were manufactured and characterized. Velocity and turbulence intensity of synthetic jets issuing at a frequency of 2200 Hz changed as a function of

geometry parameter ratios, Strouhal and Reynolds numbers. Maximum mean synthetic jet velocity of approximately 30 m/s was achieved. The influence of these synthetic jets on fully attached flows was tested at free stream velocities ranging from 3 to 20 m/s. It was found that a jet-to-free stream velocity ratio (R) of at least one was needed for the synthetic jet to penetrate the boundary layer and affect the potential flow above it.

Second part of this research was directed towards developing a basis for an analytical model that would offer flexibility for investigating the sensitivity of the actuator placements, frequency, size, issuing velocity and injection angles on aerodynamic loads and moments. Integral methods were used to predict the jet trajectory, velocity and diameter changes as a result of various synthetic jet-cross flow conditions. Fair agreement with experimental data was reached for jet-to-free stream velocity ratios above one. Solutions of this model in conjunction with a modified lifting surface theory was then used to determine the change in the lift coefficient on a 0.07 m chord rectangular flat plate with a 0.3 m span as a function of synthetic jet actuator location, diameter and velocity. An approximate 4% lift augmentation was estimated using these techniques due to a single actuator operation implying more benefits when future perturbations produced by an array of synthetic jet actuators are implemented.

EXPERIMENTAL ANALYSIS AND ANALYTICAL MODELING OF SYNTHETIC JET-CROSS FLOW INTERACTIONS

By

Sandra Ugrina

Dissertation submitted to the Faculty of the Graduate School of the
University of Maryland, College Park, in partial fulfillment
of the requirements for the degree of
Doctor of Philosophy
2007

Advisory Committee:
Professor Alison Flatau, Chair
Professor James Baeder
Professor Jewel Barlow
Professor James Duncan
Professor James E. Hubbard, Jr.

© Copyright by
Sandra Ugrina
2007

Acknowledgements

This work was supported by the NASA Langley National Institute of Aerospace (NIA) University Research Program, grant #3012-MD, and by the University of Maryland Minta Martin Research Program. Professionalism and excellence of the UMD Aerospace Engineering Department leadership, graduate students and the support from family and friends made it also a successful and enjoyable one.

Foremost, I would like to contribute the completion of this dissertation to the exceptional work and commitment of my advisor Dr Alison Flatau. Dr Alison Flatau is a remarkable mentor and researcher who provided me with direction and technical support through years. Her expertise, patience and support added considerably to my graduate experience. I feel very lucky to have been given an opportunity to work with her. I have appreciated her vast knowledge and skills in many areas as well her assistance in writing my technical papers including this dissertation. It was through her understanding, guidance and kindness that I completed my graduate degree. I grew both professionally and as a person next to Dr Flatau.

I am also extremely grateful for having had an excellent committee, a group of admirable experts in experimental dynamics and aerodynamics, computation fluid dynamics, structures and control: Dr Jewel Barlow, Dr James Baeder, Dr James

Duncan and Dr James Hubbard. Each of them provided helpful, consistent feedback and assistance at all levels of this research. I would like to recognize the generosity of Dr Duncan in allowing us full access to his laboratory and equipment without which most of this work would have been difficult to complete. I am greatly indebted to Dr James Hubbard not only for his technical advice but also for his valuable life lessons. I am also privileged to have had insightful discussions with Prof Joseph C. Majdalani from University of Tenn. Space Institute on the modeling component of this research. I owe many thanks to the people at the Aerospace Engineering Department that I had the pleasure to work with: Karthik D., Ashish P., Felipe B., Anand R., Dan C., Jared G., Sarah H., Howard G. and many others.

Most importantly, I would like to thank my family for the continuous and sincere encouragement they provided me through life. I thank my parents, Josip and Cvita, my two brothers, role models and great friends Toni and Edvard (and his wife Zvonimira), for always being there when I needed them and for their constant compassion and enthusiasm. I also want to thank Benjamin Walborn for his patience, understanding and support and for being my family away from family. This experience would have been impossible without them.

Table of Contents

List of Symbols

Latin Letters

A,B	dimensions of the rectangular cavity
a,b	dimensions of the actuator slit
A_j	local synthetic jet area
b	wing span
C	synthetic jet circumference
C_D	drag coefficient
C_L	lift coefficient
C_p	pressure coefficient
c	chord length
c	speed of sound
$c_{A,}$ c_D	damping coefficients mass (air, diaphragm)
C_μ	jet momentum coefficient
d_0	initial synthetic jet diameter
d_j	local synthetic jet diameter
D	diameter of the orifice
D_C	diameter of the actuator cavity
D^+	region of separated flow
E	Young's modulus
E_{sj}	synthetic jet entrainment coefficient
f	actuation frequency in Hz
F^+	non-dimensional frequency
H	orifice height
H_C	cavity height
i	influence coefficient
$k_{A,}$ k_D	stiffness coefficient (mass (air, diaphragm)
L	orifice length
l	load distribution
L_S	dimensionless stroke length
L_N	length of the nozzle
L_V	orifice shape factor
L/D	orifice length to diameter ratio
$m_{A,}$ m_D	mass (air, diaphragm)
p	local synthetic jet surface pressure
Q	mass flow rate
q	dynamic pressure

R	jet-to-freestream velocity ratio
Re	Reynolds number
s-n	natural coordinate system of a transverse synthetic jet
Sr	Strouhal number
St	Stokes number
t	plate thickness
T_0	inverse of the actuation frequency
U	freestream velocity
U_j	mean synthetic jet velocity
U_0	synthetic jet velocity during expulsion
V	volume of the cavity
X,Y,Z	streamwise, spanwise and wall normal coordinates

Greek Letters

α	incidence angle
γ	mass per unit length of the plate
δ	thickness of the boundary layer
ε	eddy viscosity
ζ	viscous damping coefficient
θ	angle of the synthetic jet with the Z-axis
λ	viscous effects indicator
Δ	diaphragm amplitude
ρ	freestream density
ρ_j	synthetic jet density
μ	doublet strength
τ	shear stress
ν	kinematic viscosity
φ	angular chordwise coordinate
ω_n	natural frequency of actuation in radians

Chapter 1

Introduction

1.1 Overview

Flow control research investigates techniques and strategies capable of eliminating deteriorated aircraft performance characteristics at off-design conditions by artificially changing and biasing the properties of the mean flow or its dynamics through the introduction of suitable disturbances into the flow. An example of traditional flow control concepts includes slats or flaps. They have been used for years to energize the boundary layer and/or manipulate the flow over wings to improve the aircraft take off and landing capabilities. With the demands on revolutionized aviation associated with the environmental and cost requirements, lighter and more compact flow control concepts and technologies are underway to introduce changes in aircraft designs that will reduce acoustic loads, total vehicle drag and emissions while increasing the system transport capacities, safety, endurance and range. Even though improvements in the modern aircraft over the last fifty years have remained almost unchanged and even though the suggested innovations may be drastic, risky and costly, the future of the aviation industry relies heavily on ground-breaking research areas such as the one of active flow control.

Over the years, research in active flow control technologies has included investigation of external and internal acoustic excitation, vibrating wires and flaps, steady blowing and suction **[Smith, Amitay1998]**. Some of these techniques have shown to be effective, but due to economic trade-offs, difficulties associated with system installation, maintenance and safety issues, they still haven't reached a deployable status. Innovative solutions based on smart structures and materials provide significant foundation for resolving these issues. Fluidic synthetic jet actuator technology was the most recent result of these novel solutions.

Synthetic jet actuators have been the focus of a number of important advances in flow control research since 1994. Periodic means of control along with the simplicity of their designs and versatility of their applications are what distinguish synthetic jet actuators from other mechanisms for flow control. Synthetic jet actuators have shown to be authoritative enough to successfully influence separated flows. They have also shown potential to be used for inducing pressure distribution and moment changes at a wide range of angles of attack without physically changing the aerodynamic body shape or orientation. These are characteristics that could ultimately enable lighter lifting surfaces with less total drag and the maneuverability comparable to those achieved with traditional control surfaces. In addition, this technique would allow the optimization of the vehicle performance over a range of flight conditions. It was the objective of this dissertation to address the design challenges and performance aspects of these compact, low weight active flow control devices.

1.2 Classes of flow control methods

Flow control applications are broad and can be used to eliminate or extend regions of separated flows, manipulate transition location, to influence temperature gradients and jet vectoring and to enhance mixing of flows. Choice and effectiveness of a particular control method largely depends on the flow parameters to be controlled. Some examples of potential flow control applications are presented in Figure 1.1 **[Gorton2005]**.

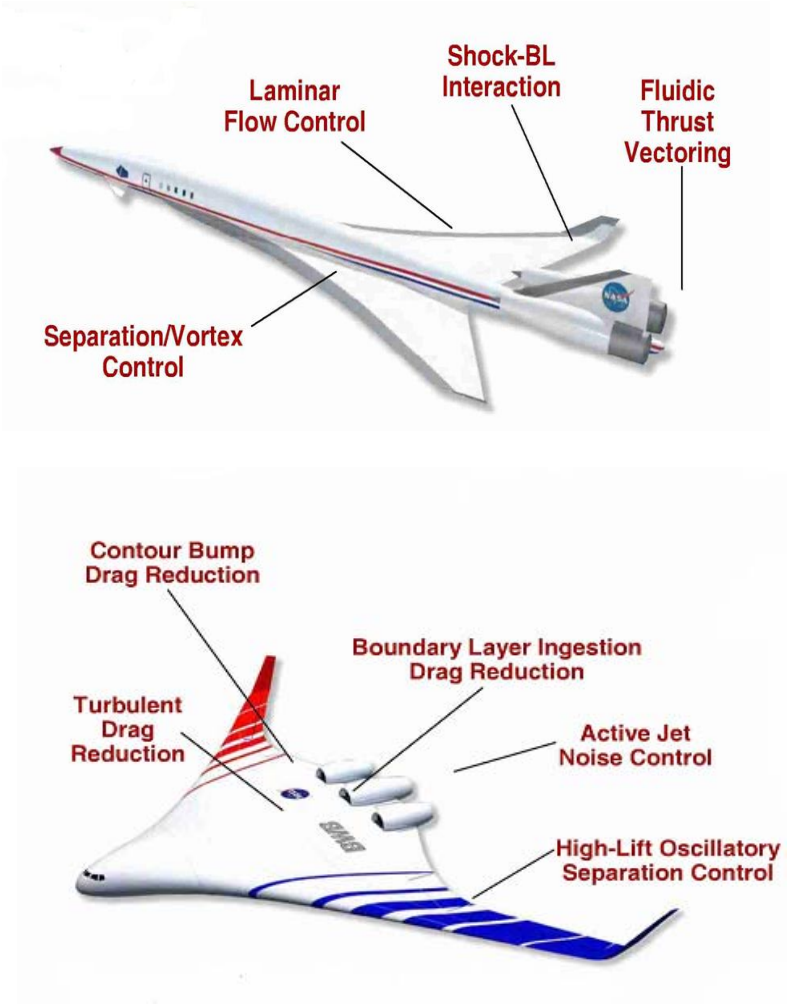

Figure 1.1 Examples of flow control **[Gorton2005].**

Energy requirements divide flow control methods into two main categories: passive and active. Passive methods are designed for a very particular objective and require no power for their operation. They cannot adapt to the changing flow conditions and are therefore operationally ineffective and sometimes even detrimental at off-design conditions. Examples of typical passive devices could be vortex generators, trip wires, grooves or any type of passive cavities. Alternatively, active methods can be designed for optimal operation over a range of conditions which makes them more attractive than fixed/passive control systems. An example of active methods includes internal or external acoustic excitation, vibrating wires, active suction and blowing and synthetic jet actuators.

1.3 Synthetic jet actuators

It was discovered in the 1950s that using a simple cavity with a small orifice on one end and releasing acoustic waves at high frequency and amplitude on the opposite end would produce a jet issuing from the cavity through the orifice **[Ingrad1950]**. Significant improvements and modifications to this idea have been made after smart structure technology has been incorporated as a novel active part of these devices. This modified and improved actuator is today known as a synthetic jet actuator. It is an autonomous and simple device requiring no heavy and intricate support systems (air supplies, clutter of hydraulic piping and connectors) for its operation.

Synthetic jet actuators can be designed and operated in several modes: (i) when activated at low frequency on surfaces at high to moderate angles of attack they can delay flow separation **[Hassan2000, Duvigneau2004]**, (ii) when operated in fully attached flows at higher frequencies and at a sufficient jet-to-free stream velocity ratio they can produce regions of recirculation flow that are capable of virtually changing the shape of the object and subsequently the load distribution **[Glezer1998]**, (iii) synthetic jets have also been successfully used to reduce acoustic loads **[Shaw2006]**, which suggest that they may be used to cancel Tollmien-Schlichting waves important for laminar flow control.

1.3.1 Synthetic jet actuator mechanism

As shown in Figure 1.2, a classic synthetic jet actuator consists of three elementary components: an oscillating diaphragm, a slit or a round orifice and a cylindrical or rectangular cavity **[Holman, Utturkar2005]**.

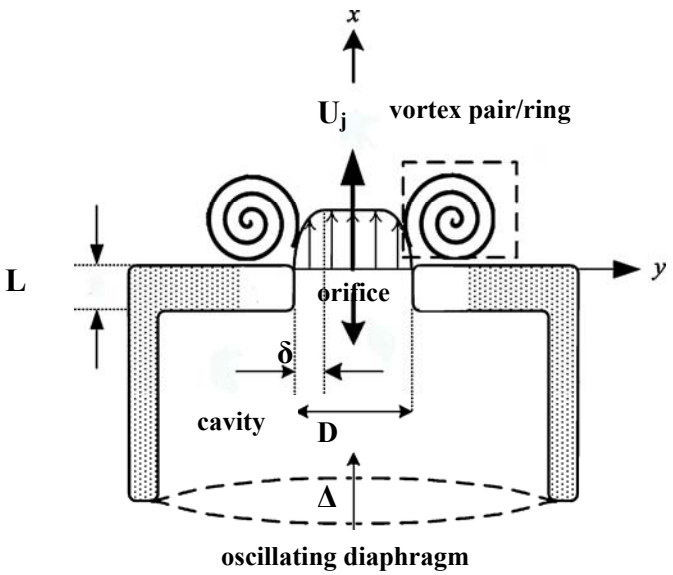

Figure 1.2 Mechanism of the synthetic jet actuator **[Holman, Utturkar2005].**

1.3.2 Synthetic jet actuator drivers

The oscillating diaphragm is an important part of the device. Its displacement amplitude is ultimately what creates the alternating pressure gradient needed to force the air in and out of the orifice. The diaphragm can take various forms including motor driven pistons, acoustic loudspeakers, piezo-electrically driven diaphragms or stacked recurve benders. Figure 1.3 depicts a few examples **[Chen2000, Gilarranz2001]**.

a) **b)**

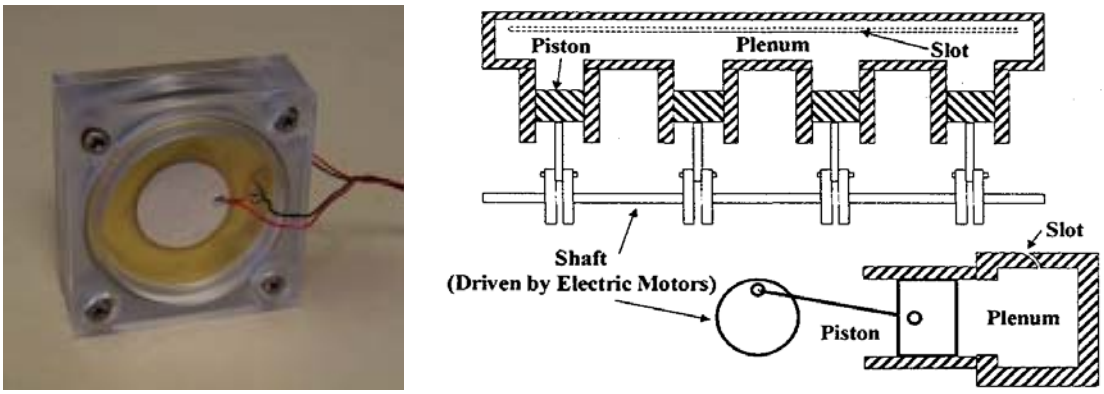

Figure 1.3 Examples of synthetic jet actuator drivers. a) Unimorph **[Chen2000]**, b) Piston configuration **[Gilarranz2001]**

Piston driven actuators are generally heavier than piezoceramic based membrane actuators and, although reliable and powerful, they are not the most optimum choice for use in confined spaces. Unimorphs have been the most widely used type of synthetic jet generator although constant effort is being engaged in developing new systems that would create more displacements at larger frequency bandwidths and lower weight. Brei

et al. from University of Michigan studied different smart material actuation systems and compared some of their characteristics in Figure 1.4 **[Brei2003]**. THUNDER actuators were placed at the higher end performance in terms of the delivered displacements. These actuators were also chosen as the basis for the synthetic jet actuators fabricated as part of this research and will be discussed in the next chapter.

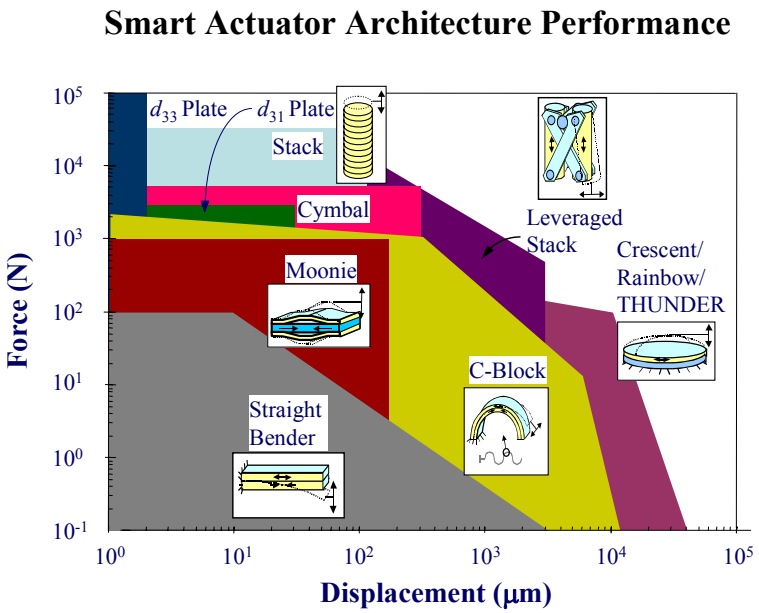

Figure 1.4 Smart Actuator Performance Table **[Brei2003].**

1.3.3 Formation of synthetic jets

Upon actuation, the diaphragm deflects at a rate dictated by the actuation frequency, creating a difference in pressures between the cavity and external ambient flow. During the blowing part of the cycle the oscillating diaphragm moves upward. Flow separates from the edge of the orifice and forms into a vortex ring. If a sufficiently large initial

impulse is given by the diaphragm, the vortex ring continues to move downstream under its own velocity leaving behind a trailing shear layer (Figure 1.5 at $\pi=90^0$). During suction the jet takes the external flow and radially entrains it back into the cavity. A vortex ring forms on the other, inner edge of the orifice as the diaphragm moves down, during the last part of the cycle. The details of these features are depicted in Figure 1.5 in the numerically predicted images developed by Rizzetta et al. **[Rizzetta1999]**. Flow characteristics of a single cycle of the synthetic jet operation at four different phase angles are presented.

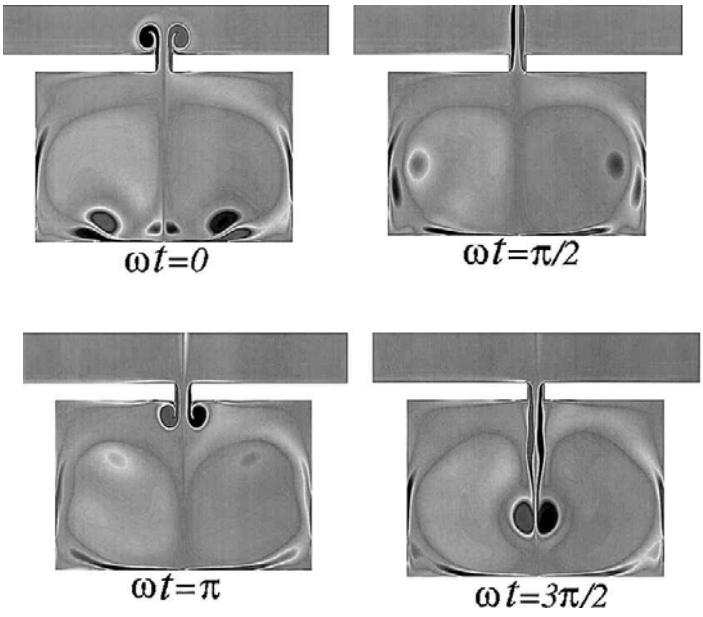

Figure 1.5 Formation of the synthetic jet locked at four main phase angles **[Rizzetta1999].**

When the diaphragm deflection cycle is repeated, a chain of vortical structures is created, which *"develops a spanwise instability and ultimately undergoes transition to*

turbulence, slows down, loses its coherence and becomes indistinguishable from the mean jet flow" **[Smith1998]**.

This description of a synthetic jet formation reveals a distinct property of synthetic jet actuators. They are able to transport momentum to the surrounding flow without adding extra mass to it. Transport of momentum is important for energizing weak flows and making them more resistant to separation. For example, during the suction part of the cycle, low momentum flow is pulled into the cavity, dragging the high momentum flow from the freestream closer to the jet exit plane. In addition, low momentum fluid captured by the cavity gets expelled back to the surrounding flow during the blowing part of the cycle, now re-energized and with more momentum.

1.3.4 Synthetic jet actuator potential applications

Synthetic jet actuators are multifunctional flow control devices. Their most common application has been the one of delaying flow separation. Georgia Tech demonstrated the success of synthetic jet actuators for flow separation control on a low speed, 50 degree swept wing UAV **[Amitay2003, Parekh2003, Washburn2004]**. By applying separation control to one or the other wing, significant roll moments were achieved at angles of attack above 15 degrees (Figure 1.6.a).

The rest of the synthetic jet application spectrum extends from fluid mixing control and thrust vectoring to acoustic noise suppression. Control of fluid mixing with

emphasis on combustor system benefits was investigated by Georgia Tech. Improved mixing could lead to improved combustor efficiency, reduced combustor size and consequently reduction of emissions **[Chen1999, Ritchie2000]**. Synthetic jet actuators were also used for jet vectoring demonstrating their ability to change the direction of much larger conventional jets **[Davis, Glezer2000]**. In cooperation with Boeing, Georgia Tech effectively applied these fluidic actuators to prevent internal flow separation inside diffusers **[Amitay2000].** Researchers at University of Bath in the United Kingdom have looked into using synthetic jets for propulsion and enhanced aerodynamics of Micro Air Vehicles **[Whitehead2003]**. Real time active flow control based on this technology was also developed and tested on a full scale F-16 aircraft by the United States Air Force **[Shaw2006]**. US Air Force researchers have demonstrated on a real platform that synthetic jets can suppress the intensity of the fluctuating pressures in the wake of weapons and as a result reduce detrimental acoustic loads. Synthetic jet actuators were also found applicable as thrust devices in underwater vehicles for low speed maneuvering (Figure 1.6.b), studied at University of Colorado **[Krieg2005]**.

a) **b)**

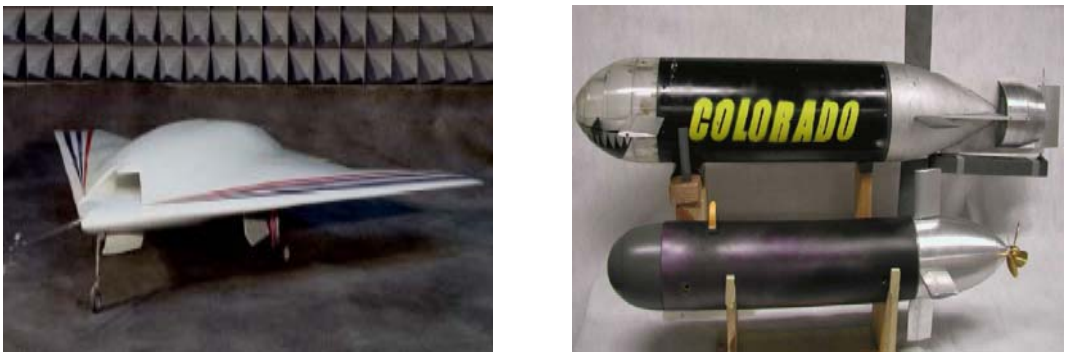

Figure 1.6 Examples of Synthetic Jet Actuator Application. a) UAV performance **[Amitay2003]**, b) Submerged Vehicles **[Krieg2005]**

1.3.4.1 Adaptive Virtual Aerosurface Shaping

The idea of using flow control techniques to create apparent changes in the shape of a surface for inducing particular pressure distributions was addressed in several analyses in the 1940s and 1950s. As an example, Perkins & Hazen increased the lift at zero angle of attack using a stationary, trapped vortex that virtually changed the local surface curvature **[Perkins, Hazen1953]**. Due to their oscillatory natures, synthetic jet actuators could be used in a similar manner.

When interacting with an external cross flow at the properly tuned operating conditions, synthetic jet actuators could create a virtual shape change by creating a recirculation region near the jet orifice **[Glezer1998]**. To the local streamlines, this region would appear as a new boundary, substantially modifying the flow field around the aerodynamic lifting surface and directly changing its lift and drag characteristics. Mechanical complexity and weight associated with the conventional control surfaces could be avoided if synthetic jet actuator activity could change the pressure distribution signature around an airfoil in the same manner as adding camber or increasing the airfoil thickness would (Figure 1.7 **[dynamicflight.com]**)

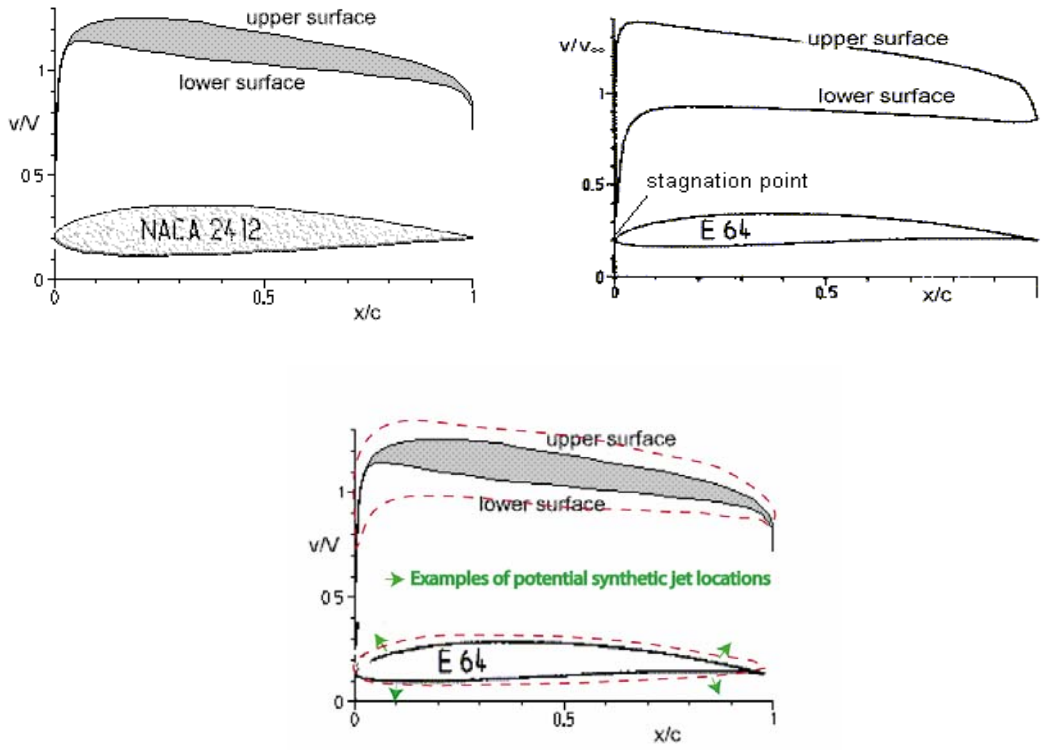

Figure 1.7 Example of the change in the pressure distributions that are desired to be achieved with solely activating synthetic jet actuators **[dynamicflight.com]**.

An experimental demonstration of using synthetic jets for a virtual shape change was reported by Glezer et al **[Chatlynne, Glezer2001]**. They combined a high frequency synthetic jet actuator with a small passive obstruction to demonstrate an increase in circulation. The passive obstruction forced the flow to separate which was then reattached with the synthetic jet actuator mounted further downstream creating the region of recirculating flow. This set-up caused an overall change in pressure distribution signature but the passive obstruction was an undesirable part of the configuration. More

studies are needed to determine how this obstruction could be removed or replaced by another synthetic jet without losing the beneficial effects.

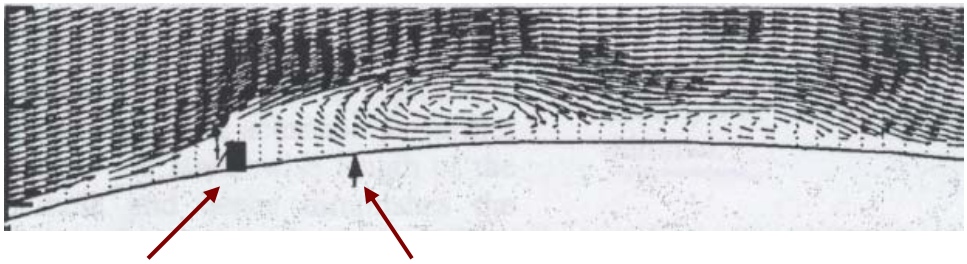

Figure 1.8 Time averaged velocity vector maps illustrating a virtual aero surface above the airfoil equipped with the synthetic jet actuator and a miniature passive obstruction **[Chatlynne, Glezer2001].**

1.4 Previous analytical studies of synthetic jet actuators

Rathnasingham and Breuer developed an inviscid, isothermal model for a resonant actuator **[Rathnasingham1996]**. They coupled a circular plate model with a control-volume model and developed a system of five nonlinear first order differential equations to estimate the vibration characteristics of the diaphragm, properties of the fluid in the cavity and the jet exit velocity. They addressed the importance of the development of the boundary layer inside the orifice. The non-dimensional Stokes number (*St*) was introduced to compare the thickness of the unsteady boundary layer inside the orifice to

the size of the orifice: $St = \sqrt{\frac{\omega D^2}{\nu}}$ (ω is the driving frequency in rad/sec). By matching the velocity solutions for the inviscid and viscous regimes they predicted a Stokes parameter of 15, for which optimum orifice diameter and maximum jet velocity were achieved. At Stokes numbers below 15, or very small orifice diameters, compressibility and unsteadiness lead to fluid non-linearities. Predicted velocity magnitudes were only in qualitative agreement with the measured data.

A lumped element model of a piezo-driven synthetic jet actuator was carried out by Cattaffesta et al. from University of Florida **[Gallas, Cattfaesta2003]**. Individual components of the actuator were modeled as elements of an electronic circuit. Volume flow per applied voltage was predicted as a function of a range of geometry and material properties. The damping coefficient of the diaphragm had to be tuned for good agreement with the measurements. More accurate models should incorporate the effects associated with the unsteady flow in the orifice.

Tang and Zhong presented another lumped element model of the synthetic jet actuator. They decoupled the mechanical and fluid phenomenon and predicted the temporal variation of the synthetic jets, but only when the actuator was operating away from the Helmholtz frequency **[Tang, Zhong2006]**. They also provided analytical relations between performance and structural-geometry parameters of the actuator. Assuming incompressible flow their analysis suggested that the time averaged ejected mass flow rate at the orifice is proportional to the Reynolds number (*Re*) and inversely proportional to the Strouhal number (*Sr*) **[Tang, Zhong2005]**.

Analytical models suffer from the ability to account for large number of loss mechanisms of the orifice. Flow in the orifice region and the orifice length-to-diameter ratio effects on the flow are complex and need to be further studied. Nonlinear effects due to large amplitude pressure oscillations and compressibility effects in the orifice remain as important effects that need to be incorporated in analytical models.

1.5 Previous numerical studies of synthetic jet actuators

Simplified classes of numerical models used harmonic functions to set the jet velocity as a boundary condition at the orifice exit completely ignoring the fluid behavior inside the cavity. Research from McDonnell Douglas Corporation demonstrated that such a boundary condition captures the essential features of the jet without having to model the details of the cavity flow **[Kral1997]**. Their two-dimensional incompressible simulations also indicated that steady, pulsed and synthetic jets show the same behavior in the mean.

Utturkar et al. modeled the entire geometry of the actuator including the diaphragm **[Utturkar2003]**. They used incompressible simulations to demonstrate that the details of the synthetic jet actuator cavity design and the placement of the diaphragm do not play a significant role in synthetic jet characteristics. Lee and Goldstein, on the contrary, used direct numerical simulation results to conclude that the shape of the orifice and the depth of the cavity were important parameters for the resulting synthetic jet flow **[Lee, Goldstein2002]**.

In 1999 Rizzetta et al. from the U.S. Air Force carried out direct numerical simulations of the unsteady compressible Navier- Stokes equations for both the flow inside the cavity and the flowfield outside the orifice **[Rizzetta1999]**. They simulated the formation of vortices in and out of the orifice and characteristics of the synthetic jet outside the orifice plane.

Mittal et al. used an incompressible Navier Stokes solver to simulate the diaphragm as a moving boundary acting on the flow inside the cavity **[Mittal2001]**. They discussed the interaction of the synthetic jet with the flat plate boundary layer and published results that captured the formation of recirculation bubbles at jet-to free stream velocity ratios of three and higher.

1.5 Previous experimental studies of synthetic jet actuators

Measuring complex oscillatory flows like synthetic jets particularly inside the orifice and in the near-orifice region presents several difficulties. Experimentally determining a Reynolds number for example, would require measurements of the average velocity during the expulsion part of the cycle only **[Utturkar2003]**. Obtaining pressure fluctuation and temperature measurements inside the cavity are particularly challenging for small scale actuators.

Particle Image Velocimetry (PIV), Laser Doppler Velocimetry (LDV) and constant temperature anemometry (CTA) are the common tools used to acquire synthetic jet flow

field measurements. NASA Langley Research Center (LaRC) performed a very detailed analysis comparing different techniques available **[Yao, Chen2004]**. Profiles of jet maximum velocities, obtained with either hot wire measurements, LDV or PIV were similar to the mean profiles. Each of these techniques has associated with it a set of advantages and disadvantages and there is still an ongoing debate as to which technique is the most convenient and accurate. Other techniques used to document the synthetic jet flow fields and actuator properties, include flow visualization **[Lachowicz1998, Shuster2004]** and diaphragm displacement measurements **[Chen, Bryant2000]**, respectively.

Experimental analysis of the complex fluid physics associated with synthetic jet formation has been performed on several different scales and at a different number of synthetic jet actuator operational parameters. The design of these actuators varied significantly from one research group to another. Sometimes, the design was governed by the size of the diaphragm and in other studies by the size of the test bed or the need to satisfy specific fundamental research objectives. Key actuator parameters (dimensions and operating frequency range) and output flow velocity from five actuator representation of those described in the literature are summarized on the next page:

1. Georgia Tech

- Operating frequency: 500-1000 Hz
- Cavity dimensions: A=76.2 mm, B= 12.7 mm, H=71 mm (where *A* is the length of the cavity, *B* is the width and *H* is the cavity height)
- Exit slot dimensions: a=75 mm, b=0.5 mm (where *a* is the length of the slot and *b* is the width)
- Maximum reported jet velocity: 25 m/s **[Smith, Glezer1997]**

2. NASA Langley Research Center

- Operating frequency: 500 Hz
- Cavity dimensions: A=57 mm, B=57 mm, H=20 mm
- Exit slot dimensions: a=35 mm, b=0.5 mm
- Maximum reported jet velocity: 100 m/s **[Chen, Bryant2000]**.

3. Boeing: PVdf Active Diaphragm

- Operating frequency: 25 Hz
- Cavity dimensions: A=75 mm, B= 25 mm, H=19 mm
- Exit slot dimensions: a=19 mm, b=0.75 mm
- Maximum reported jet velocity: 9.7 m/s **[Bailo2000]**

4. <u>Air Force Academy</u>

- Operating frequency: 700 Hz
- Cavity dimensions: D_C=30 mm, H= 2-7.62 mm (where D_C is the diameter of the cavity)
- Exit orifice dimensions: D=0.25-1.27 mm, L=0.5 mm (where D is the diameter of the orifice and L is the orifice thickness)
- Maximum reported jet velocity: 8 m/s **[Guy2001]**

5. <u>Other: Piston- cylinder apparatus by Texas A&M University</u>

- Operating frequency: 200 Hz
- Cavity dimensions: A=25 mm, B= 10 mm, H=60 mm
- Exit slot dimensions: a=76 mm, b=16 mm
- Maximum reported jet velocity: 40 m/s **[Gilarranz2001]**

As demonstrated with this list of actuators, observations about the impact of an actuator structural and geometric design effects on the synthetic jet flow have been mainly based on devices with a cavity diameter of 7-10 cm and operating at frequencies of up to 1000 Hz. More specifically, Shuster and Smith experimentally analyzed a 10.2-cm diameter piston driven actuator with a 1.27-cm thick and 2.54-cm diameter orifice and concluded that increasing the Reynolds number increases the strength of the vortex rings but not vortex ring location or interaction **[Shuster, Smith2004]**. Gillaranz et al. obtained PIV measurements of another piston-driven actuator, operating at 300 Hz with a 7-cm long chamber. According to their measurements, the prevalence of the suction part

of the cycle could be kept to a minimum by decreasing the actuator's Strouhal number to 0.2 and lower **[Gilarranz1998]**.

In summary, a spectrum of useful insights on the importance of non-dimensional parameters has been provided by a number of researches. However, design of smaller scale actuators (<7 cm) operating at higher frequencies (>1000 Hz) will be further complicated by the presence of strong non-linearities associated with larger pressure oscillations inside and around the orifice and compressibility effects. These effects don't scale well and are more likely to influence smaller actuator performance than they would the actuators analyzed by, for example, Shuster or Gilarranz. Development of optimization algorithms that integrate unsteadiness, compressibility effects and scaling issues require more investigation.

1.6 Important synthetic jet actuator parameters

Actuator geometric, structural and flow parameters directly influence the formation and evolution of the synthetic jets they produce. Understanding the coupling of these effects on the resultant jet and finding their optimum relationship for meeting a specific flow control objective is critical in the design of effective actuators. Synthetic jet actuator parameters are generally divided as follows:

Actuator operating parameters:

1. Actuator amplitude (A)
2. Actuator Frequency (f)

Actuator geometric parameters:

1. Orifice Diameter (D)
2. Orifice Thickness (L)
3. Cavity Diameter (D_C)
4. Cavity Height (H)

Fluid parameters:

1. Density (ρ)
2. Viscosity (ν)
3. Temperature (T) **[Lachowicz1998, Utturkar2002, Tang, Zhong2005]**

Non-dimensional Parameters:

A synthetic jet is generally scaled with the characteristic dimension of the orifice. Tang and Zhong used the Buckingham-Pi Theorem to determine the independent non-dimensional parameters that will govern the synthetic jet flow. They used the diameter of the orifice, frequency and density to represent length, time and mass to define the following parameters: $\pi_1 = \frac{\Delta}{D}, \pi_2 = \frac{D_C}{D}\ \pi_3 = \frac{H}{D}\ \pi_4 = \frac{L}{D}\ \pi_5 = \frac{fD^2}{\nu}$ **[Tang, Zhong2005],** where Δ is the amplitude of the diaphragm displacement, D is the orifice diameter, D_C is

the cavity diameter, H is the cavity height, L is the orifice length, f the operating frequency and ν the kinematic viscosity.

Findings regarding the Reynolds number which can be recognized in the last π term above (π_5) are discussed in Section 1.6.1. The Strouhal number, not emphasized by Tang and Zhong, is another very important non-dimensional parameter used in analyzing synthetic jet formation and evolution and is discussed in Section 1.6.2. In the case of the non-zero external cross flow, the jet momentum coefficient (Section 1.6.3) and the non-dimensional frequency (Section 1.6.4) are the two additional important non-dimensional parameters used to describe the synthetic jet flow control capabilities.

1.6.1 Reynolds number (*Re*)

Reynolds number is most frequently defined based on the actuator orifice diameter (D) and spatial and time-averaged jet velocity ($\overline{U}_0$) during an expulsion stroke **[Utturkar2003]:**

$$\mathrm{Re} = \frac{\overline{U}_0 D}{\nu} = \frac{fD^2}{\nu} \tag{1.1}$$

Reynolds number indicates whether or not the strength of the vortex generated will be sufficient for the fluid to separate from the orifice. At higher Reynolds numbers the vortex rings have a greater ability to move further away from the orifice and as a result are less affected by the suction part of the oscillating cycle. At a Reynolds number of

approximately 50 or less, the jet will not separate from the orifice edge and the flow will become reversible with the blowing and suction phases being identical in value but opposite in direction **[Wu, Breuer2003]**.

Figure 1.9 shows the structure of the vortex rings captured at a selected range of Reynolds number increasing from 320 to 2300 **[Crook, Wood2001]**. The diameter of the rings increased as the Reynolds number increased. There was a limiting *Re* after which the growth of the vortex rings ceased and instead, an appearance of tail like structures behind the ring began. As the *Re* increased above ~2300, secondary vortices developed behind the primary vortex ring. This flow behavior was shown to be dependent on the actuator geometry (Figure 1.9 shows the change of the flow structures at different orifice lengths *L*). Authors of this study concluded that *"if the total circulation produced exceeds that which can be contained within the vortex ring then this excess circulation is shed in the form of a tail and/or secondary vortices"* **[Crook, Wood2001].** Gharib et al. confirmed the existence of maximum circulation produced by studying the limiting non-dimensional fluid stroke length or the Strouhal number **[Gharib1998]**. Flow character of the synthetic jet as a function of the Strouhal number will be discussed next.

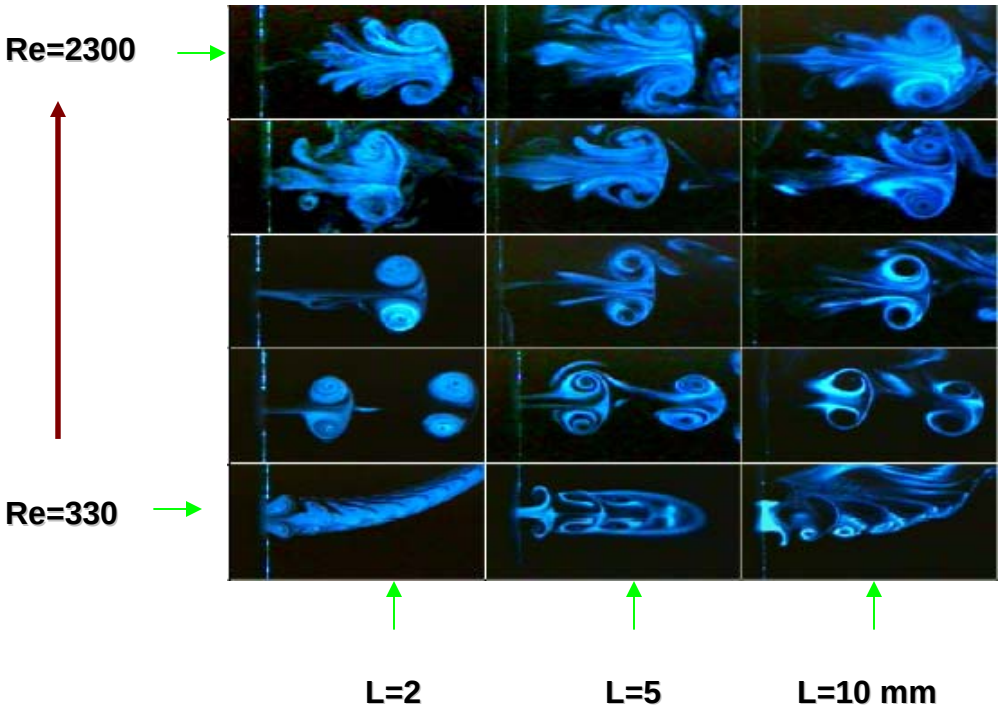

Figure 1.9 Change of the vortex rings structures as a function of the Reynolds number and the orifice length **[Crook, Wood2001].**

1.6.2 Strouhal number (*Sr*)

The Strouhal number is the ratio of inertia forces caused by local unsteady acceleration at a point and the inertia forces caused by the convective acceleration over a region in the neighborhood of that point. It is a non-dimensional parameter that compares the excitation frequency to the amount of time it would take an element of fluid to pass through the orifice:

$$Sr = \frac{fD}{U_j} \tag{1.2}$$

where f is the frequency of disturbance, D is the orifice diameter and U_j is the average jet velocity **[Wu, Breuer2003]**.

A synthetic jet actuator takes air in and out of a cavity at a pace determined by the actuation frequency. Strouhal number at which neither blowing nor suction dominates the flowfield is believed to be the optimum Strouhal number **[Wu, Breuer2003, Rediniotis1999]**. Strouhal numbers of approximately two and above, indicate the dominance of inertial effects associated with the local oscillations in the flow. Under these circumstances an actuator will undergo several suction-blowing cycles before the fluid manages to convect away from the orifice region. In contrast, at Strouhal numbers of less than two an element of fluid passes through the orifice in fewer cycles as inertial effects associated with the larger spatial velocity gradient in the flow overwhelm the local oscillation inertial effects.

Majority of the jets studied in the literature operate at relatively low Strouhal numbers, i.e. $Sr<1$ (less unsteadiness and more directivity) and high Reynolds number, i.e. $Re>50$ (lower viscous losses). This combination of non-dimensional parameters creates strong jets with high momentum flux **[Wu, Breuer2003]**.

1.6.2.1 Non-dimensional stroke length

Glezer proposed a simple "slug" model, for the synthetic jet, and explained that during actuation a specific amount of fluid is forced from the inside of the cavity out through the

orifice. Depending on the actuation frequency and amplitude, the length of the column of fluid L_0 pushed through the orifice of diameter D during the ejection part of the cycle will travel at some velocity U_0 for a time T_0 (inverse of the actuation frequency). This length can be approximated as: $L_0 = \overline{U}_0 T_0$. This relationship is a crude estimate because of the variation of the exit velocity and geometry effects but it is used to define an important dimensionless parameter for synthetic jets: the dimensionless stroke length: $L_S = \frac{L_0}{D}$. This is also recognized as the inverse of the Strouhal number: $Sr = \frac{fD}{\overline{U}_0} = L_S^{-1}$ as the actuation frequency and velocity term normally associated with the Strouhal number are incorporated within the fluid stroke length term L_0. **[Smith, Glezer1998]**.

1.6.3 Jet momentum coefficient (C_μ)

The jet momentum coefficient is a key parameter for characterizing jet interaction with the external cross flow. It is defined as the ratio of the synthetic jet momentum flux to the freestream momentum flux:

$$C_\mu = \frac{2\rho_j U_j^2 b}{\rho U^2 c} \tag{1.3}$$

ρ_j and ρ are the jet and freestream fluid densities, U is the freestream velocity and U_j is the averaged jet velocity, c is the length of the area to be influenced (normally the chord length) and b is the width or the diameter of the actuator's orifice **[Smith, Amitay1998]**.

For flow separation control C_μ is normally on the order of 10^{-3}. A minimum jet momentum coefficient of 0.002 is needed for the actuator to have any effect on separated flows. The effect of the synthetic jet on the separated flow will grow as the jet momentum coefficient increases. It can be seen in Figure 1.10 that without actuation the flow is completely separated and the size of the separated region decreases as the jet momentum coefficient increases until finally being eliminated at $C\mu$ of 0.04 **[McCormick2000]**. Higher jet momentum coefficients are generally needed if the jet is located further away from the separation location.

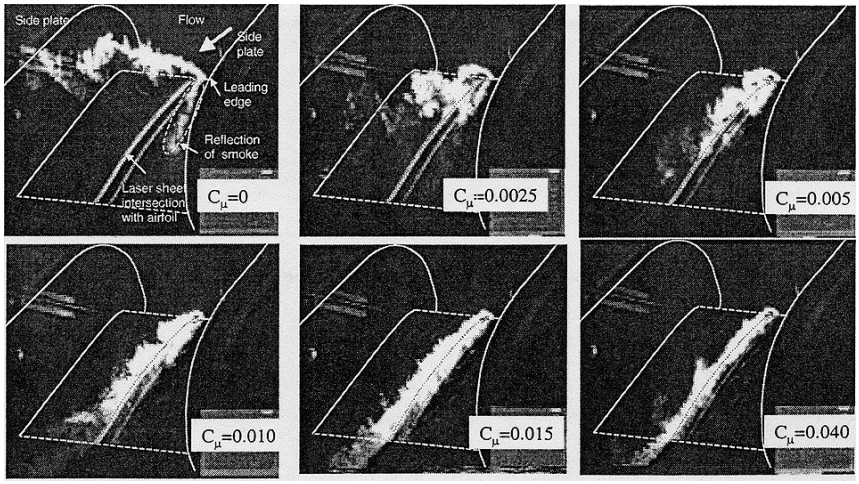

Figure 1.10 Effect of the jet momentum coefficient on flow separation control **[McCormick2000].**

A closely related non-dimensional parameter that is commonly used to define the efficiency of synthetic jets in cross flow is known as the jet-to-free stream velocity ratio (R) and it compares the magnitude of the peak velocity of the jet to the velocity of the

free stream. *"For low subsonic speeds it is typical to have U_j/U of 3. For micro UAV applications this ratio can be as high as 10, so the achieved aerodynamic benefits due to active flow control are sensitive to the characteristic Reynolds number of the lifting surface"* **[Hassan2005]**. The optimum velocity ratio depends on the type of flow control strategy in use.

1.6.4 Non-dimensional frequency (F^+)

Non-dimensional frequency is defined using the actuator operating frequency and a length scale (D^+) that is on the order of the size of the flow region to be influenced **[Gilarranz2001]**:

$$F^+ = \frac{fD^+}{U} \tag{1.4}$$

There are two generally accepted actuation frequency choices. When the synthetic jet actuator is used for flow separation it is operated at frequencies that are of the same order as the natural shedding frequencies of the main flow: $F^+=1$. In such cases coincidence of the unsteadiness of the jet to the instability of the working flow amplifies the control input causing flow reattachment **[Seifert, Wygnansky1996, Seifert, Pack1999]**.

Second option is to operate the actuator at much higher frequencies such that it influences the main flow independently of its internal operating frequency: $F^+ \sim 10$. In

such cases the interaction of a jet with the flow occurs at a smaller length scale which suppresses the shedding frequency and leads to local modification of the apparent shape of the given surface **[Chatlynne, Glezer2001]**.

1.7 Importance of the actuator location on the control authority

The naturally developing flow field over an arbitrary surface is not uniform. Governed by the applied control strategy, it matters where on such surfaces a perturbation is introduced. Some locations are more influential than others. In the case of reattaching separated flows, the closer the control perturbation is located to the separation point, the more effective the actuation and the lower the actuator power required. If the separation point is unknown, a combination of control location and momentum coefficient can be adjusted to achieve the best performance for a particular configuration **[Amitay, Smith2001]**.

Flow reattachment of separated flows was observed by Smith et al. when using flow perturbations applied at various locations on the pressure side of the surface. Such abilities suggests that the *"control is effecting a global change in the flowfield and is a strong evidence that the control input is not simply a local coupling with a boundary layer or shear layer instability"* **[Smith, Amitay1998].** In 1998, Nae observed similar results. He used an unsteady Navier Stokes code to conclude that at relatively small angles of attack (zero and five degrees) synthetic jets may be used for lift improvement if

they are used on the lower side of the airfoil starting at around 10% from the leading edge **[Nae1998]**.

In the case of fully attached flows, actuators mounted in the front half of the wing could potentially change the camber of the airfoil, while actuators in the second half could influence the suction peak pressure and the stagnation point **[Glezer1998]**. Both of these phenomena would effectively change the aerodynamic properties of the lifting surface, however, the evidence of such control remains to be demonstrated.

1.8 Interaction of adjacent synthetic jet actuators

It is not likely that axisymmetric synthetic jets will ever be applied on real time platforms as single units. Their use will be combined in a form of arrays. It is important to understand how the spacing between these actuators and the sequence of actuation affects their mutual interaction as well as the flow field properties around them.

Two adjacent jets, when operating together, could produce a single resultant jet. Strength, form and direction of this ensuing jet could easily be manipulated by exciting the two actuators with different wave forms. This is unique for synthetic jets due their oscillatory nature and vortex ring formation. It was observed in numerical simulations that when excited with 0 degree phase offset, two adjacent jets attract each other and merge into a single large jet. With a 60 degree phase offset the merged jet was vectored to the side of the actuator leading in phase therefore leading the relevant blowing and

suction strokes **[Kral2000]**. Smith et al. experimentally studied this dynamic vectoring of synthetic jets and its effect on the entrainment of ambient fluids in the near region: *"In the far field the scaled velocity distribution of the combined jets and the single jets are very similar. However, the volume flow rate of the jet pair in the far field is substantially larger than the corresponding flow rate of the single jet even though the rate of increase is similar. This is attributed to a large increase in entrainment in the near field due to vortex interactions"* **[Smith, Trautman, Glezer1999]**.

It is likely that changing the relative phase angles of excitation of adjacent actuators to produce needed effects may be the major parameter in control strategies of the future. Preliminary experiments and simulations have implied that a combined use of orifice spacing and phase shift angles could be used to control the degree of vortex interaction to suit particular flow control needs.

1.9 Importance of the synthetic jet injection angle

Numerical studies have been conducted to explore the effects of jet injection angles on the aerodynamic performance. An array of transverse (jet ejecting normal to the surface) and tangential (jet ejecting at angles between 0 and 45 degrees) synthetic jets was simulated on a NACA 0012 and NACA 0015 airfoils **[Hassan, Munts2000]**.

Transverse jets, when placed on the lower surface of the airfoil, demonstrated an increase in the mean lift force. These benefits were particularly pronounced at lower

angles of attack. It was also observed that the use of an array of transverse synthetic jets increased the airfoil drag.

The near tangent synthetic jets were relatively ineffective at small angles of attack. At higher angles of attack, in the post stall region and regardless of the jet angle, improvements in lift with simultaneous reductions in drag were achieved. However, the percent reduction in the airfoil drag for a jet angle of 45 degrees was less than that achieved for a jet angle of 35 degrees suggesting an optimum jet angle required to maximize the airfoil's aerodynamic benefits at a given free stream velocity and angle of attack.

1.10 Shape of the orifice

Milanovic et al. studied the effect of the orifice shape on the synthetic jet in cross flow penetration abilities. Straight, tapered, pitched and a cluster of nine orifices were investigated. Strength of the jet issuing from the tapered and straight orifices was very close. The flow field of the orifice cluster was similar to the single orifice of the same area. Flow from the cluster, however, had a slightly lower strength. The pitched configuration had the lowest penetration length of all **[Milanovoic2003]**.

Shuster and Smith studied straight, rounded and beveled orifice geometries and effects of various non-dimensional stroke lengths on jet formation. Their observations showed that the value of the non-dimensional stroke length below which the jet formation

will not occur depends on the shape of the orifice. Shape also dictates whether a pulsed or synthetic jet will be created. Along with the non-dimensional stroke length, orifice shapes also govern the location of the vortex breakdown **[Shuster2004]**.

1.11 Organization of the dissertation

Chapter 1: Introduction

Chapter 1 described the mechanism of a synthetic jet actuator. Structural and geometric properties related to the formation of the synthetic jets were discussed. Non-dimensional parameters, important for both analysis of synthetic jets in quiescent and cross flow conditions, were separately defined and analyzed including the discussion on their efficient ranges and limits. Major contributions in analytical, numerical and experimental studies have been highlighted and referenced. A short discussion on some of the actuator application parameters, like actuator location in the flow, injection angles and their mutual interaction, was provided at the end of the chapter.

Chapter 2: Synthetic jet actuator design and characterization

The initial motivation for this research was an interest in investigating the potential for using synthetic jets to maneuver a small scale aerial vehicle without the need to apply any control surfaces. A THUNDER-based axisymmetric synthetic jet actuator operating at 2200 Hz was designed, fabricated and characterized for this purpose. Some of the intricacies of this process including the difficulties in assigning the most efficient values

for the actuator geometry parameters have been addressed. Special care was given to the fluid-structure coupling of such a device by analyzing the system fundamental frequencies.

Chapter 3: Measurements of flow fields from synthetic jets in quiescence conditions

Viscous effects and compressibility effects are pronounced in actuators of smaller scale and operating at higher frequency. These are the type of actuators used in this project and because study of actuators of a similar size were not found in the literature detailed experimental analyses were conducted to study these particular synthetic jet actuators. A constant temperature anemometer, in conjunction with a single and dual sensor probe, was used to obtain detailed synthetic jet velocity field measurements in a two-dimensional plane centered above the orifice. The isolated effects of the orifice diameter, orifice length and cavity height on the streamwise and cross stream velocity component and on turbulence intensity were presented separately. The orifice was labeled a key influence parameter for synthetic jet actuator performance and its shape/dimensions were used to define the non-dimensional parameters like the Reynolds number and the Strouhal number.

Chapter 4: Characterization of synthetic jet actuators in cross flow

This chapter included the analysis of the individual synthetic jet actuators operating in fully attached cross flows. Actuators were mounted flush to the wind tunnel test section floor with the wind speeds changing from 3 m/s to 20 m/s. Different jet-to-free stream

velocity ratios were tested to determine the range of this ratio under which the actuator would have a distinguished effect on the given free stream. It was seen that for velocity ratios above one the synthetic jet had enough momentum to emerge through the boundary layer and significantly affect the external flow. Transverse synthetic jet cross section measurements showed that the jet area and shape changed more dramatically at smaller velocity ratios. Additional measurements included the effects of the variation of the orifice diameter with respect to the boundary layer thickness, at constant velocity ratios. Measurements and observations of similar types synthetic jet actuators in such external conditions have not been found in literature.

Chapter 5: Modeling of synthetic jets in cross flow

Details of the model predicting the synthetic jet trajectory, velocity decay and the jet area as it propagates in the external cross stream are covered in this chapter. The approach was developed using semi-empirical integral methods. A slug of jet flow was identified as a control volume and integral techniques were used to follow its properties along the jet centerline. It was demonstrated that the jet deflects, spreads and deforms due to flow entrainment and due to pressure imposed on the jet boundaries. The primary drawback of this type of modeling is that empirical calibrations are required when assuming the jet cross sectional shape, entrainment rate and surface forces coefficients. Comparison with experiments, however, demonstrated the practicality of this theory for estimating the location, size and velocity of the jet with respect to the orifice location in different cross flow conditions. The advantage of having such a model is emphasized in the next chapter.

Chapter 6: Prediction of the induced pressure distribution on a flat plate due to synthetic jet actuation

The interaction between a jet and a lifting surface to estimate aerodynamic loads due to synthetic jet actuation were simulated through the distribution of sets of sinks and doublets along the width and centerline of a jet trajectory. Total velocity induced on the surface due the presence of the jet was determined using the Biot Savart Law. Jet-induced downwash was presented as an effective camber created on the surface due to such flow interactions. Information on the jet induced downwash allowed the application of the lifting surface theory integral to solve for the pressure loading caused by the presence of a synthetic jet. Similar modeling of single jets in cross flow and their effect on the lifting surface have not been found in the literature. Only a single synthetic jet was studied here. Modeling of the interaction of these jets and their total effect on an entire surface is considered part of suggested future work.

Chapter 2

Synthetic Jet Actuator Design and Characterization

2.1 Introduction

The experimental approach of this research included the design, manufacturing and characterization of synthetic jet actuators in both quiet and cross flow conditions. This chapter highlights the design and fabrication aspects including the system analysis.

Initial design constraints were related to the objective test bed size (unmanned/micro aerial vehicles) and the targeted control strategy (influencing fully attached flow). Control of fully attached flows to induce significant pressure distribution changes, e.g. changes needed for maneuverability tasks, requires a global influence on the flow field that is decoupled from the operating frequency of the actuators **[Amitay2002, Wu, Breuer2003]**. This requires actuators that can generate high frequency flow perturbations.

Information on actuators of the desired size and operating frequency was not found in the literature. Some insights from the available design characterization studies were applied to design of these high frequency (~1 kHz-2 kHz) miniature (~10 mm in height)

actuators. However, due to this particular scale and frequency combination, some of those observations were not applicable. As clarified by Rathnasingham, the dynamics of each newly manufactured actuator needs to be well understood and accurately characterized before being used in flow control **[Rathnasingham1996]**. As a result, this chapter focused on developing transfer functions between the input (voltage) and the output (acoustic signal and velocity) for a range of synthetic jet actuator configurations. Details on the design concept and on the experimental and theoretical characterization of the synthetic jet actuators manufactured and used in this research are also discussed.

2.2 Synthetic jet actuator design

Synthetic jet actuators developed and analyzed in this project were axisymmetric and based on piezoelectric composite technology. Considering the chosen small (MAV type) scale test bed, all other available diaphragm options (i.e. piston driven actuators) were too complex and/or too heavy for such an application. Axisymmetric actuators were chosen to simplify the analysis by avoiding the non-uniform velocity profile along a 2D slit. Additionally, strategically engineered adjacent actuator interactions could provide more flow control strategy opportunities over the one of a continuous slot.

PZT based synthetic jet actuators provide maximum displacement when operating at their resonant frequency so for maximum jet velocity they should be forced at the resonant mode of the PZT diaphragm. This condition, however, significantly restricts the frequency band of unimorph and bimorph type synthetic jet actuators. As an example, for

a half inch PZT-brass shim diaphragm the operating frequency can reach up to 7-8 kHz. After the initial studies, building half inch PZT-5 single crystal-metal shim unimorphs **[Ugrina, Flatau2003]**, the choice for the synthetic jet actuator driver for this research was shifted and finalized to the commercially available THUNDER® actuator (Figure 2.1). These actuators provided greater displacement and output velocity for less weight and power than the alternative PZT-brass shim based unimorph design **[FACE Inc]**. The operating frequency of the actuators was reduced from ~8000 HZ for the PZT-5-brass shim unimorphs to ~2000 Hz for the THUNDER based actuators.

Figure 2.1 Thunder actuator TH-5C **[FACE Inc]**.

2.2.1 PZT piezoceramic and piezoelectricity

By nature piezoelectric materials (such as Lead Zirconate Titanate) are polycrystalline. Crystals contain positive and negative electrical charges which are distributed such that the crystal is electrically neutral (they are isotropic cubic before poling as shown in Figure 2.2.a). These sites form electric dipoles which align themselves in regions called

Weiss domains. Before poling these domains are oriented in random directions as needed to satisfy the minimum energy state within the material. However, these domain orientations can be aligned through poling, during which a strong electric field is temporarily applied across the material. This leaves the domains oriented mostly along the direction which that field was applied (Figure 2.3). This reorientation of the domains results in a mechanical deformation usually reflected through a change of dimensions of the PZT material. The material expands along the axis of the field and contracts perpendicular to that axis (Figure 2.2.b).

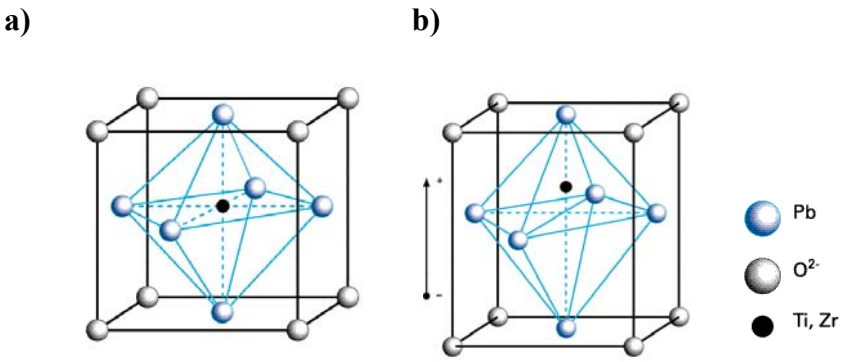

Figure 2.2 Piezoelectric elementary cell a) before and b) after poling **[pi.ws].**

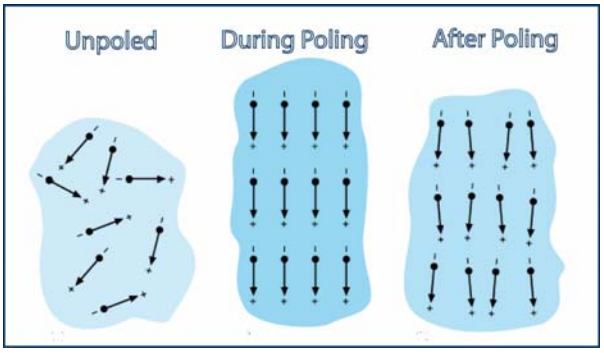

Figure 2.3 Dipoles in Weiss Domains

Piezoelectricity can be used for actuator or sensor applications. In the case of a sensor application when pressure is applied to this type of material it causes the dipoles to rotate producing an electrical charge, while in the actuator application the material changes dimensions when an applied voltage produces a reorientation of these domains.

2.2.2 THUNDER actuator technology

"THUNDER is an acronym for Thin Layer Unimorph Ferroelectric Driver and Sensor" **[FACE Inc]**. It is composed of a thin PZT layer that is bonded on one side to an electrically conductive stainless steel shim and on the other side to an aluminum layer (Figure 2.4). The bonding of these individual elements was achieved using a high performance epoxy developed by NASA. The piezoceramic is held in a state of compression and the stainless steel in a state of tension. The resultant actuator in its neutral, "unexcited" state is arched into a dome-like shape. Piezoceramic crystal would normally break under such curvatures but this patented manufacturing process strengthens the PZT providing a THUNDER with much larger deflections than of any other commercially available unimorph in this category.

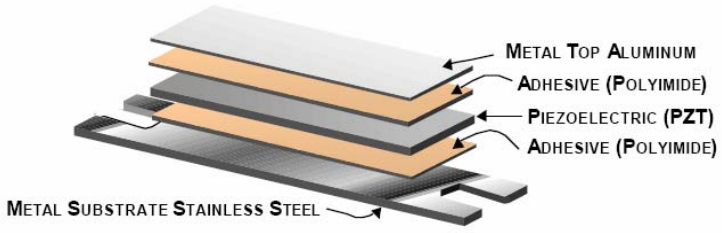

Figure 2.4 Major components of the THUNDER actuator **[FACE Inc].**

THUNDER elements are polarized such that the actuator flattens, when positive voltage is applied to the top layer. Applying positive voltage reduces the size of the PZT and in turn reduces the internal compression of the PZT which flattens the stainless steel and causes the THUNDER to move downward. When negative voltage is applied PZT grows in size increasing the internal stresses. This forces the stainless steel to adapt by arching, which causes the THUNDER to move upward.

2.2.3 THUNDER actuator-a synthetic jet generator

To minimize research costs, pre-designed, off the shelf THUNDER actuators were chosen for driving the synthetic jet actuators used in this research. Round, 32-mm diameter and 1.30-mm dome height TH-5C THUNDER actuators (weighing ~2.6 g) were selected. The piezoceramic thickness of this particular model is 0.18 mm and the total thickness of the unimorph is 0.41 mm. When simply supported and excited at 1 Hz with maximum voltage of +60 V/mil and -30 V/mil the maximum displacement reported by the manufacturer is 0.13 mm.

The main disadvantage of these actuators for "pump type" applications is their dome shape. Unimorphs are normally flat so clamped boundary conditions are easily implemented. This is not true for the THUNDER actuator. Rigidly clamped boundary condition is not realizable due to its "saddle" shape. Clamping it loosely between two O-rings damped out its displacement capabilities. To overcome this mounting problem a cavity was developed that incorporated a recessed section at its base. A controlled

amount of silicone was placed on this edge for the THUNDER to rest on. The layer of silicone provided an air-tight seal and held the actuator in place without restricting its ability to change shape thereby providing the desired displacement when excited. Silicone provided a low mass bonding condition for the active synthetic jet membrane.

2.2.4 Experimental analysis of the THUNDER actuator

Analysis of the isolated diaphragm, with a silicone layer forming the boundary condition, was conducted using the Polytec Scanning Vibrometer (PSV). The diaphragm was excited with a sine sweep over a frequency range of 10 Hz to 3 kHz (in 5 Hz increments) while measuring spatial and temporal distribution of the actuator vibration. More constricted boundary conditions reduced the maximum allowable excitation voltage from 400V (at free boundary conditions) to 150V. 3D visualizations obtained with PSV were accompanied with the velocity and displacement data at each frequency the diaphragm was excited at. Animated diaphragm motion showed diaphragm modes at different frequencies and allowed a quick and easy verification of the uniformity of the boundary condition all around the actuator circumference. It was a useful test for both the final tuning of the actuator as well as for the guarantee of the symmetry of the bonding. Once assuring that a uniform boundary condition was established the fundamental resonant frequency of the diaphragm at these conditions was measured to be 2200 Hz with maximum displacement of 0.06 mm when driven at 150V. Figure 2.6 shows the velocity of the diaphragm when excited at 75V. Maximum membrane velocity for this case was measured to be 60 mm/s.

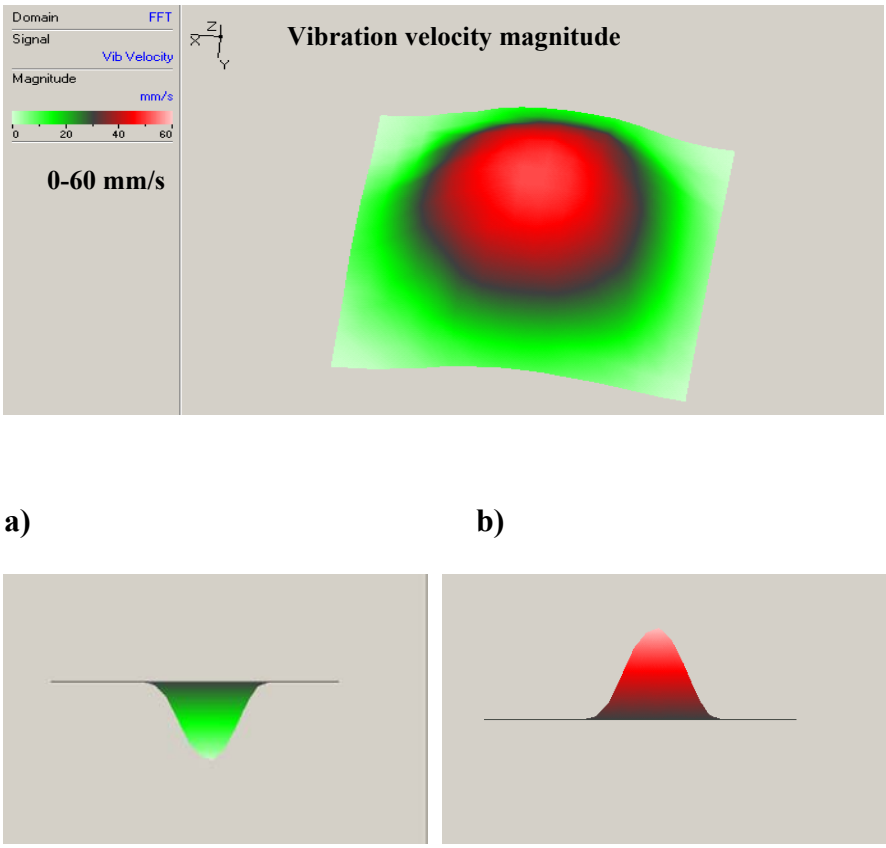

Figure 2.6 Figure of the THUNDER response when excited at 75 V captured with the Polytec Scanning Vibrometer at its a) minimum and b) and maximum velocity peaks.

2.2.5 Specifics of the actuators manufactured in this project

For ease of construction and analysis (to maintain axisymmetric conditions) round shape diaphragm (TH-5C THUNDER discs) predetermined a cylindrical cavity of the same size (D_C). The optimum height of the cavity (H), diameter (D) and thickness (L) of the orifice were determined by experimental analysis. A parametric study had to be conducted to

identify design configurations that would ensure jet formation and development of coherent flow structures.

Modular components were manufactured to provide flexibility for assembling different actuators. The plate to which the THUNDER was bonded operated as the base housing and had an associated cavity height of 1.1 mm. One or more plates of the same thickness were interchanged or stacked on top of the existing one, providing a simple way to change the volume of the cavity. The cavity was closed with aluminum top plates of different thickness and orifice dimensions providing means to study the sensitivity of jet formation and evolution on orifice properties. Circular orifice diameters of 1 mm, 2.5 mm, 5 mm and 7 mm were used and the lid thickness ranged from 0.5 mm to 2 mm. Figure 2.7 shows some of the synthetic jet actuator components. It shows a THUNDER actuator bonded to the base plate along with the sample plates that were used to change cavity volume and orifice thickness and area.

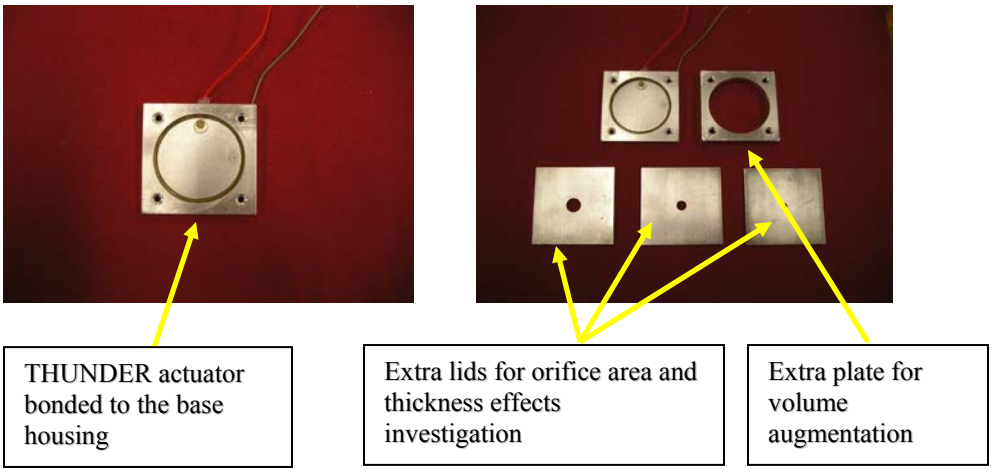

Figure 2.7 Components manufactured to assemble the most efficient synthetic jet actuator.

2.3 Theoretical analysis of synthetic jet actuators

Synthetic jet actuator was represented as a two degree of freedom model in terms of inertia, stiffness, damping and forcing coefficients. Both the diaphragm and the vibrating air have their own respective mass (M), damping (C) and stiffness (k) coefficients (Figure 2.8).

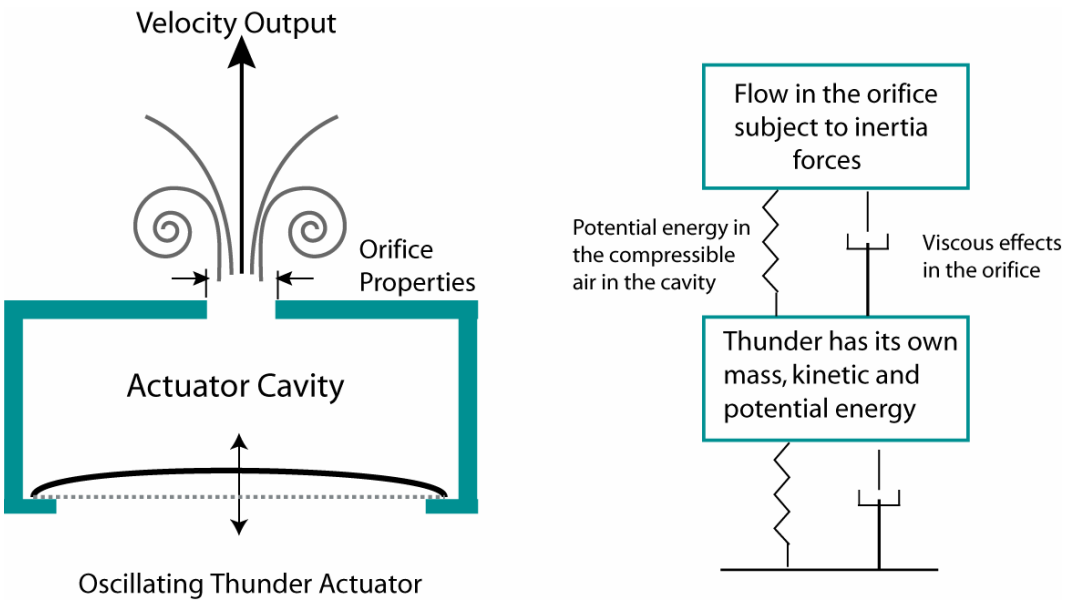

Figure 2.8 Physical representations of the synthetic jet actuator components

Air moves with high velocities so the energy required to accelerate the air mass is significant. Viscosity and boundary layer separation cause major energy losses in the orifice through dissipation of kinetic energy of the oscillating air mass. This is reflected in the damping terms of the model. Stiffness terms are associated with potential energy

stored as air inside the cavity is compressed **[Gallas, Cattafesta2003]**. Forcing terms result from the oscillating diaphragm of a given mass whose damping and stiffness terms were determined experimentally.

2.3.1 Synthetic jet actuator fundamental frequencies

A synthetic jet actuator is a coupled mechanical-Helmholtz resonator system. Periodic motion of the diaphragm is coupled with the air oscillating in the actuator's orifice. The final response of such a system will be a function of the structural properties of the THUNDER diaphragm (mechanical resonant frequency), the geometry properties of the actuator and the physical characteristics of the operating fluid (acoustic or Helmholtz resonant frequency). For the most efficient output, it is desirable to tune the actuator so that the acoustic or Helmholtz resonant frequency of the cavity and structural resonant frequencies of the Thunder diaphragm coincide.

Helmholtz recognized that the slug of air in the orifice of a closed cavity would oscillate at a frequency associated with the mass of the air in the orifice and the stiffness or compressibility of the air in the cavity, i.e. at what is known as the Helmholtz frequency. By exciting the diaphragm in the cavity at the cavity Helmholtz frequency a small displacement and hence a small pressure variation within the cavity can produce a large mass flow through the orifice **[Blevins1979]**. Higher synthetic jet velocities are, therefore, expected when the diaphragm oscillates at the cavity Helmholtz frequency.

Tang and Zhong observed that the Helmholtz resonant frequency can be suppressed by viscous effects **[Tang, Zhong2005]**. They defined a non-dimensional parameter lambda (λ) to estimates the strength of the viscous effects: $\lambda = \frac{c^2 D^6}{256 \nu^2 H L D_c^2}$, where c is the speed of sound and ν is the kinematic viscosity. They observed that if lambda is greater than ten, Helmholtz resonance will occur. Otherwise the jet produced is in proportion to the diaphragm displacement alone.

2.3.2 Synthetic jet actuator model coefficients

Helmholtz frequency of the cavity was estimated using a simplified equation **[Blevins1979]**:

$$f = \frac{c}{2\pi}\left(\frac{A}{VL}\right)^{\frac{1}{2}} \tag{2.1}$$

where c is the speed of sound in air, A is the cross sectional area of the orifice, V is the volume of the cavity and L is the length of the orifice. In the case of a larger orifice diameter-to-length ratio, Blevins provided a formula that takes into account the inertia of the fluid in the cavity and the motion of the fluid outside the orifice. The acoustic natural frequency is then represented by:

$$f = \frac{c}{2\pi}\left[\frac{A}{1.2\left(V + AL_N\right)L_1}\right]^{1/2} \tag{2.2}$$

Where L_N is the length of the nozzle/orifice and L_1 is an expression that takes into account the factor of the orifice shape L_V, which for our case of a cylinder with a circular hole corresponds to $L_V = \frac{1.88r^2}{L}$. The expression for L_1 is as follows:

$$L_1 = \left\{ L_V + L_0 + \left(L_N + L_0\right)\left[1 + \frac{L_N + L_0}{2L} + \frac{A\left(L_N + L_0\right)}{2V} + \frac{A(L_N + L_0)^2}{3VL}\right]\right\} \frac{VL}{V + A(L_N + L_0)(L + L_N + L_0)} \tag{2.3}$$

where $L_0 = 0.24r$ and r the radius of the orifice.

To model the dynamic behavior of a piezoceramic-metal unimorph the classical plate equation $\nabla^2 D\nabla^2 w = p$ is usually used, where D is the bending modulus defined as $D = \frac{Et^3}{12(1-\nu^2)}$ **[Leissa1993]**. The expression for the natural frequency of a plate is given by:

$$f = \frac{\lambda^2}{2\pi a^2}\left[\frac{Et^3}{12\gamma(1-\nu^2)}\right]^{1/2} = \frac{\lambda^2}{2\pi a^2}\sqrt{\frac{D}{\gamma}} \tag{2.4}$$

Where λ is the eigenvalue, a the radius of the plate, E is the Young's modulus, t the thickness of the plate, ν the Poisson's ratio, γ the mass per unit length of the plate. Eigenvalues are tabulated and widely documented for different boundary conditions. Since the THUNDER actuator is a composite plate that has undergone a particular

manufacturing process, these classical plate equations were not entirely applicable. Instead, the resonant frequency of the diaphragm was obtained experimentally and used in conjunction with analytical models to extract the effective stiffness and damping coefficients of the THUNDER actuator. The following simplified relation was used: $f = \frac{1}{2\pi}\sqrt{\frac{k}{m}}$. Damping coefficient was determined using $C = 4\pi fm\varsigma$, where ς is a viscous damping factor estimated from the measured data using the quality factor or the half power point method **[Meirovitch2001]**. These coefficients were then implemented in a set of two degree of freedom equations of motion to estimate the response of the system to harmonic excitation: $\ddot{x}(t) + 2\varsigma\omega_n\dot{x}(t) + \omega_n^2 x(t) = \omega_n^2 A\cos\omega t$. This was written in the matrix equation form as follows:

$$\begin{Bmatrix} F_D(t) \\ 0 \end{Bmatrix} = \begin{bmatrix} m_D & 0 \\ 0 & m_A \end{bmatrix}\begin{Bmatrix} \ddot{x}_D \\ \ddot{x}_A \end{Bmatrix} + \begin{bmatrix} c_A + c_D & -c_A \\ -c_A & c_A \end{bmatrix}\begin{Bmatrix} \dot{x}_D \\ \dot{x}_A \end{Bmatrix} + \begin{bmatrix} k_A + k_D & -k_A \\ -k_A & k_A \end{bmatrix}\begin{Bmatrix} x_D \\ x_A \end{Bmatrix} \quad (2.1)$$

where $c_{A,}$ and c_D are the damping coefficients of the air in the orifice and the diaphragm respectively, m_A and m_D are the masses of the two and k_A and k_D are their stiffness coefficients.

Figure 2.9 presents the prediction of the frequency response of a set of synthetic jet actuators with various orifice diameters. The values of the geometry parameters modeled were taken directly from the as-built modular components. An increase of the orifice diameter caused a significant change in the Helmholtz frequency which is reflected in the different frequency response curves shown. The normalized magnitude of

the response increased as the two fundamental frequencies of the system approached one another with the increased orifice size.

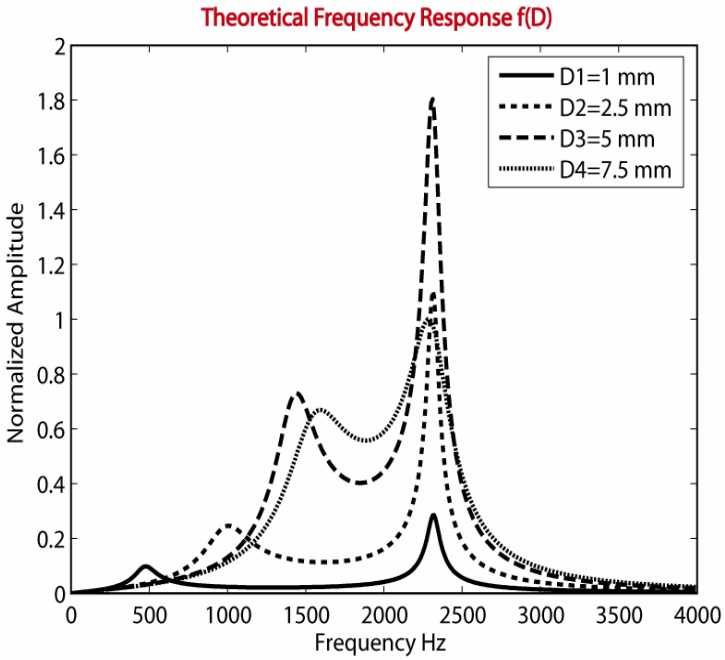

Figure 2.9 Prediction of the frequency response of synthetic jet actuators with orifice diameters of 1, 2.5, 5 and 7.5 mm.

2.4 Experimental analysis of the synthetic jet actuator

To validate the model, synthetic jet actuator frequency response was measured for a wide set of configurations. Experiments were performed using a condenser microphone in conjunction with the virtual sine sweep program (SigLab software). The microphone had a flat frequency response (from ~DC to over 20 kHz). It was calibrated, indicating 12 mV/Pa. In all tests the microphone was placed at a constant distance of 2 mm from the orifice. Results are presented as the frequency response of the measured mean jet acoustic pressure (normalized) relative to the Thunder actuation voltage at a given frequency.

The baseline actuator model consisted of a cavity with the height of 1.1 mm and the orifice diameter and thickness of 1 mm and 0.5 mm, respectively (L/D =0.5). A first glance at the frequency response of the actuator as a system, shown in Figure 2.10.a, demonstrates suitability of a two-degree of freedom model. Two peaks, the lower one associated with the Helmholtz resonant acoustic response and the second associated with the diaphragm resonant response, correspond to the two lowest resonant modes of the assembled system. For comparison, the experimental frequency response of just the diaphragm was shown in Figure 2.10.b, with the resonance peak at ~ 2200 Hz (as measured with the Laser Vibrometer).

a) **b)**

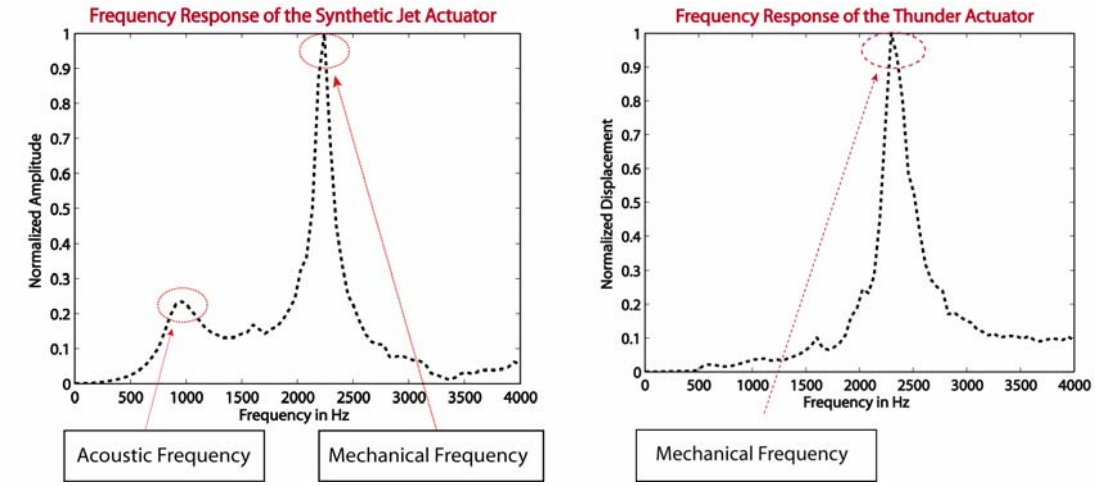

Figure 2.10 Experimental data of the frequency response of the a) synthetic jet actuator and b) diaphragm

By comparing experimental data to the model, in Figure 2.11, it was demonstrated that both the resonant frequency of the diaphragm and the resonant frequency of the cavity were well captured.

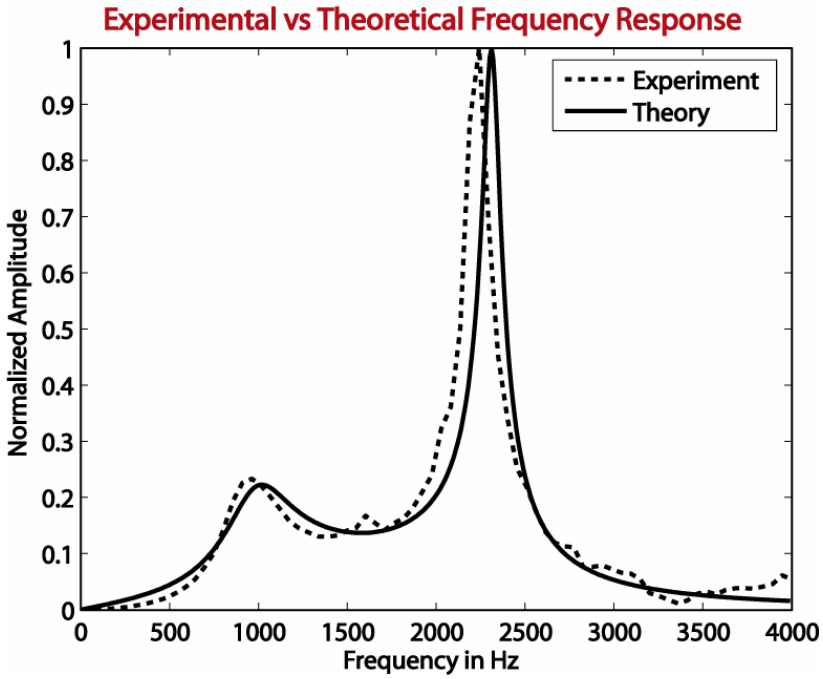

Figure 2.11 Comparison of theoretical frequency response prediction to experiment.

A significant assumption in the model is that the damping coefficient is associated with both the viscous losses and the oscillatory boundary layer in the orifice. All of these effects were stored in the damping coefficients that were empirically determined so that the frequency response magnitude matched the experimental data. Expressions to predict these effects and incorporate them into the model are needed for a better model. Agreement between this simplified theory and the experimental data were acceptable only for cases where the acoustic frequencies were lower than the mechanical resonance frequency.

2.4.1 Experimental results and discussion

The following set of experiments focused on analyzing the sensitivity of the frequency response curve to orifice size. The orifice diameter was varied from 1 mm to 7.5 mm shifting the Helmholtz resonant frequency from ~450 Hz to ~1800 Hz. The larger diameter reduced the orifice resistance decreasing damping and improving the systems efficiency. As the Helmholtz frequency approached the structural frequency of the device, the overall amplitude of the response curve increased, as seen in Figure 2.12. These trends validated the predictions observed in the theoretical analysis section.

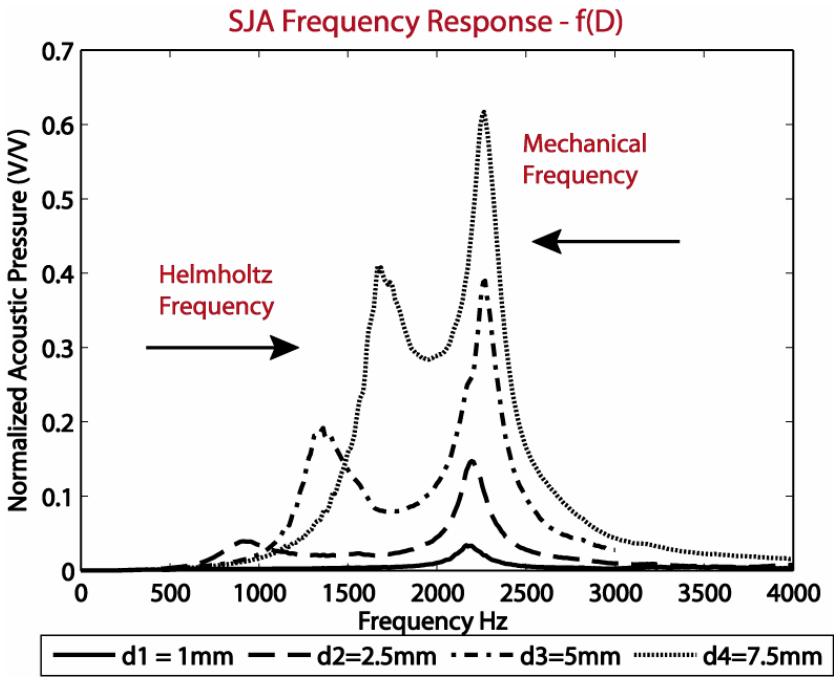

Figure 2.12 Experimental data of the frequency response of the synthetic jet actuator at different orifice areas.

Cavity height was varied next, from 1.1 mm to 6.1 mm, reducing the stiffness terms of the system and thus lowering the Helmholtz resonance from ~3400 Hz to ~1800 Hz. In comparison to the cavity height of 6.1 mm, smaller cavity heights (1.1 mm and 3.1 mm) suggested higher stiffness that shifted the mechanical resonant frequency position down by approximately 100 Hz. In such cases, resonant peak associated with the oscillating air was higher than the resonant peak associated with the diaphragm (Figure 2.13).

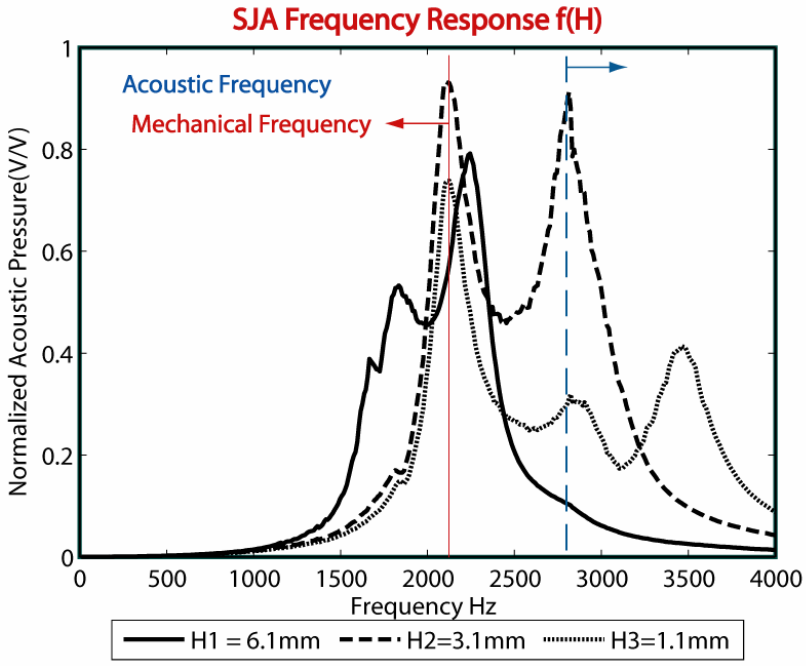

Figure 2.13 Experimental data of the frequency response of the synthetic jet actuator at different cavity heights.

Lastly, sensitivity of actuator frequency response curves to the orifice length was tested. The influence of this parameter was expected to be lower than of the previously

studied parameters. This is because the Helmholtz frequency is inversely proportional to the length of the orifice but it changes as the square of the diameter and the cube of the cavity height. As shown in Figure 2.14 decreasing the length of the orifice by three times caused the Helmholtz frequency to increase by approximately 200 Hz.

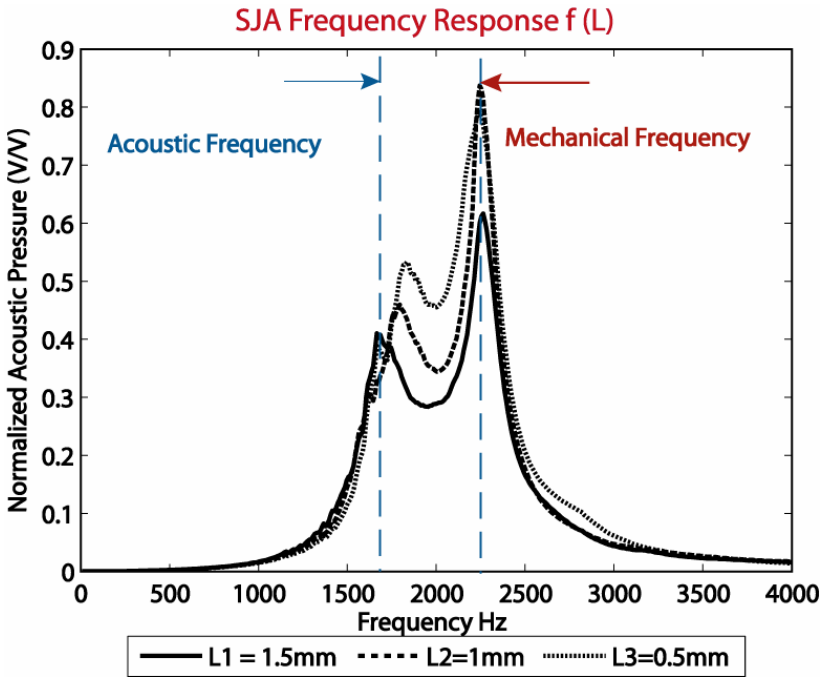

Figure 2.14 Experimental data of the frequency response of the synthetic jet actuator at different orifice nozzle lengths.

2.5 Synthetic jet actuator operating regimes

Constant temperature anemometer experiments were conducted to relate the mutual interaction of the two frequencies to the actual synthetic jet velocity. Synthetic jet

velocity measurements were taken at mechanical, acoustic and off resonance frequencies for various geometries. Mean synthetic jet velocity was recorded 1 mm above the orifice exit plane at several locations in the radial direction (up to +/-5 diameters away from the orifice center).

2.5.1 Non-Helmholtz Regime

In the non-Helmholtz regime presented in Figure 2.15, the system is considered over damped and significant amplification at the Helmholtz resonance doesn't occur. The first (Helmholtz) and second (Thunder) resonant frequency peaks are distinct and the actuator creates a jet with largest velocity peaks when excited at the resonant frequency of the diaphragm. The next largest jet peak velocity was produced when the driver was excited at the first, Helmholtz, resonant frequency of the system.

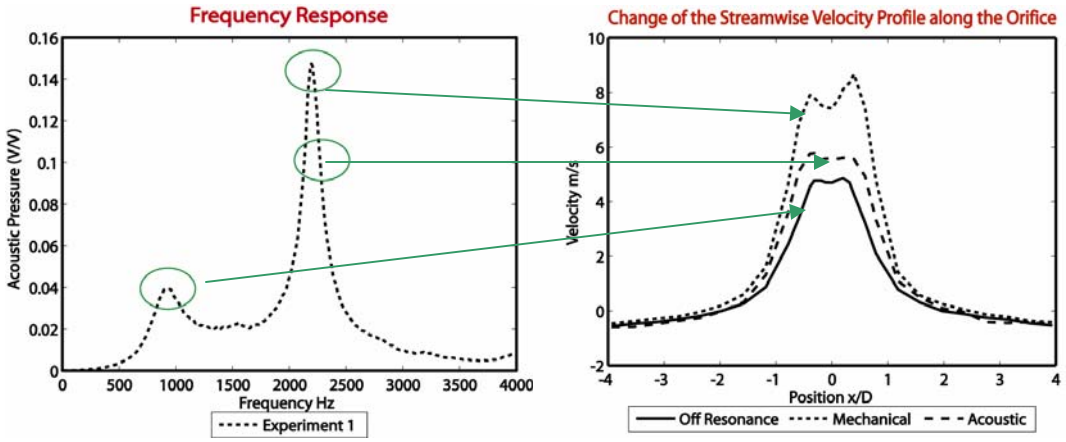

Figure 2.15 Correlation of the cross stream jet velocity measurements at different frequencies to the frequency response plot.

2.5.2 Helmholtz Regime

Once the two resonance peaks merge or once they are in each others near vicinity the actuator operates in a Helmholtz regime. The system is considered under-damped and the performance of the actuator at such conditions is different (Figure 2.16). The overall maximum jet velocity achieved occurred at actuation frequency equivalent to the mechanical resonant frequency of the system. However, under these conditions the maximum jet velocity produced was significantly (almost twice) higher than the maximum jet velocity produced when operating in the non-Helmholtz regime. The jet velocity remained as high over a bandwidth of 20 Hz near the mechanical resonant frequency but excitation at frequencies outside that range caused a significant reduction in the jet peak velocity.

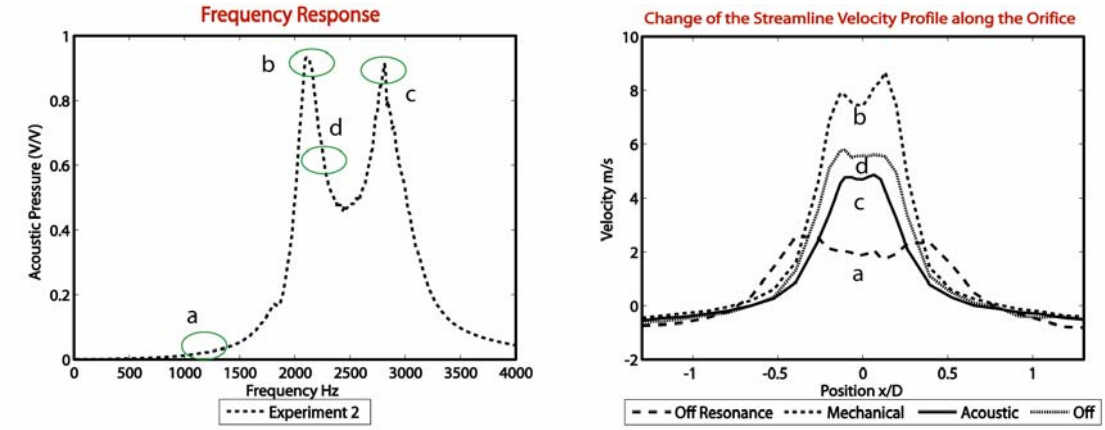

Figure 2.16 Correlation of the cross stream jet velocity measurements to the frequency response plot at four different frequencies: off resonance (a), mechanical resonance (b), near mechanical (c), acoustic (Helmholtz) resonance.

2.6 Conclusion

A THUNDER-based synthetic jet actuator was manufactured and its operational capabilities investigated. Its geometry parameters were varied and their influence on the system frequency response analytically and experimentally determined.

The actuator was modeled as a two-degree of freedom system. Simplified equations for the Helmholtz frequency and the mechanical frequency were used to predict frequency response curves for differently configured actuators. A condenser microphone was used to validate the predictions. Air damping coefficients had to be identified empirically to match the model to the experimental results, but otherwise responses of the first two resonant frequencies were well predicted. It was demonstrated with mean synthetic jet velocity measurements that being able to closely match these two natural resonant frequencies provided a higher resultant velocity jet. Once the mechanical resonant frequency of the system is known, the model can be used to change the different cavity parameters to tune the Helmholtz frequency so it approaches the mechanical frequency and thereby maximizes performance.

This parametric study revealed that inclusions of compressibility effects, viscous and orifice losses effects are of great importance. Care needs to be taken if the actuator is operating in the Helmholtz regime and/or if the orifice of the actuator is of the size where viscous effects could be the prevailing loss mechanism. The non-dimensional parameter *lambda* was cited as an approximate indicator of the level of viscous effects.

Accordingly, attention had to be given to identifying the regime the actuator was operating in. A simple comparison of the various geometry parameter ratios is not enough to predict the jet velocity or its impact on the surrounding flow. The frequency response of the actuator, unsteadiness effects, viscous effects, non-dimensional parameters all have to be understood and taken into consideration when stating facts about the performance and capabilities of any newly designed and manufactured synthetic jet actuator.

Chapter 3

Measurements of Flow Fields of Synthetic Jets in Quiet Conditions

3.1 Introduction

Geometry of the actuator and the dynamic behavior of the active membrane govern the flow character of the synthetic jet produced. Resultant jet velocity and momentum are important actuator performance parameters that determine the impact of synthetic jets on the surrounding flow. As Crook and Wood stated: *"…one should pay close attention to the geometry of the synthetic jet….failure to do so could lead to incoherent structure being ejected into the surrounding flow or possibly nothing at all,"* **[Crook, Wood2001]**.

The deliverables of this chapter include information on the flow topology of synthetic jets in quiet (zero cross flow) conditions. Measurements that illustrate changes in streamwise and cross stream jet velocity signature above the orifice as a function of the actuator design parameters are presented. Additionally data that highlight the importance of the influence of non-dimensional parameters, such as the Strouhal and Reynolds numbers, on jet formation and evolution are presented and discussed.

3.2 Experimental set up

Synthetic jet flow field analysis was based on an extensive experimental flow field database built using a constant temperature anemometry (CTA) technique. By design, a constant temperature anemometer collects spatial and temporal flow field information. The technique is based on convective heat transfer. Any changes in the fluid that affect the heat transfer from the heated ("hot") wire are detected by the CTA system. The CTA used here was the TSI Inc. model (IFA 300) constant temperature anemometer with a flat DC to 300 kHz frequency response shown in Figure 3.1 **[TSI Inc]**.

Figure 3.1 IFA 300 Constant Temperature Anemometer **[TSI Inc]**.

Two different probes (Figure 3.2) were used for all measurements: a model 1260A miniature straight end probe and a model 1249A miniature dual "X" cross flow probe with sensors suitable for close-to-wall measurements and minimal flow disturbance **[TSI Inc].**

a)

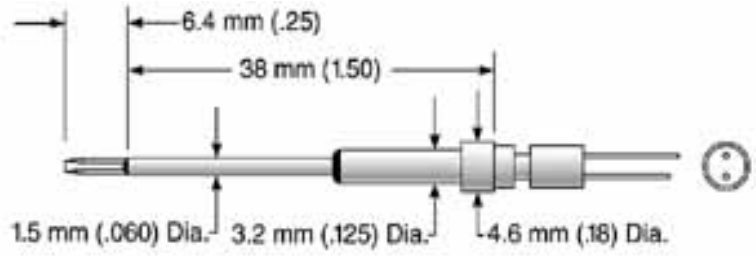

b)

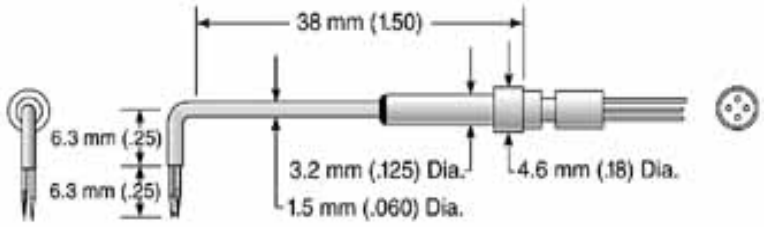

Figure 3.2 Miniature straight end probe (a) and miniature dual sensor cross flow probe (b) **[TSI Inc]**.

Sensors were calibrated by the provider for use in 0 to 40 m/s flow fields. Data were collected at a sample rate of 200 kHz and 8 kilopoints per channel (one kilopoint has 1024 samples). Accordingly, at each point in the flow field the system was collecting data for a total of 0.04096 seconds before it moved to the next point. All measurements were taken in a 12 x 12 x 24 inch test section of an Engineering Laboratory Design model 402 wind tunnel similar to the one shown in Figure 3.3 **[ELD Inc]**.

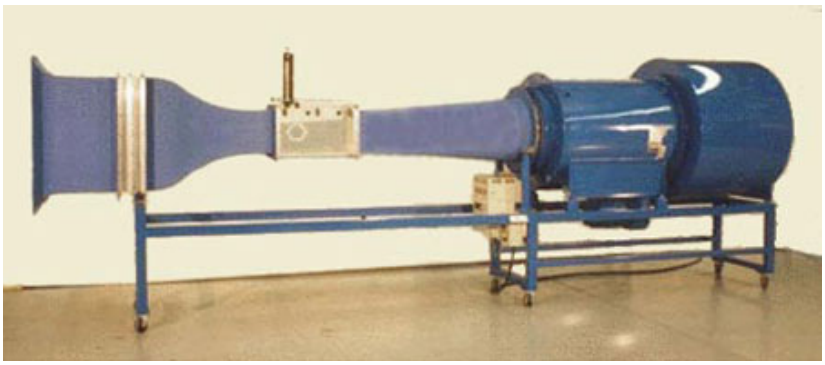

Figure 3.3 Model 402, wind tunnel manufactured by Engineering Laboratory Design **[ELD Inc]**.

An appropriate housing for the actuator was designed to continuously hold the actuator flush to the wind tunnel test section wall, regardless of its external dimensions and height (Figure 3.4). An aluminum plug, with a rectangular pocket wide enough to accommodate two actuators (side by side), was designed to fit the opening in the wind tunnel test section floor. As the thickness of the actuator lid or the height of the cavity was varied for the different parametric studies overall actuator height varied. To keep the actuator flush to the working surface, the difference between the various geometry configurations was easily adjusted by using a wheel (one for each actuator) that was held at the bottom of the plug by a threaded pin. The wheel was designed as a resting bed for the actuators and their position in the plug were regulated by turning the wheels either clockwise or counterclockwise.

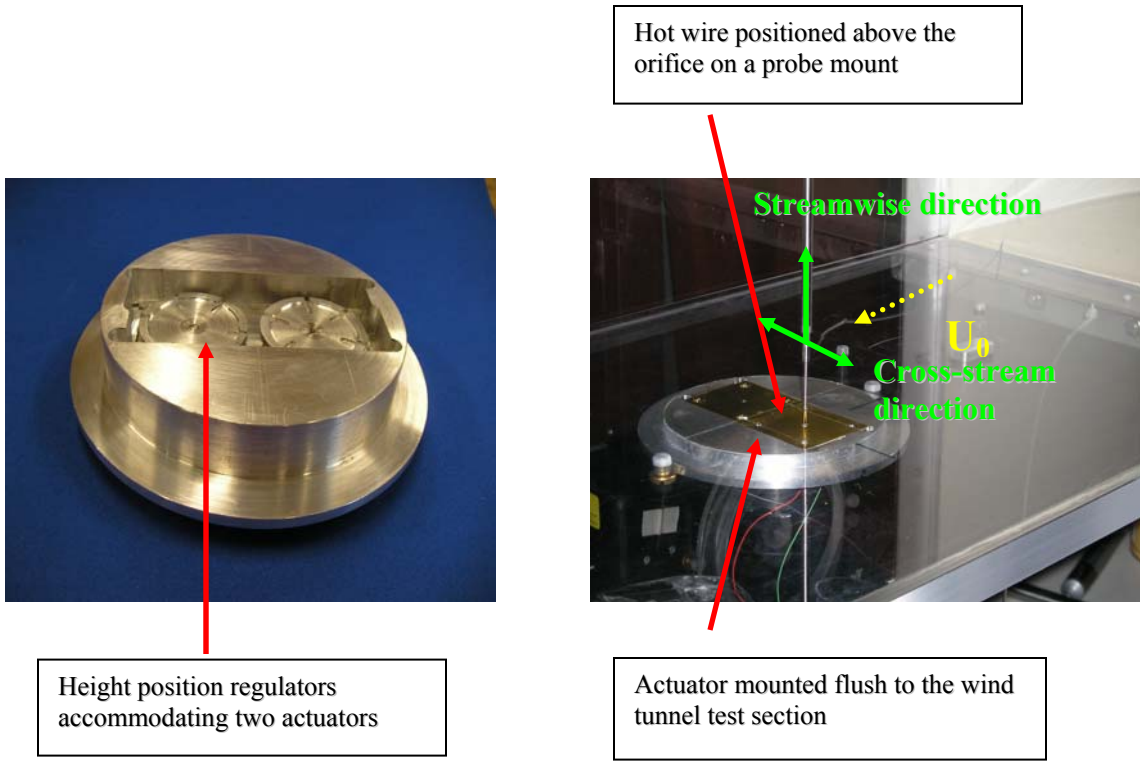

Figure 3.4 Customized aluminum "plug" designed to hold the actuator flush to the wind tunnel test section floor.

The hot wire sensor was positioned to map out the flow field above the orifice using a two axis, computer controlled, motorized traversing mechanism with a 600 x 600 mm travel length. The system was programmed to move the sensor automatically along a predefined path or grid. The grid selected was a 10 x 50 mm region in 1 mm increments in the jet cross stream direction and a 0-50 mm range in the vertical or jet streamwise direction, with a total of 350 measurement points. The origin of the grids was centered 0.5 mm above the center of the orifice. High spatial resolution was applied closer to the orifice exit and a lower spatial resolution in the far field. The flow field was phase

averaged and it presents a time smoothed motion of the synthetic jet over the entire time span of actuation.

3.2.1 Basic principles of constant temperature anemometry (CTA)

Thermal anemometry is a common method used to measure instantaneous fluid velocity. A hot-wire sensor is a solid metallic cylinder made of tungsten or platinum. It usually has a diameter on the order of 10^{-4} mm and is 1 to 2 mm long. Sensors used for measurements in this research were 1.5 mm long. Constant Temperature Anemometer electronic circuitry is designed to keep the resistance in the sensor high and constant. The sensor is electrically heated to maintain a constant temperature that is higher than the ambient temperature. When the sensor is placed in a test fluid, the changes in the velocity of the fluid are reflected through the heat transfer or heat loss from the heated sensor to the surrounding. The heat convected away by the fluid is determined by measuring the current required to maintain a constant wire temperature. Heat lost can then be converted into a fluid velocity in accordance with convective theory **[Bruun1995]**. The hot wire measurement technique used herein rectifies the measured velocity, thus it is not possible to differentiate between the positive and negative velocities. It is sensitive only to the absolute value of the velocity component perpendicular to the wire.

3.2.2 Experimental error analysis

Potential sources of the errors in the velocity measurements can be attributed to uncertainty in hot wire initial position (+/- 0.5 mm in the *x* and *y* direction and +/- 0.25 mm in the *z* direction) and experimental repeatability. Size of the hot wire probe affected some of the measurements as velocity is averaged over the length of the wire. The wire length, for the smallest orifice area configuration tested, slightly exceeded the orifice diameter.

Error bars were used to graphically illustrate the variability in the data. The plot shown in Figure 3.5 was based on averages of three different velocity measurements for the same test configuration. Data were obtained on different days and set-up rearrangements occurred between measurements. Synthetic jet velocity was collected in the cross stream direction and approximately 1 mm above the jet exit plane. Deviation of the data from the mean is expected to be highest in this region due to the presence of high oscillatory flow in the near fields. Particularly high errors would be expected to occur at the orifice edges. It is shown in Figure 3.5 that the ends of the error bars are most far apart in this particular area, the +/- 0.5D region.

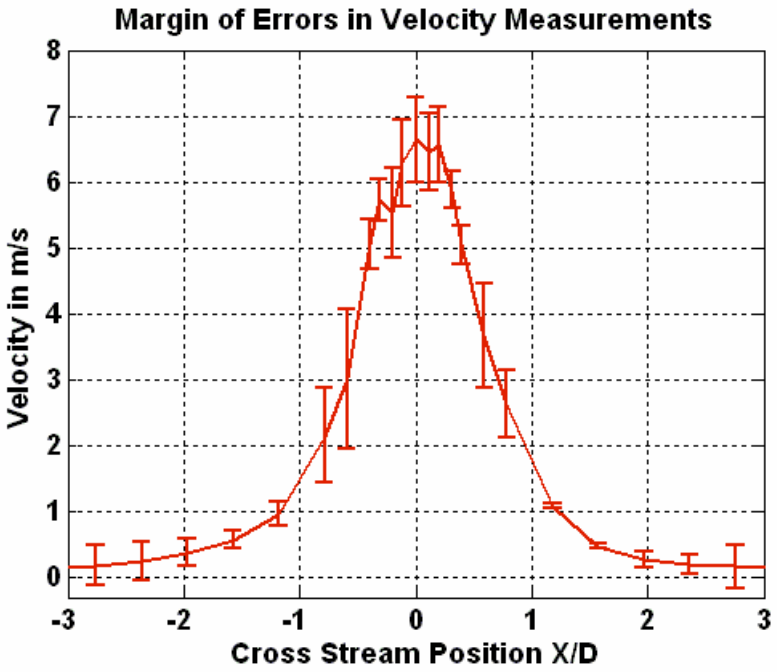

Figure 3.5 Standard deviation in jet velocity measurements.

Higher turbulence levels that occur near the orifice could also have caused errors. Namely, hot wire measurement techniques are restricted to low and moderate intensity flows. Higher than experienced velocity could have been, therefore, indicated by the measurements in the near orifice region where turbulence intensity is higher **[Bruun1995]**.

Figure 3.6 shows a sample of the time history of the jet velocity measured at three different distances above the orifice: immediately above the center of the orifice, and 2 and 15 diameters distances above the orifice. The actuator was operating at 2200 Hz and according to the presented data the jet was oscillating at 2200 Hz as well (at least in the near field region). Peaks in velocity and the oscillatory nature of the jet reduced with

distance from the orifice plane. It was difficult to estimate the effect of the reversed flow. If a sensor capable of measuring reversed effects was placed inside the orifice the probe would have been expected to indicate a velocity of zero as flow direction was changing. However, just a few millimeters above the orifice, the jet was already formed. As seen in Figure 3.6 it gained a velocity that was oscillating around some mean between an average of 17 m/s and an average of 11 m/s. At 15 diameters above the orifice, the unsteadiness of the flow was mitigated and it seemed that the hot wire was placed high enough above the orifice where suction effects were not as considerable.

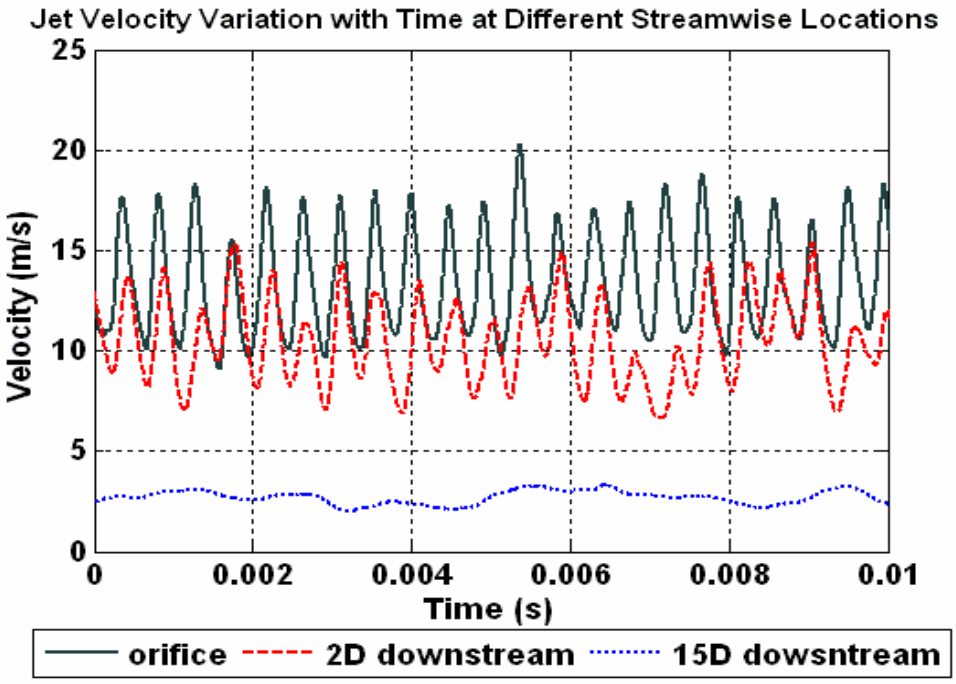

Figure 3.6 Time history of the velocity of the jet measured immediately above the orifice, 2D and 15D above the orifice.

Studies at NASA indicated that hot wire measurements are fairly reliable. They found that hot wire measurements were off in comparison with PIV and LDV measurements but only near the orifice exit. Comparison improved downstream, where the jet oscillatory amplitudes were significantly reduced **[Chen2004]**.

3.3 Effects of the geometry parameters on the jet peak velocities

For best efficiency, combinations of actuator parameters should be adjusted so that the Helmholtz frequency (associated with the cavity and orifice) approaches the THUNDER diaphragm resonant frequency. The Helmholtz resonance frequency is a function of three parameters. Different combinations of these parameters can result in a same frequency; however, they will generally not result in a same mean synthetic jet. Viscous and unsteady effects, mainly associated with the orifice characteristics, also have a significant influence on output velocity. Proper balance between the inertia and viscous forces (Reynolds number) and between unsteady and inertia forces (Strouhal number) has to exist to generate a synthetic jet with the right coherence level and directivity and to be useful for effective flow control **[Wu, Breuer2003]**. Accordingly, geometry properties of the actuators used were tuned to maximize synthetic jet effectiveness. To assist this study, a baseline actuator was chosen whose geometry is specified in Table 3.1 below. This actuator and variations of its baseline dimensions were used in succeeding experimental studies.

Table 3.1 Geometry properties of the baseline synthetic jet actuator used in this work.

Actuator Parameters	Value
Orifice Diameter (D)	1.1 mm
Orifice Depth (L)	1.5 mm
Cavity Diameter (Dc)	32 mm
Cavity Height (H)	6.1 mm
Diaphragm Displacement (Δ)	0.065 mm
Diaphragm Frequency (f)	2200 Hz

3.3.1 Effects of the orifice area on the synthetic jet velocity flow field

Increasing the diameter from 1.1 mm to 7.5 mm (L/D=0.5 to 0.05) increased the Helmholtz frequency from ~480 Hz to ~ 1800 Hz. According to Bernoulli's law for incompressible flows it was natural to expect that the velocity would decrease as the area increased. However, the jet did not behave in this manner (Figure 3.7). The velocity increased as the orifice diameter increased. Such behavior can be explained by considering that the Helmholtz frequency approached the Thunder diaphragm resonant frequency as the orifice diameter increased and by taking into account viscous effects within the orifice. Viscous effect indicator *lambda* (discussed in Section 2.3.1) was less than ten for the first two cases and greater than ten for the last two cases. Accordingly, for the higher orifice diameters the actuator was operating in the Helmholtz resonance regime which was manifested in the actual greater velocity jet. On the other hand, viscous effects and the resultant boundary layer growth dominated the small orifice diameter

cases. In this non-Helmholtz regime the jet was produced by the oscillating diaphragm only and the added velocity due to the Helmholtz resonance was suppressed by viscous effects. In these cases the unsteady boundary layer dominates flows within the orifice and significantly reduces the mass flow through this area. On the other hand, in the extreme case of an even larger area orifice Bernoulli's Law will describe the flow physics causing the centerline velocity to rapidly decay suggesting, that a true jet flow couldn't even be established. Therefore, a balance between these two opposing mechanisms exists for optimum results. Based on this theory, Rathnasingham et al. determined an optimum Stokes number of 15 **[Rathnasingham1996]**.

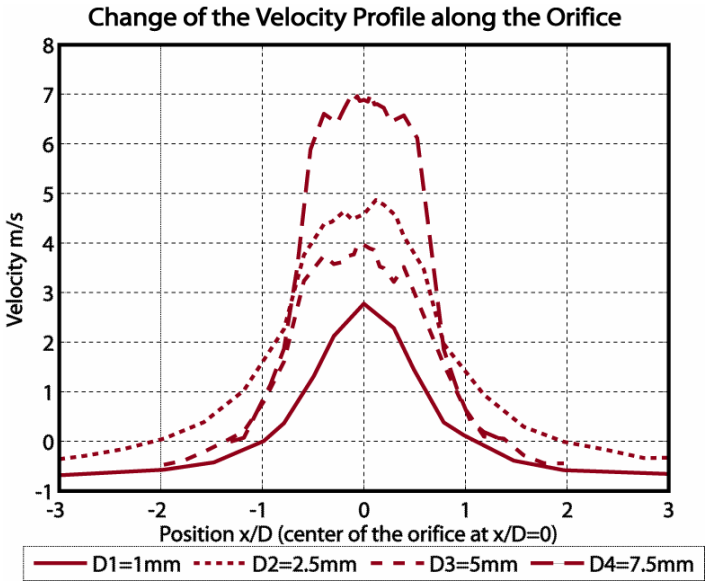

Figure 3.7 Cross stream jet velocity profile 1mm above the jet exit plane for synthetic jet actuators of different orifice areas.

3.3.2 Effects of the orifice length on the synthetic jet velocity flow field

Synthetic jet actuators with varying orifice lengths were assembled. Orifice diameter and cavity height in all cases were constant and equal to 2.5 mm and 2 mm, respectively. Changing the orifice length didn't have much effect on the frequency response curves of acoustic pressure per volt but they had a significant effect on the jet peak velocities. Decreasing the length of the nozzle from 1.5 mm to 0.5 mm, corresponding to decreasing from L/D=0.6 to L/D =0.2, increased the jet output velocity from roughly 8 m/s to almost 20 m/s (Figure 3.8). For all cases the lambda coefficient was within the Helmholtz resonance regime. Orifice losses associated with viscous effects are assumed to explain this difference in output velocities. As the orifice length increased, the pressure gradient decreased while the viscous effects increased, reducing the jet-exit velocity.

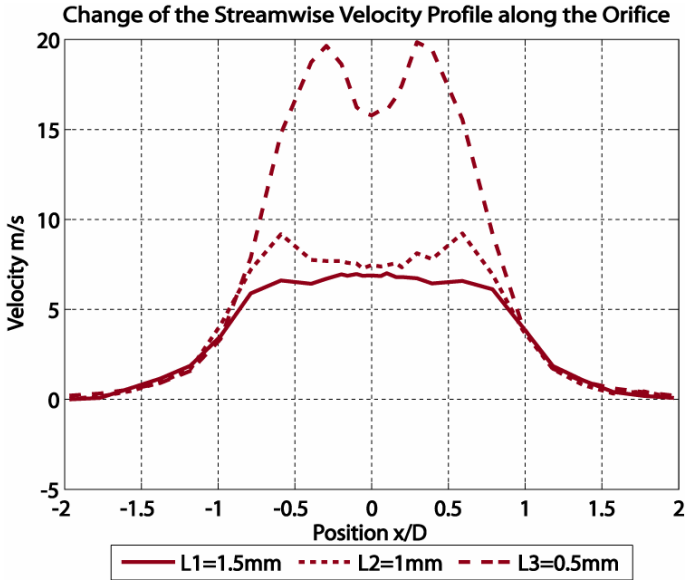

Figure 3.8 Cross stream jet velocity profile 1 mm above the jet exit plane for synthetic jet actuators with a 2.5 mm diameter but different orifice thicknesses.

Another set of tests examined synthetic jet actuator configurations in which the diameter of the orifice was reduced by two. Tested actuators had the same cavity height (2 mm) and the L/D ranged from 0.12 to 0.4. The smaller diameter caused the viscous effects to be significantly more pronounced. Viscous effects didn't influence the peak centerline velocity (Figure 3.9.b) as much as they influenced the jet's penetration length (Figure 3.9.a). Even though the maximum velocity for all three cases was very close (difference of 1-3 m/s between the extreme cases) it appeared that the breakdown of the vortex rings occured further downstream for the case with the smallest L/D. Possible explanations were sought for the aggravated viscous effects. The actuator with the largest L/D ratio was operating in the non-Helmholtz resonance regime (λ=7.12). The lambda for the second case was marginal (λ=10.7) and the case with the lowest L/D ratio was operating well within the Helmholtz resonance regime (λ>>10). Depending on its severity, the viscous layer can occupy large portion of the orifice area reducing mass flow. It is speculated that the energy needed for the jet to maintain its strength may have been lost in this viscous layer. So the smaller the nozzle length for a given nozzle diameter, the less the viscous effects that will interfere with the development of the synthetic jet at such significantly smaller orifice diameters, hence the apparent lack of sensitivity to this parameter in the range of dimensions studied.

a) b)

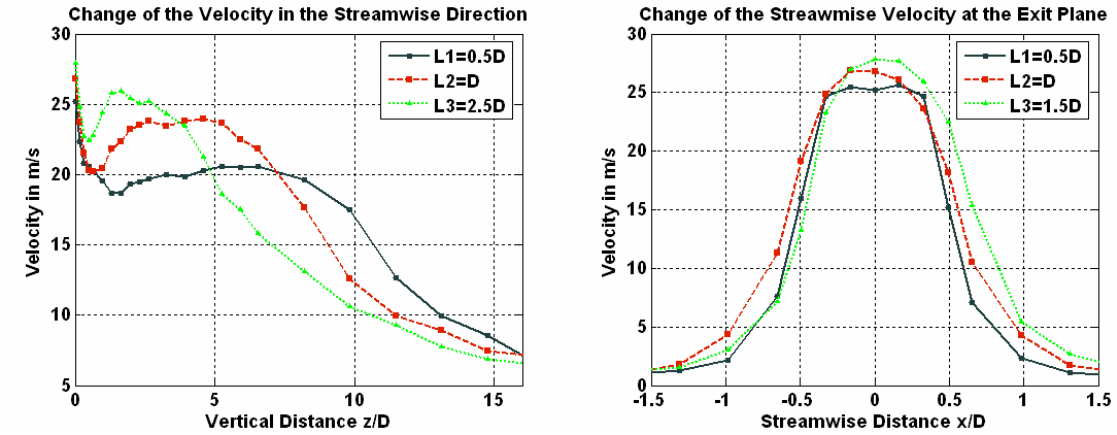

Figure 3.9 Streamwise (a) and crosswise (b) jet velocity distribution of synthetic jet actuators with different orifice thicknesses.

Tang and Zhong observed that for a very thin orifice an accelerated region of flow is present at both ends of the orifice that can induce high pressure gradients and augment the velocity **[Tang, Zhong2005]**. However, the thinnest orifice used in this study did not exhibit any significant velocity changes (Figure 3.9.b). Viscous effects dominated the smaller diameter orifice set of actuators used in this particular test run. It is therefore important to present the orifice length effects with respect to the orifice diameter. This re-emphasizes the need to take into considerations all the non-dimensional parameters and all flow phenomena involved in the spatial and temporal development of these synthesized jets. Results of the velocity maps for these three cases (L/D =0.12, 0.8 and 0.4) along with their turbulence intensities are plotted in Figure 3.10. Figures show that actuators with larger L/D ratios produce jets with lower turbulent intensities.

a)

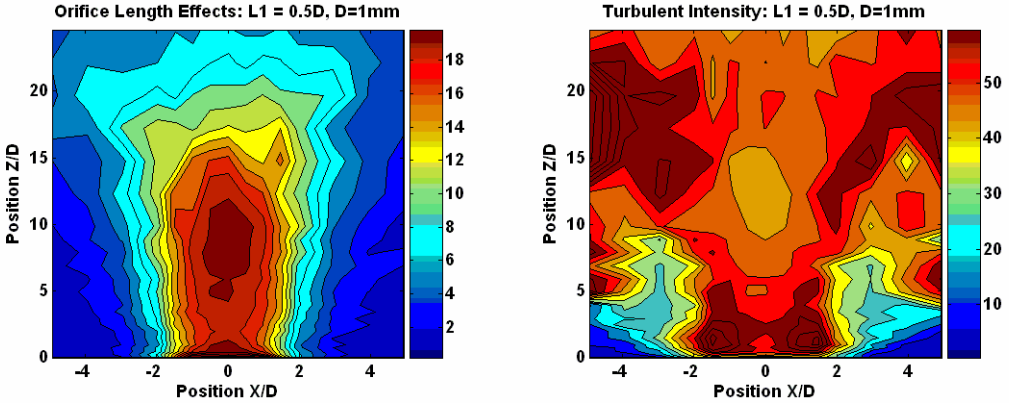

b)

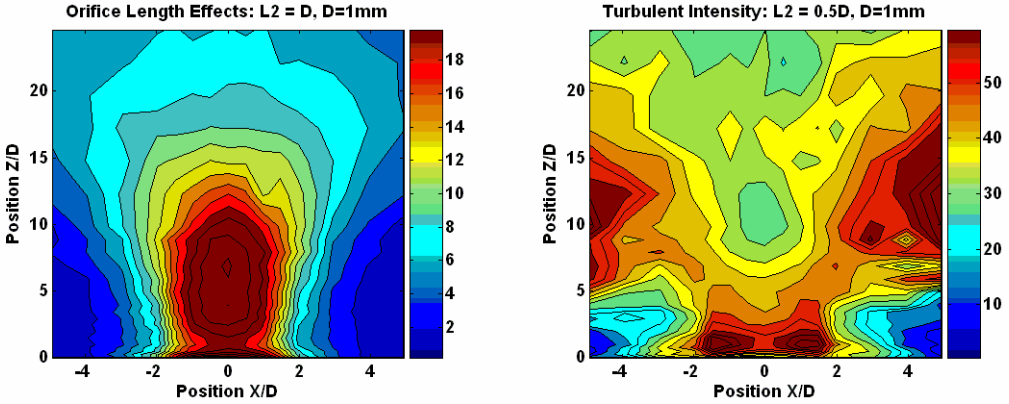

c)

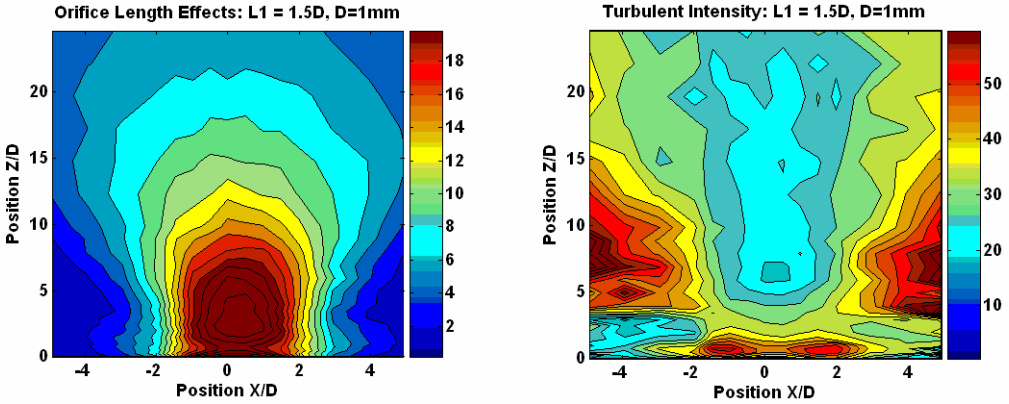

Figure 3.10 Effect of the orifice depth on the velocity contour (left images) and turbulence level intensity (right images). a) L/D=0.4, b) L/D=0.8, c) L/D=0.12.

3.3.3 Effect of the cavity dimensions on the jet velocity

"The cavity is the lever between the diaphragm motion and the jet expulsion", **[Tang, Zhong2005]**. Its behavior is central to the actuator system so the next study included investigation of the sensitivity of synthetic jet development to the size of the internal cavity. The baseline cavity was decreased by two, three, five and six times (H/D = 0.4, 0.8, 1.2, 2 and 2.4). Orifice length for all cases was 0.5 mm and the orifice diameter 7.5 mm (purposely kept large enough not to cause major deterioration in the performance due to the high viscous influence). From the lambda parameter analysis, viscous effects in all of these cases weren't pronounced enough to deteriorate the actuator's output. As the height of the cavity was reduced from 6.1 mm to 3.1 mm to 1.1 mm (H/D=2.4, 1.2 and 0.4) the first resonant frequency of the system increased from ~2000 Hz to ~2300 Hz to ~3200 Hz. The difference between the first two cases, in which two resonant frequencies were closer, didn't significantly affect the velocity of the jet even though the volume of the actuator cavity was reduced by almost two times (Figure 3.11). However, further reduction in the cavity height pushed the Helmholtz acoustic mode beyond the Thunder actuator resonant mode, which was reflected in the small reduction in jet velocity.

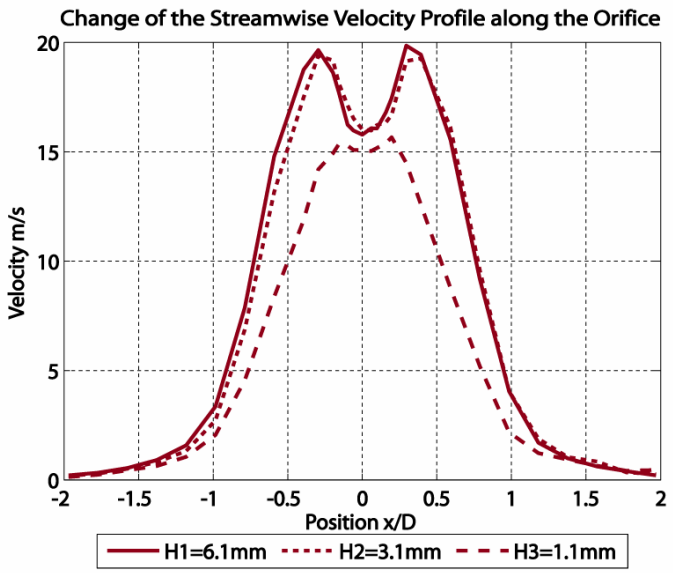

Figure 3.11 Cross wise distribution of the velocity profile of synthetic jets with different cavity heights.

Effects of the cavity height were then partially isolated by freezing the Strouhal and the Reynolds number through manipulation of the diaphragm parameters. Two cases are presented in Figure 3.12 where the cavity heights were changed and the velocity of the jet was tuned to 10 m/s, corresponding to a *Re*= 2000 and *Sr*= 0.6.

a) b)

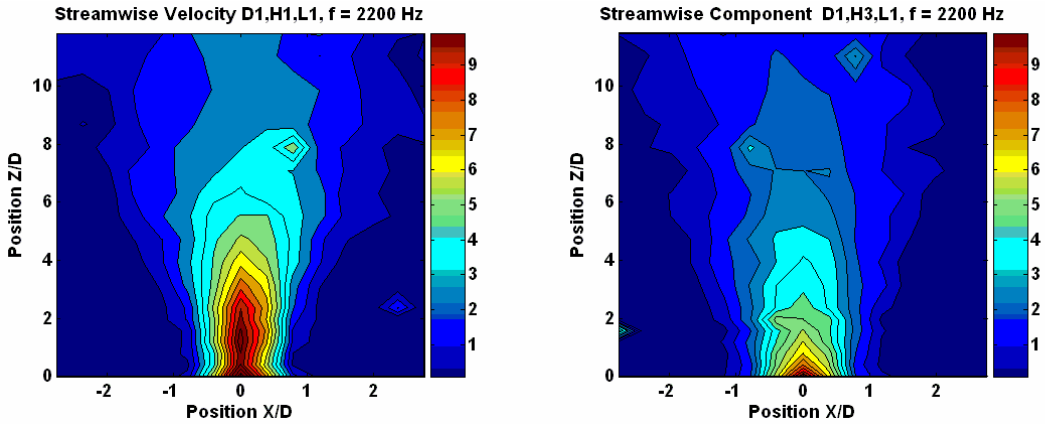

Figure 3.12 Streamwise velocity contour plots for a) H/D=2.4 and b) H/D=0.4

The actuator with a larger cavity height to diameter ratio (H/D=2.4) produced a synthetic jet with more momentum. In this case, the volume of the air in the cavity was larger and it appeared that the oscillating diaphragm had enough energy stored to displace all of the air above it. A larger volume traveling at the same velocity, in comparison to the smaller volume, therefore added more momentum to the flow. This can be observed in Figure 3.12. There exists an optimum ratio of the amplitude of the diaphragm displacement to the cavity height. This is expected to be limited by the maximum displacement of the diaphragm and its blocked force rating. This is another parameter to be considered when choosing specific geometry and flow parameters.

3.3.4 Strouhal number (Sr) effects

To study the influence of Strouhal and Reynolds numbers on jet formation and evolution, excitation parameters were varied to change the diaphragm frequency/displacement and force these non-dimensional parameters to fall in a particular range. In this section actuators were configured and excited to obtain a different Strouhal number but a constant Reynolds number for the flow exiting the orifice according to equations $Sr = \frac{fD}{U}$ and $\mathrm{Re} = \frac{\overline{U}_0 D}{\nu}$.

Figure 3.13 shows four different velocity field contours. They correspond to synthetic jets with Reynolds number of 2000 and the Strouhal number increasing from 0.25 to 3.5. For the Strouhal number of 0.25 (Figure 3.13.a), an actuator with L/D =0.6 was operated at an actuation frequency of 1000 Hz. Figure 3.13.b shows the synthetic jet flow field of an actuator L/D =0.6 operating at 2200 Hz and Strouhal number of 0.5. The last two figures represent the measured velocity fields of synthetic jets developed with an L/D =0.2 actuator operating at 1740 Hz and 1500 Hz forcing the Strouhal number to be 1.76 and 3.5 respectively. These figures show that the jet formation weakened and was limited to the near orifice region as the Strouhal number increased. At the Strouhal number of 1.76 (Figure 3.13.c), hints of the synthetic jet were still observed but as *Sr* was increased even further (Figure 3.13.d) it appeared that unsteady effects overpowered the inertia effects.

Under conditions in which the Strouhal numbers are higher than ~2 the actuator barely perturbed the flow. It appears that for Strouhal numbers larger than ~2 a vortex ring will not have enough induced velocity to fully escape the orifice region. As a result it gets pulled back into the cavity before a jet had an opportunity to form. These experimental data suggested that under conditions with Strouhal number greater than 2 the appearance of the directed jet is not likely to occur. This is because Strouhal numbers reflect the ratio of oscillatory fluid dynamic forces to mean inertial fluid dynamic forces. This range of Strouhal numbers imply strong unsteadiness and that the flow is not likely to move downstream, while numbers of less than one indicate much higher mean flow inertia.

The relationship between the Strouhal number and the non-dimensional fluid stroke length L was mentioned in the *Introduction* chapter. The inverse of the non-dimensional stroke length was equated to the Strouhal number. The existence of an inversely proportional change in the normalized stroke length as the Strouhal number is varied is also evident in this experimental data. As seen in the contour plots just discussed, for a high Strouhal number case a much smaller amount of fluid is ejected. Low Strouhal number cases present the opposite physical effect, in which the long stroke length causes large amounts of fluid to be ejected, so the growth of the jet progressed further downstream.

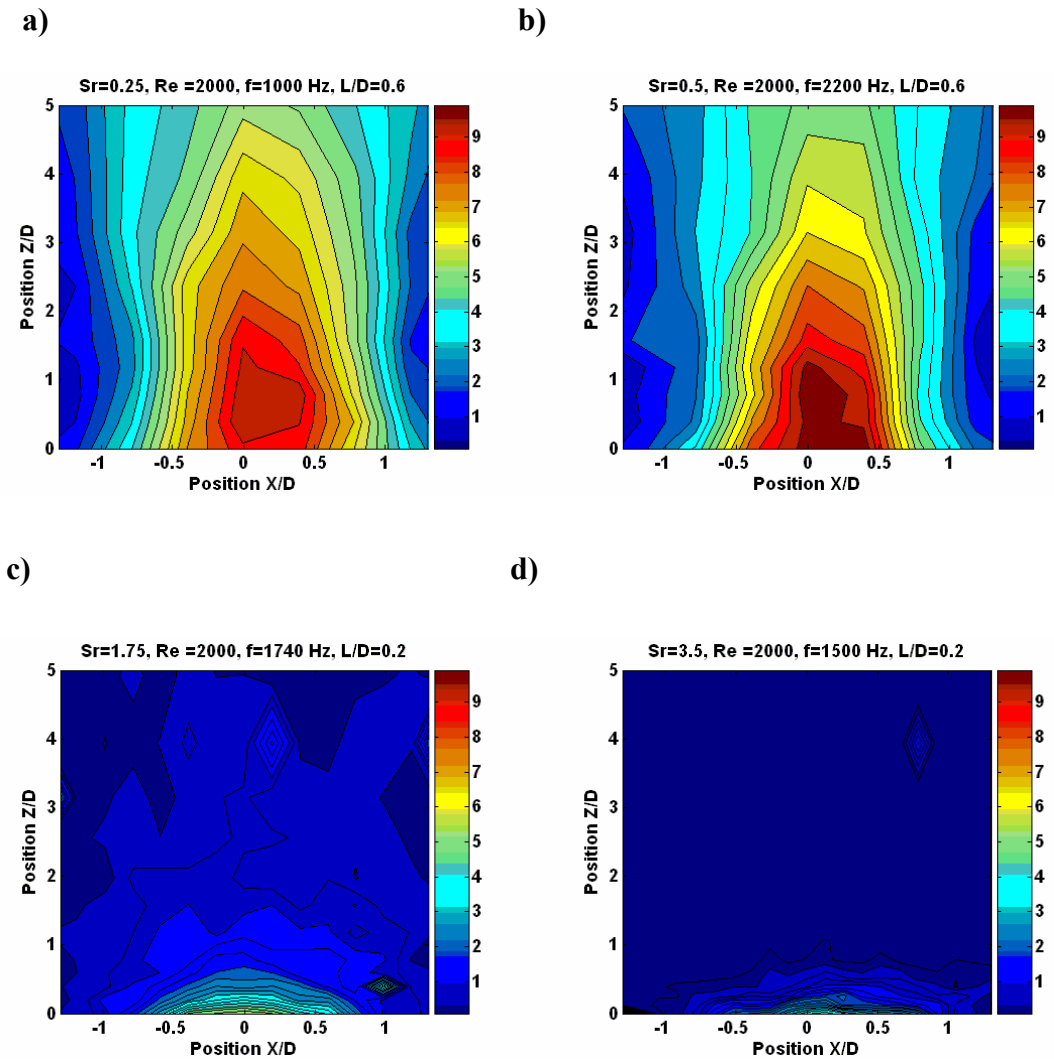

Figure 3.13 Effect of the Strouhal number on jet formation. a) Sr=0.25, b) Sr = 0.5 c) Sr=1.75. d) Sr=3.5.

To conclude, a comparison of the shape of the velocity profile at the jet exit plane for different *Sr* is presented in Figure 3.14. The jet velocity at the orifice increased with decreasing Strouhal number, reaching a maximum at *Sr*=0.5 at which time further

increase in the Strouhal number caused a slight decrease in velocity. The trend of exhibiting a parabolic velocity profile was similar for all of these cases. We will see in the next section this is not the case for different Reynolds number jets.

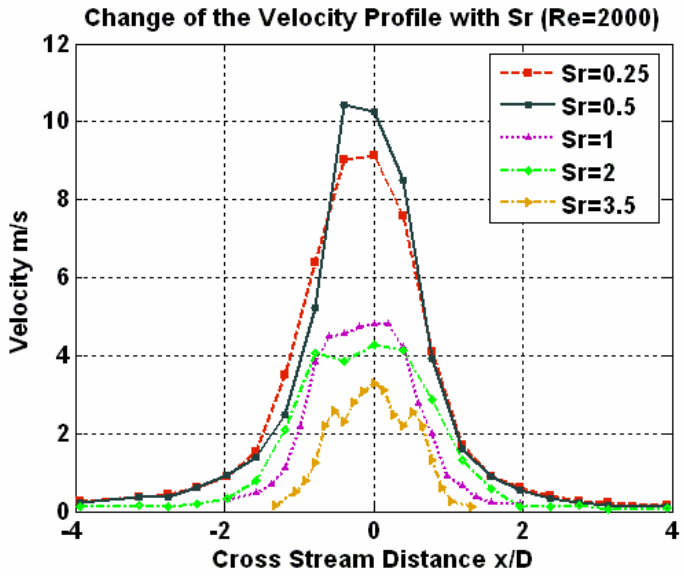

Figure 3.14 Comparison of cross wise variation in the streamwise velocity distribution of synthetic jets operating at the same Reynolds number but different Strouhal numbers.

3.3.5 Reynolds number (Re) effects

Reynolds number dependence was examined by maintaining the Strouhal number constant (approximately 0.9) while increasing the Reynolds number from ~1000 to ~10000. Effects of Reynolds number variation on the synthetic jet characteristics were plotted in terms of the streamwise jet velocity at 1 mm above the jet exit plane for four different cases (Figure 3.15).

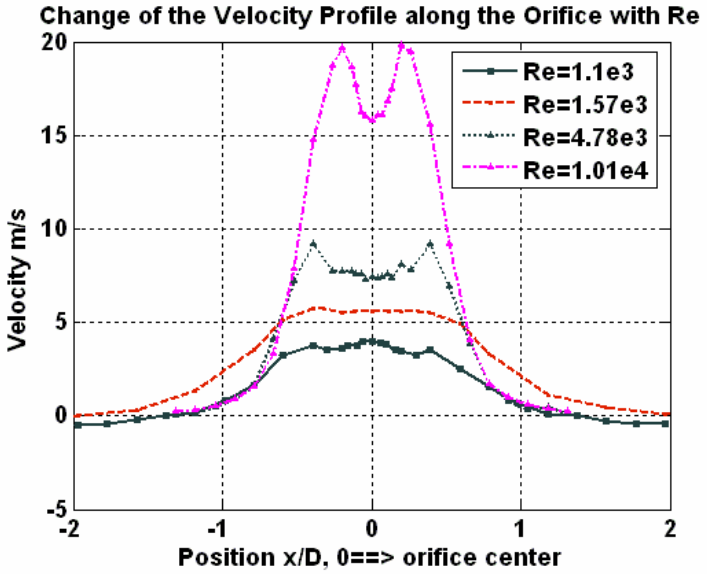

Figure 3.15 Plot of the streamwise velocity distribution for synthetic jets of various Reynolds numbers.

As expected, the mean vertical velocity component increased with the Reynolds number. In general, synthetic jets with higher Reynolds number have more momentum which helps the synthetic jet overcome adverse pressure gradient caused by the suction part of the oscillation cycles. If the Reynolds number is too low there will be no transition from the reversible flow to a synthetic jet. The suction part of the oscillating cycle is therefore more pronounced at low Reynolds number so synthetic jets with higher Reynolds number generally have a higher range of operational use.

Velocity profiles across the orifice changed as well. At higher Reynolds number, the jet velocity profile lost the flattened parabola profile. The location of the velocity

peak, located at the center of the orifice at lower Reynolds numbers, split and shifted towards the orifice edges as the Reynolds number increased. The boundary layer formed inside the orifice grows proportionally to: $\sqrt{\frac{\nu}{\omega}}$. Two peaks occurring at higher Reynolds number are the result of the thinner boundary layer in the orifice and are common to oscillatory flows **[Lee, Goldstein2002]**.

3.3.6 Coherent vs. incoherent structures

A synthetic jet is generally characterized by large scale coherent motions known as vortex pairs. However, under certain circumstances these coherent structures may disintegrate. For example, increasing the jet velocity causes the spacing between the adjacent vortex rings to reduce. This increases the mutual interaction of the vortex rings which (depending on the value of the Strouhal and the Reynolds numbers) could lead to the expulsion of a synthetic jet with incoherent structures **[Shuster2004]**. An example of incoherent structures being ejected can be seen in Figure 3.16.a, showing the velocity flow field and vorticity contours for a case with a Strouhal number of ~1.7 and a Reynolds number of ~6000. Once the Strouhal number was reduced down to ~0.6, as contoured in Figure 3.16.b, the coherence of the ejected structure increased. For clarity of presentation purposes, the coherent structure was plotted in a frame larger than the one of the incoherent structures. Range of the *X* and *Z* axis, equivalent to Figure 3.16.a, is outlined with the dotted border in Figure 3.16.b.

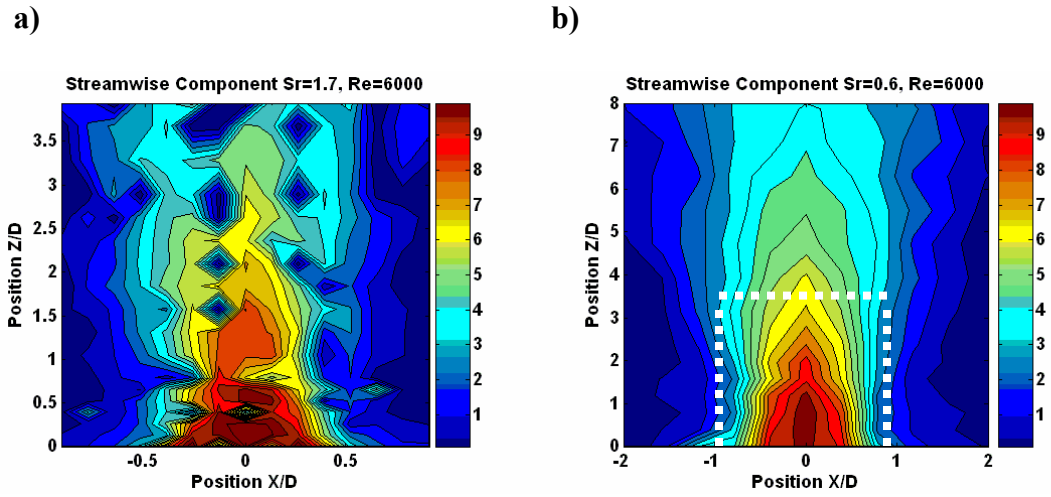

Figure 3.16 Example of a) incoherent structure being ejected from the synthetic jet actuator (Re=6000, Sr=1.7) and b) coherent structure being ejected from the synthetic jet actuator (Re=6000, Sr=0.6).

These two different sets of test data (which were collected at relatively high Reynolds number but different Strouhal numbers) suggested that a high Strouhal number causes an undesirable effect on the jet flow structure. This occurrence implies that of these two non-dimensional parameters, the Strouhal number is the one responsible for disturbing the vortex rings. Given the results observed above, it appears that a synthetic jet with a higher Reynolds number and a lower Strouhal number would minimize the viscous losses in the orifice and produce jets with a higher momentum flux. Overall, the non-dimensional fluid stroke length L or the Strouhal number, in conjunction with the Reynolds number, can be used to predict the likelihood of formation and the nature of evolution of synthetic jets.

3.4 Study of the velocity spectra

Additional insight into the evolution of the synthetic jet may be gained from observing the frequency content of the streamwise velocity. Power spectra were obtained with a hot wire anemometer and are presented in Figure 3.17 for two different synthetic jets: one oscillating at 1000 Hz (Figure 3.16.a) and the other at 2200 Hz (Figure 3.16.b).

a) **b)**

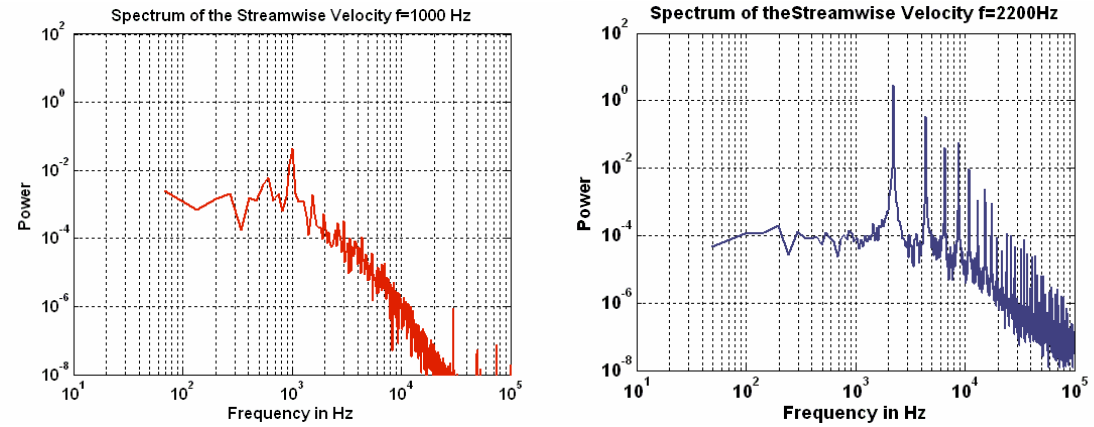

Figure 3.17 Velocity spectra of jets developed at excitation frequencies of a) 1000 Hz and b) 2200 Hz.

Flow introduced with actuator activation is visible in both cases through distinct peaks present at the actuation frequency. These are followed by peaks of decreasing amplitude at higher harmonic frequencies. This is an expected trend and is typical of velocity spectra of turbulent shear flows. Energy was falling from the primary large flow fields that form a jet, down to smaller scales at which dissipation occurs **[Smith, Glezer1997]**. At frequencies below the actuation frequency flat response characteristics are shown.

The velocity spectrum at the exit was then compared to the velocity spectrum at different stations above the orifice in Figure 3.18. At distances further away from the exit plane the higher harmonics decreased suggesting loss of coherence of the vortical structures. At some point even further away from the orifice these spectral peaks disappeared and a slight increase in lower frequency content of the flow was observed. The oscillating membrane no longer affected the flow on this region and the spectra were showing up as if due to the presence of just a steady jet.

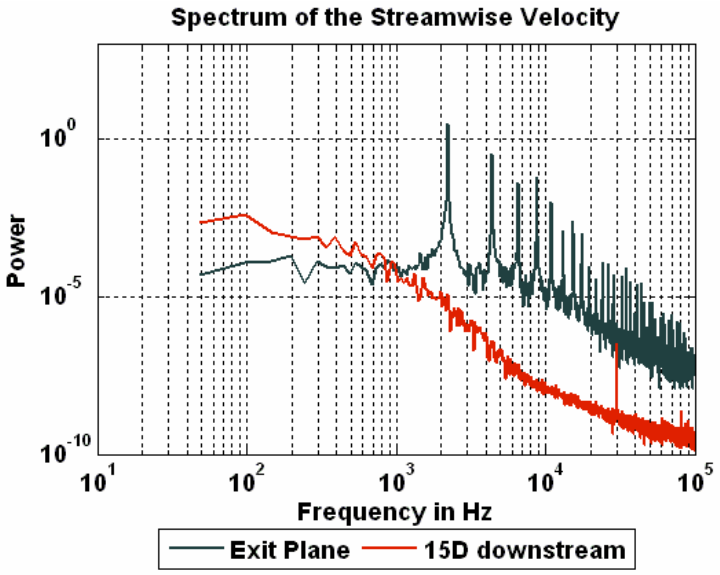

Figure 3.18 Comparison of the power spectra at the orifice exit and further downstream.

3.5 Conclusion

This chapter concludes the discussion on synthetic jet actuator mechanisms as individual units acting in quiet (zero cross flow) external conditions. The first chapter was an introduction to the terms and definitions as well as the summary of the potential synthetic jet actuator applications. Second chapter focused on the frequency response and fluid structural coupling powers of such a device. The objective of this chapter was to observe detailed flow properties of the synthetic jet in a region extending above the jet orifice plane. We first observed the importance of understanding the capabilities of the actuator driver. The stronger the driver, the less impact the cavity domain will have on its performance. Once the maximum volume displaced by the given diaphragm has been established another crucial aspect in the synthetic jet development to be considered was the actuator orifice. Very complex flow phenomena are direct consequences of the viscous effects present in this region. Tied to this parameter was the actuation frequency responsible for oscillation and unsteadiness effects. Based on the orifice diameter, two primary non-dimensional parameters have been defined and studied: the dimensionless stroke length or the Strouhal number and the Reynolds number. For a given Reynolds number we observed a distinct formation of a directed jet for a range of Strouhal numbers below approximately two. For Strouhal numbers larger than two, the ejected fluid was significantly influenced by the unsteadiness effects. For high Reynolds numbers (~6000) and relatively higher Strouhal numbers (~2) occurrence of very incoherent structures was observed.

This chapter offers a spectrum of observations on the effects of the structural and geometry parameters on the flow characteristics of small scale (~30 mm diameter) synthetic jets. There was a suggestion in the literature that the ratio of the cavity diameter to the orifice diameter needs to be at least 50 before the viscous effects start dominating the synthetic jet flow **[Tang, Zhong2005]**. In the case of our particular actuator scale, with the cavity diameter held constant at all times and equal to approximately 32 mm, this conclusion would imply that one could have an orifice diameter of almost half a millimeter before the viscosity comes into effect. The velocity contours in this chapter demonstrate that their observation is not applicable to all scales.

Attempts to classify different non-dimensional parameters into certain "inviscid-viscous" or "incompressible-compressible" categories are numerous and have overwhelmed the synthetic jet technology literature. The work presented here hasn't provided the clear and practical answers to all the issues raised, nor did it result with the needed "manual" for the design of the optimum actuator. However, most issues that need to be considered when designing a new synthetic jet actuator have been highlighted. Discussion and results of the experimental measurements of these, smaller scale high frequency synthetic jets contributed to the field of synthetic jet technology.

Chapter 4

Characterization of Synthetic Jet Actuators in Cross Flow

4.1 Introduction

All synthetic jet actuator applications imply a manipulation of some type of external flow. In order to improve the understanding of synthetic jet actuators and advance their use for aerodynamic performance enhancement it is imperative to understand the fundamentals behind synthetic jet-cross flow interactions.

In the current investigation experiments were carried out to capture flow field signatures of high frequency synthetic jets acting at 90^0 to ambient flows developed over an infinite plate at zero angle of attack. Synthetic jet actuators were placed in several different cross flows: 3, 6, 10, 15 and 20 m/s, with boundary layer thicknesses ranging from 2.5 to 5 mm. Synthetic jet velocities were adjusted from 10 to 25 m/s and orifice diameters of the actuators varied from 1 to 7.5 mm. The influence of a combination of these parameters (jet-to-free stream velocity ratios, orifice diameter-to-boundary layer thickness ratio) and consequent direct and indirect flow phenomena that occurred (jet

trajectory variations, velocity decay, shape change of the jet cross sectional area) were observed and recorded with constant temperature anemometry techniques. The objective was to determine jet characteristics which are needed to produce the right amount of control authority to have a significant impact on such boundary layer flows. The content of this chapter also examines the design space in which synthetic jets might cause regions of recirculating flow to occur.

4.2 Non–dimensional parameters

The jet momentum coefficient (C_μ) and non-dimensional frequency (F^+) are parameters often used when discussing control authority of synthetic jets in various external flows. The influence of synthetic jets on a non-zero cross flow depends on the ratio of "strengths" of the synthetic flow and the external flow field. A non-dimensional term that will be used in this text to quantify the actuator performance in the presence of the moving ambient flow (more convenient for studying flows over flat plates and also often used to compare the performance of synthetic jets to the equivalent continuous jets) is the velocity ratio (R) defined as:

$$R \equiv \left(\frac{\rho_j U_j^2}{\rho \overline{U}^2} \right)^{\frac{1}{2}} \tag{4.1}$$

where U_j is the velocity of the jet, U the freestream velocity and ρ_j and ρ are the jet and crossflow densities, respectively **[Mungal, Smith1998]**.

4.3 Synthetic jets in cross flow state-of-the art

Basic research on synthetic jet-cross flow interactions has not been as detailed and extensive as research on isolated synthetic jet actuators exhausting into quiet flow conditions. Publications are limited to a few investigations that mainly focused on the influence of the orifice shape and orientation on the resulting flow fields.

Milanovic et al. studied synthetic jet actuators with the orifice diameter and thickness of 20 mm and 25.4 mm, operating at 24 Hz and producing a 6 m/s synthetic jet. Straight, tapered, pitched, yawed and clustered orifices were investigated **[Milanovic2004]**. Schaeffler et al. from NASA used PIV to examine and compare the behavior of actuators with circular and elliptical orifices in turbulent boundary layers. They observed that the amount of penetration into the boundary layer is reduced at higher free stream velocities **[Schaeffler2003]**. Shuster studied actuators with straight and inclined circular orifices operating at a Reynolds number of 250 and Strouhal numbers of 1 and 0.5. The inclined orifice demonstrated more control authority at even higher Strouhal numbers. Possible virtual dynamic shaping capability was observed as well: *"In the mean there is a rapid thickening of the boundary layer at the orifice suggesting an apparent change in the surface shape"*, **[Shuster2005]**. Mittal et al. have numerically studied the interaction of two-dimensional synthetic jets with a flat plate boundary layer. They observed the existence of recirculation zones on the surface of a flat plate for high velocity jets. The results of these numerical solutions are shown in Figure 4.1 **[Mittal2001]**. They defined the jet to free stream velocity ratio of approximately three as

the threshold for onset of the actuator virtual shaping capabilities. These findings, however, were not validated with experimental data.

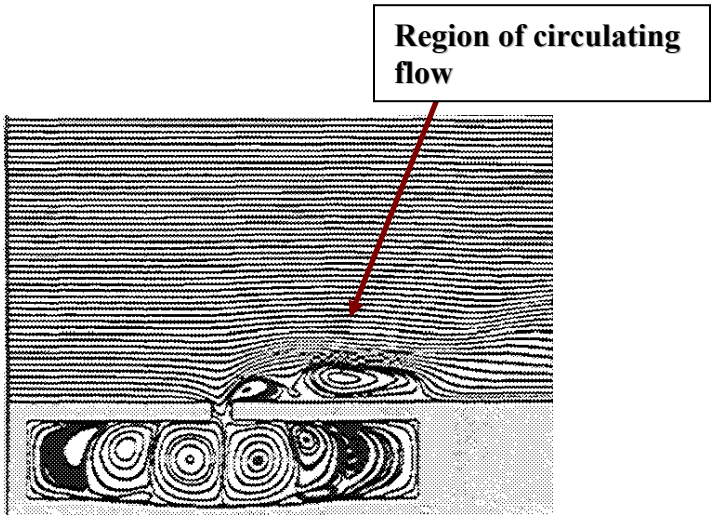

Figure 4.1 Numerically produced region of recirculating flow due to the synthetic jet-cross flow interaction **[Mittal2001]**

4.4 Synthetic jet in cross flow characteristics

A jet issuing from a flat plate into a cross flow causes an intense mixing between the two streams of fluid creating a complex flow field structure. Depending on its strength, the synthetic jet profile gets deflected into a specific trajectory by the existing horizontal forces, experiencing continuous cross section deformation and eventually completely transforming into the direction of cross flow. Similarly, the presence of the jet causes changes in the cross flow streamlines as the jet both deflects and entrains the external fluid. In an attempt to adjust to the apparent obstruction due to the presence of the synthetic jet, cross flows follow the jet boundary, separates towards the jet exit trailing

edge creating a region of low energy flow downstream of the jet orifice, also known as the wake.

An example of measured flow contours of first the boundary layer over a flat plate, then the isolated synthetic jet acting in quiet conditions and finally the interaction of the two flows are shown in Figure 4.2.a-c. The rest of this chapter discusses the jet-in-cross flow structures through experimental data to advance the comprehension of this intricate mixing flow.

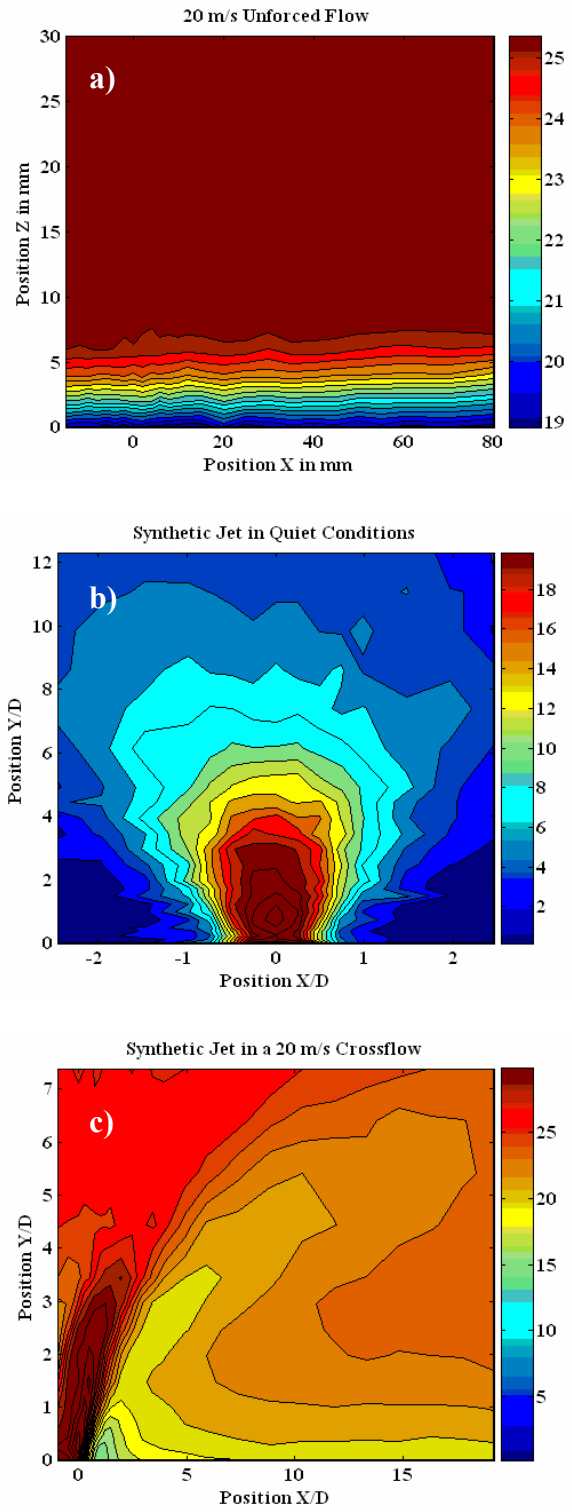

Figure 4.2 The difference in the two types of flow when investigated separately and when they mutually interact. a) 20 m/s no actuation b) synthetic jet at 0 m/s cross flow, c) synthetic jet in 20 m/s cross flow.

4.5 Contribution to the Experimental Analysis of Synthetic Jets in Cross Flow

Since synthetic jet is formed entirely from the working flow in which it is embedded its dynamics will be influenced by the given external conditions. Structural and geometry effects on synthetic jet formation and evolution in a quiet ambient environment were studied in Chapter 3. This study was continued herein by collecting constant temperature anemometer data to compare the resemblance in trends when same synthetic jet actuator configurations where subjected to various cross flow conditions. The discussion on this data can be found in Appendix A. This chapter will concentrate on experimental data of the jet-cross flow mixing regions as a function of various velocity ratios and jet orifice diameters. A dual cross wire sensor for measuring the *u* and *w* velocity components was used for mapping the flow.

4.5.1 Velocity Ratio Effects

Several different jet-to-free stream velocity ratio cases were tested. All actuators were excited at the same frequency but excitation voltages were varied to establish the desired synthetic jet mean velocities. The wind tunnel speed was changed from 3 to 20 m/s and with the synthetic jet velocities tuned between 5 and 30 m/s a total of six velocity ratios was tested. Velocity ratios studied ranged from 0.25 to 6 as given in Table 4.1. Each jet exit velocity was based on the measurements in quiet conditions, before being subjected to external cross flow.

Table 4.1 Velocity Ratios Investigated.

Velocity Ratio	Synthetic Jet	Cross Flow
0.25	5 m/s	20 m/s
0.5	10 m/s	20 m/s
1.5	30 m/s	20 m/s
2.7	27 m/s	10 m/s
3.6	22 m/s	6 m/s
6	18 m/s	3 m/s

4.5.1.1 Low Velocity Ratios (*R<1*)

Depending on the self induced velocity and strength of the vortex ring formed (during the actuator cycle) it was expected that the synthetic jet would block the boundary layer, causing the cross flow to be diverted over and around the jet. However, at low velocity ratios, i.e. ratios less than 1, cross flow exerted sufficient pressures on the orifice that did this not occur. Figures 4.3.a-c show that there is no strong vertical jet momentum visible and the vortices generated during discharge did not have enough momentum to escape the near wall region. It appears that the jet is quickly deflected, losing its structure to the dominating influence of the external cross flow. The influence of the synthetic jet remained completely buried inside the boundary layer, just barely perturbing and shuffling the near-wall flow. The synthetic jet was swept along with the cross flow,

introducing turbulence to the flow and inducing just a slight lift up of the oncoming flow immediately above and slightly downstream from the orifice, effectively causing a minor thickening of the boundary layer. As the jet-to-free stream velocity ratio increased so did the synthetic jet ability to push the boundary layer away from the wall. The amount of displacement of these streamlines could arguably be used as a measure of control authority of the actuator.

Vorticity plots in the right column of Figure 4.3.a-c shows hints of vortex-like flow structures developing in the streamwise direction. Clear vortex dipole structure normally seen with the inert external flow (Figure 1.2, 1.5 or Figure 1.9) did not appear in these images. It seems that the freestream boundary layer turned the clear vortex dipole structures into a shear layer.

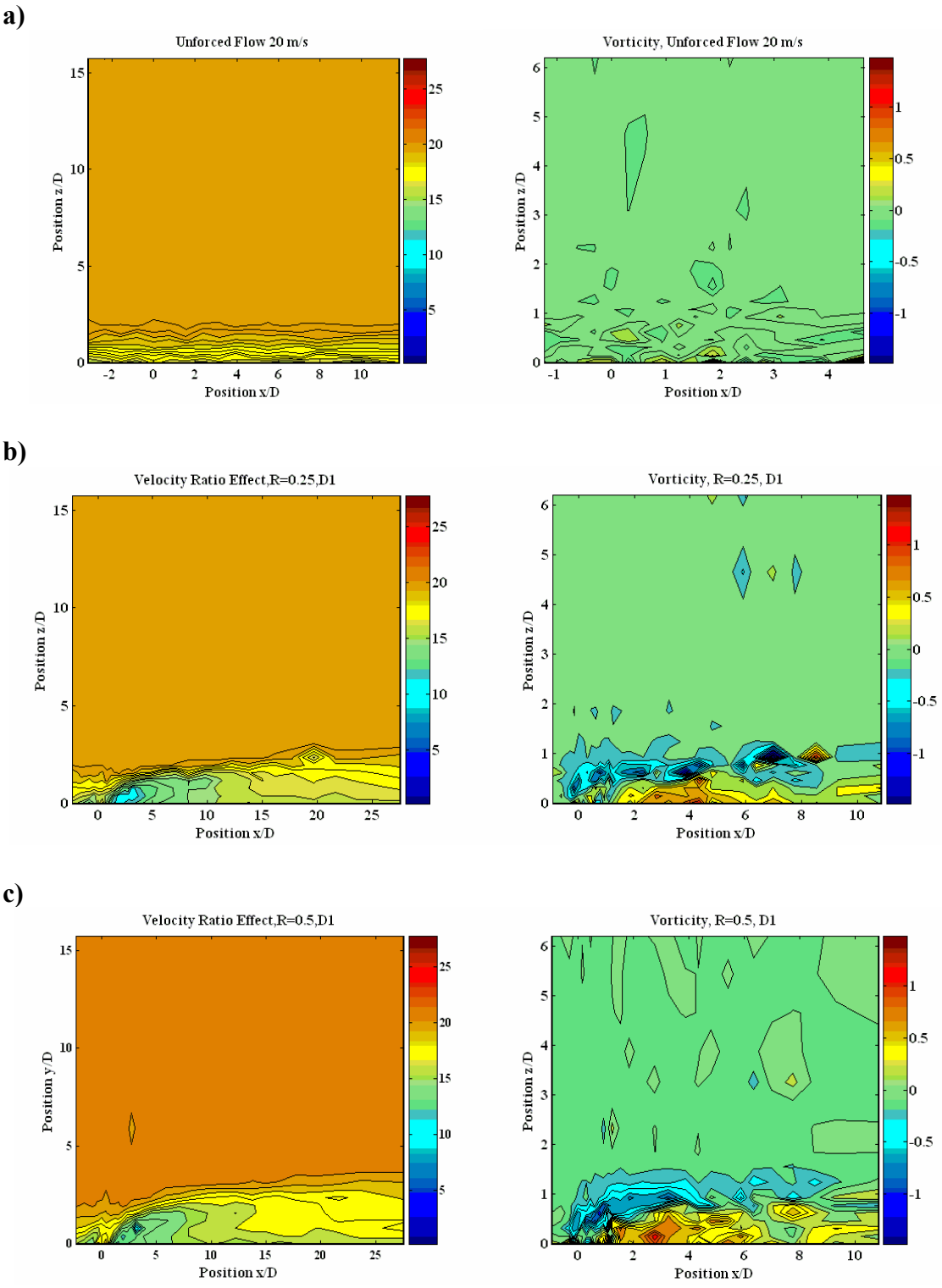

Figure 4.3 Velocity ratio significance on the flow field velocity signature (first row) and the vorticity signature (second row). a) no control, b) R=0.25, c) R=0.5.

4.5.1.2 High Velocity Ratios (*R>1*)

At higher velocity ratios, i.e. R>1, velocity contour plots depict decidedly different flow patterns. In these cases the jet is stronger and can shift the external flow momentum. The synthetic jet perforates much deeper into the cross flow and well beyond the edge of the boundary layer. The forming of a vortex ring appears to block the boundary layer flow entirely, slowing it down, causing the external streamlines to partially divert around and to partially become entrained in the forming vortex rings.

Four examples were tested in which the velocity ratio was increased from 1 to 6. Synthetic jet is obviously strongest at its source where it has the highest momentum. As such it is least affected in the near field region and it meets the external cross flow almost perpendicularly. A minimum jet-to-free stream velocity ratio of one was observed as the threshold for the jet to completely escape the boundary layer region. As the velocity ratio was further increased so did the slope of the synthetic jet trajectory, an indication of a much stronger jet (Figure 4.4). At a velocity ratio of six, the synthetic jet was standing in the cross flow almost entirely vertically, rising out of the cross flow resembling a fluid pole. In all cases, a region of separated, low pressure flow was created downstream of the jet orifice as a result of the actuator effect.

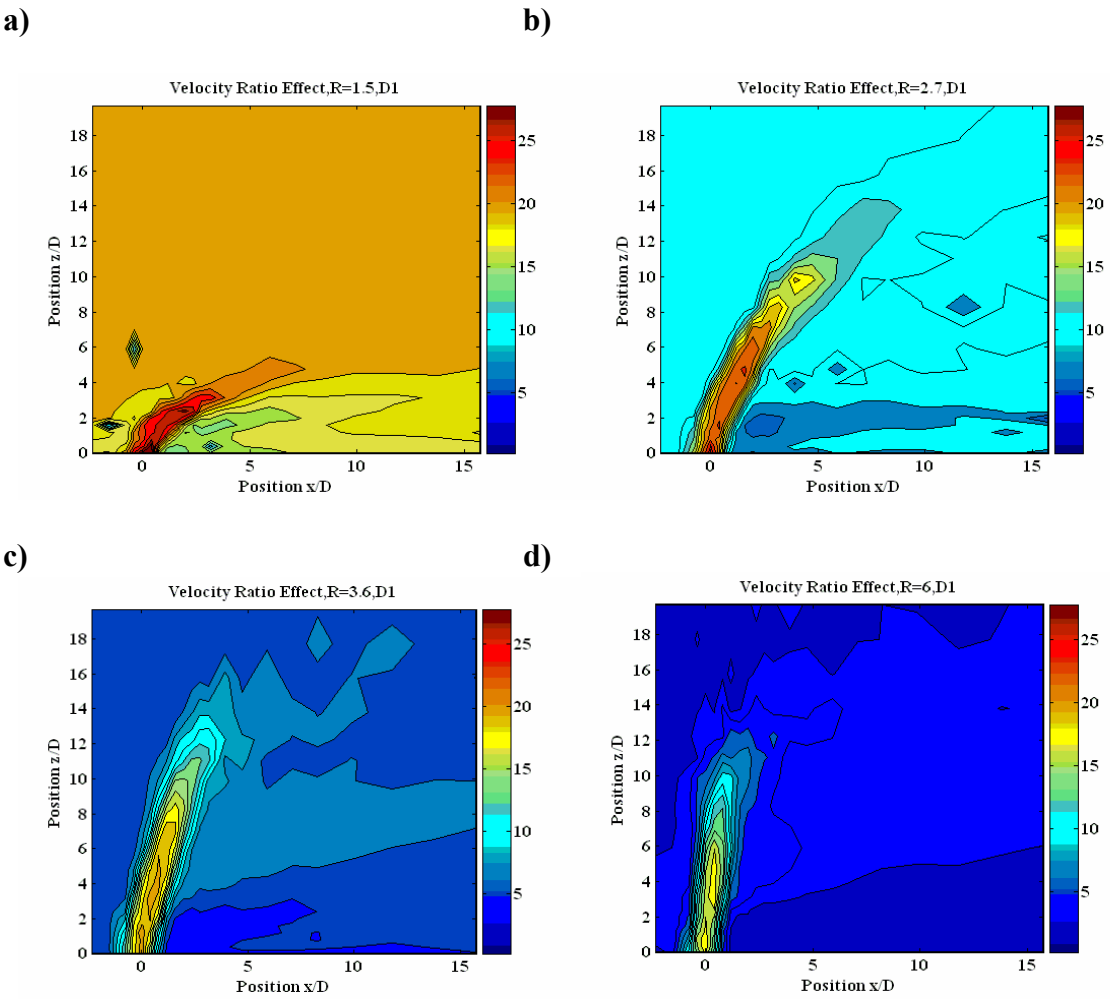

Figure 4.4 Jet to free stream velocity ratio effect on the flow field signature in the region above the orifice and further downstream. a) R =1, b) R =2.7, c) R=3.6, d) R=6.

The flow field contours presented are all phase averaged, mean velocity data. Due to the limitations of our experimental tools we were not able to observe the time periodic formation and development of the vortices in the boundary layer during synthetic jet operation. The experiments performed provide a qualitative assessment of the global flow

field effects. They provide the potential influence of a synthetic jet of this intensity and actuated at this frequency range on a fully attached flow of known boundary layers.

4.5.2 Boundary layer thickness to orifice diameter ratio

The ratio of the orifice diameter to the thickness of the boundary layer is an interesting non-dimensional factor that influences the global jet-in-cross-flow flow field topology. The importance of this parameter on flows has barely been mentioned in the literature. Thinner boundary layers imply a flow with more momentum. They impose a stronger impact on the oncoming jet causing it to deflect earlier so a non-dimensional parameter taking this into consideration should be mentioned when discussing scaling and authority of synthetic jets.

The dispersion height of a synthetic jet in cross flow increases with increasing stroke length L/D or decreasing the Strouhal number, as discussed in Chapter 3. This was also observed in the cross flow velocity contour plots presented in Figure 4.5 for Strouhal number of 0.2 to 0.9. Isolated effects of the boundary layer thickness-to-orifice diameter ratio could have been better assessed if the Strouhal number was held constant.

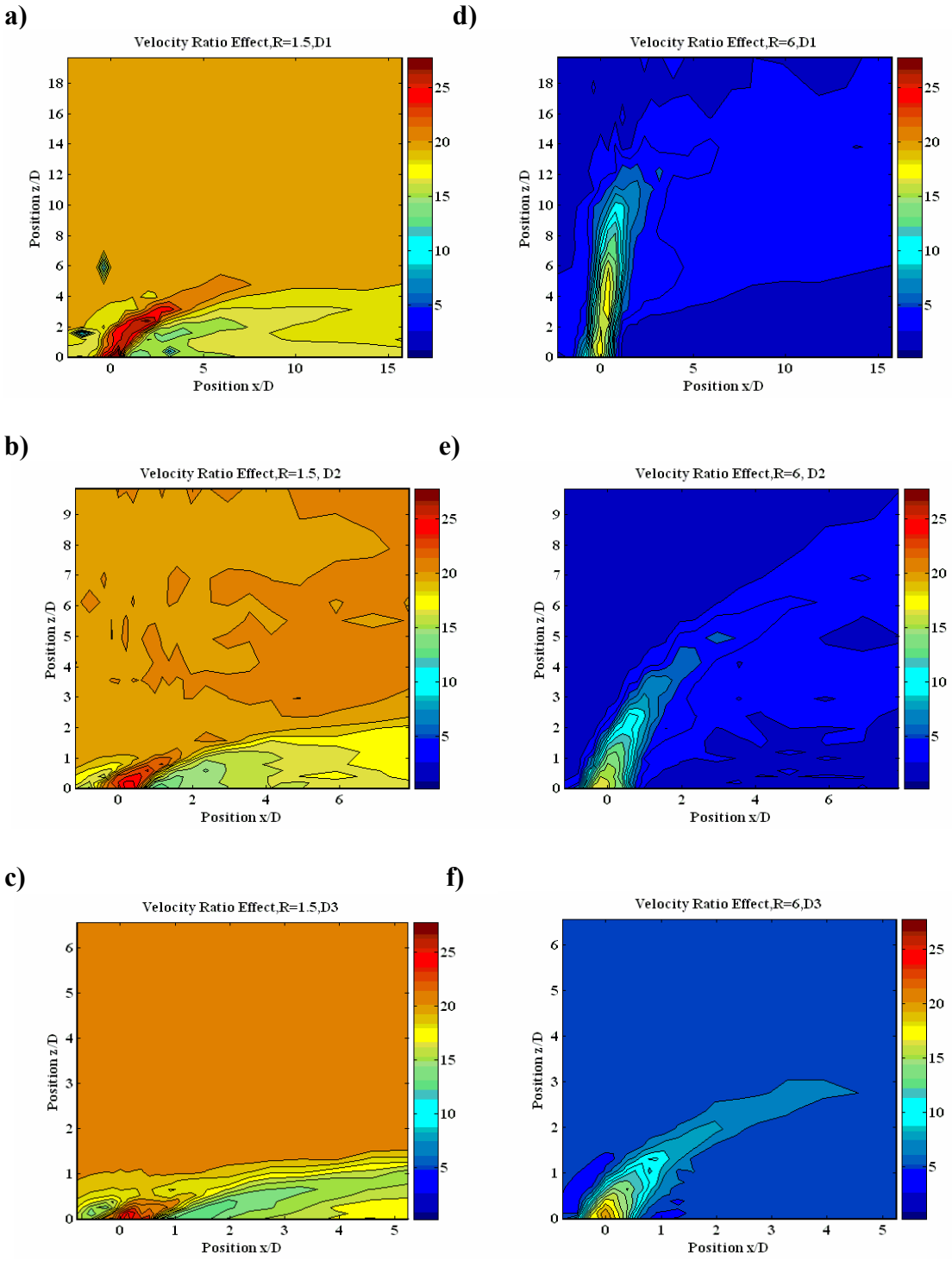

Figure 4.5 Effect of the different orifice diameters on the synthetic jet development in the same cross flow (case for the 20 m/s (top row) and 10 m/s cross flow (lower row). **a)** R=1,D1=2.5mm, Sr=0.2 **b)** R=1,D=2D1**,** Sr=0.4 **c)** R=1,D=3D1, Sr=0.6, **d)** R=1,D1=2.5mm, Sr=0.3 **e)** R=1,D=2D1**,** Sr=0.6 **f)** R=1,D=3D1, Sr=0.9.

4.5.3 Pressure induced on the flat plate behind the synthetic jet

To gain a better understanding of the synthetic jet integrated impact on the main aerodynamic properties, our experimental set up was modified to allow for pressure distribution measurements on the surface behind the actuator. One of the "compartments" of the aluminum plug module (*discussed in Chapter 2*) was reserved for the actuator and the other was used for a plate instrumented with four rows of static pressure ports (Figure 4.6). Pressure ports consisted of tygon tubing placed flush to the plate and they were connected to a 48 channel pressure scanner. Due to space restrictions pressure ports were placed along only one half of the plate and symmetry was assumed to get the entire pressure field contour behind the actuator. Plug was rotated such that the plate with the pressure ports was downstream of the actuator. It was very difficult to measure pressure immediately behind the orifice due to the actuator design constraints. The plate covering the actuator cavity was very thin and restricted the placement of pressure ports in this region. The only pressure information collected was from locations beyond the trailing edge of the actuator (from approximately 8 to 18 diameters downstream of the orifice).

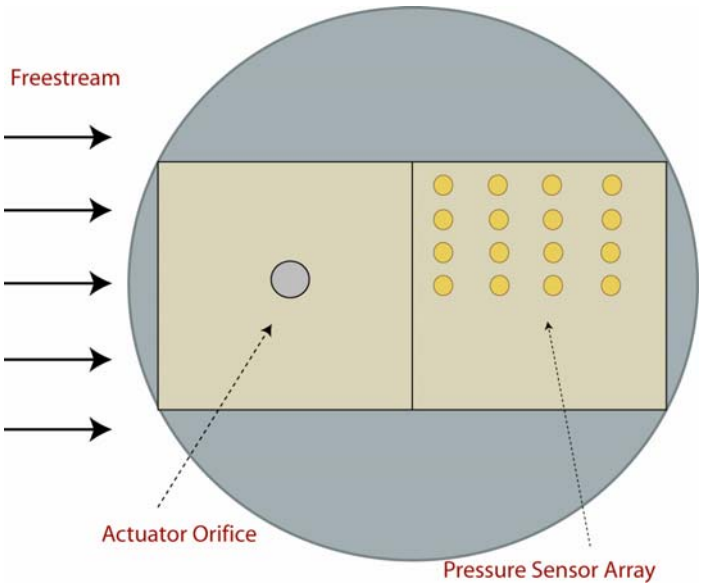

Figure 4.6 Pressure Distribution Measurement Set-up.

Pressure measurements were collected for all the cases listed in Table 4.1. The difference between atmospheric pressure and static pressure at each of the ports was measured for both the controlled and uncontrolled flows. The induced pressure, due to synthetic jet actuation, is presented in the contour plots in Figure 4.7. The low pressure region zone terminated roughly 12 diameters downstream for the higher jet velocity ratios (R>1), and approximately 16 diameters downstream for the lower velocity ratios (R<1). For most of these cases the measurable pressure differences were outside the designated pressure sensor area region. The exception was the case in which the jet to velocity ratio was approximately one. In the velocity contour plots for this case, at the distance furthest downstream, there was still a slight difference between the actuated and non-actuated velocity profiles implying that the impact of the jet at these conditions was maintained further downstream. Operating these high frequency synthetic jets in fully attached flows

created a net increase in the pressure downstream of the jet. The maximum difference of 22 Pa was noted for the jet operating in cross flow at a jet to free stream velocity ratio of one (Figure 4.7.a). All other configurations created much smaller, if at all distinguishable, differences in pressures between the control and uncontrolled flows, with results similar to the image shown in Figure 4.7.b.

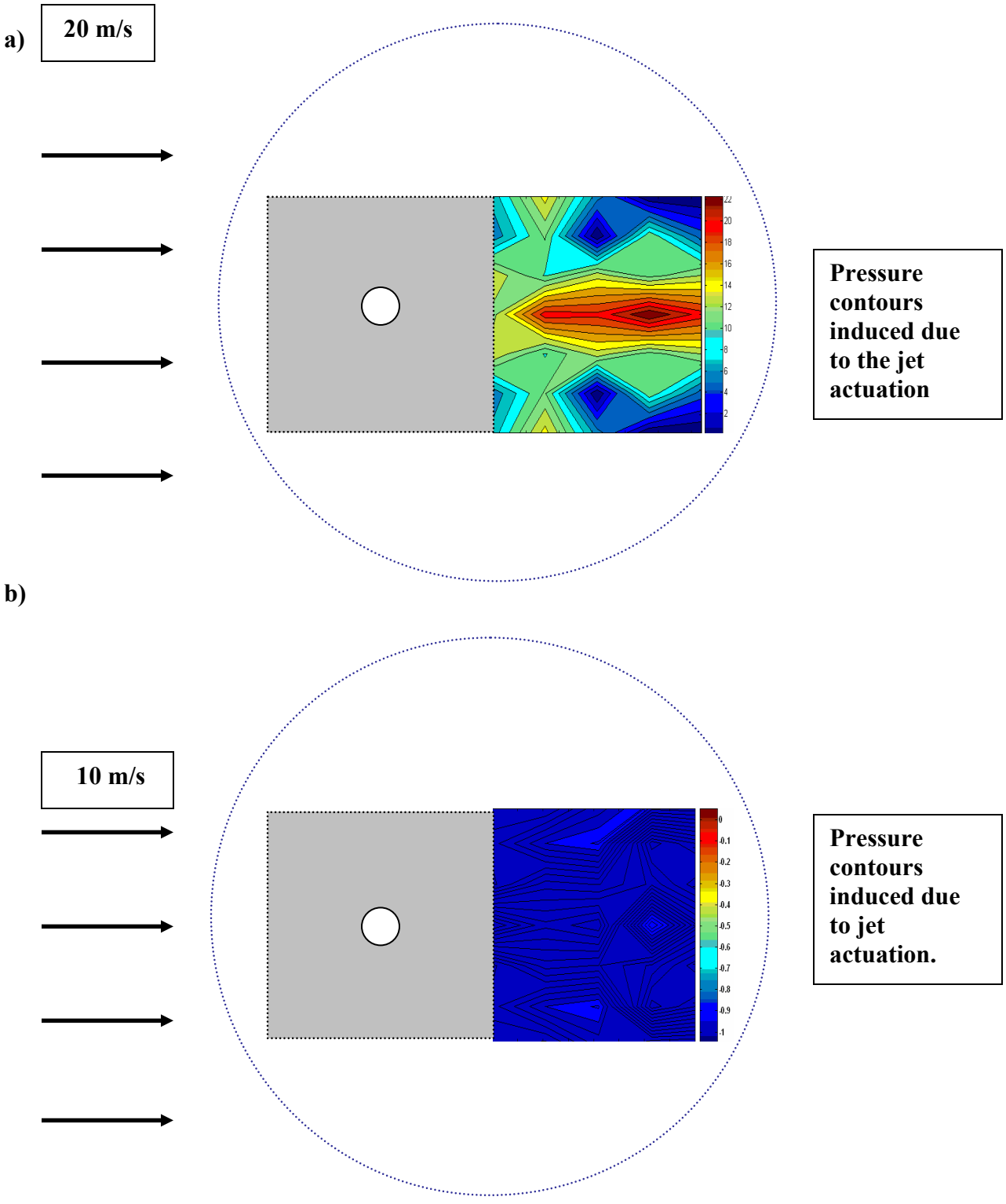

Figure 4.7 Pressure Distribution Measurement for R =1 and R =6.

4.5.4 Study of the jet cross sectional area changes

Velocity flow field surveys of the jet cross sections (in the *y-z* plane) at several locations downstream of the orifice were measured to advance the understanding of the effect of the jet-to-cross flow velocity ratio on the synthetic jet cross stream spreading rate and consequently the change in its circumference and area. Jet-to-free stream velocity ratios of 3.6, 2.7 and 1.5 were investigated. For all cases the jet originated from a same size circular orifice and as such it had the same initial circular shape with the diameter equivalent to the diameter of the orifice. Figures 4.8-4.10 present velocity contour snapshots, in the *y-z* plane, at four different downstream locations for the three jet-to-free stream velocity ratios tested. The size of the frames for all instances was the same. Concentrated regions of higher velocities representing the location and size of the synthetic jet at that particular location were visible in most frames. These concentrated regions were stretched in a spanwise direction, the extent of which depended on the strength of the cross flow relative to the strength of the jet. Increased mixing at lower velocity ratios caused the span of the synthetic jet to increase faster. In those cases the shape of the cross section of the synthetic jet changed significantly, immediately downstream of the orifice (Figure 4.10). In all cases the shape of the cross section changed from a circle to an ellipse as it progressed downstream. The circle to ellipse transformation was more pronounced for lower velocity ratios. In some instance the concentrated region wasn't captured with the frames defined (Figure 4.8.d, 4.10.d). For low velocity ratios this implied the jet asymptotically approached and was blended with the cross flow conditions and for the high velocity ratios cases it meant that the jet deflection wasn't strong enough to be captured with those low profile frames.

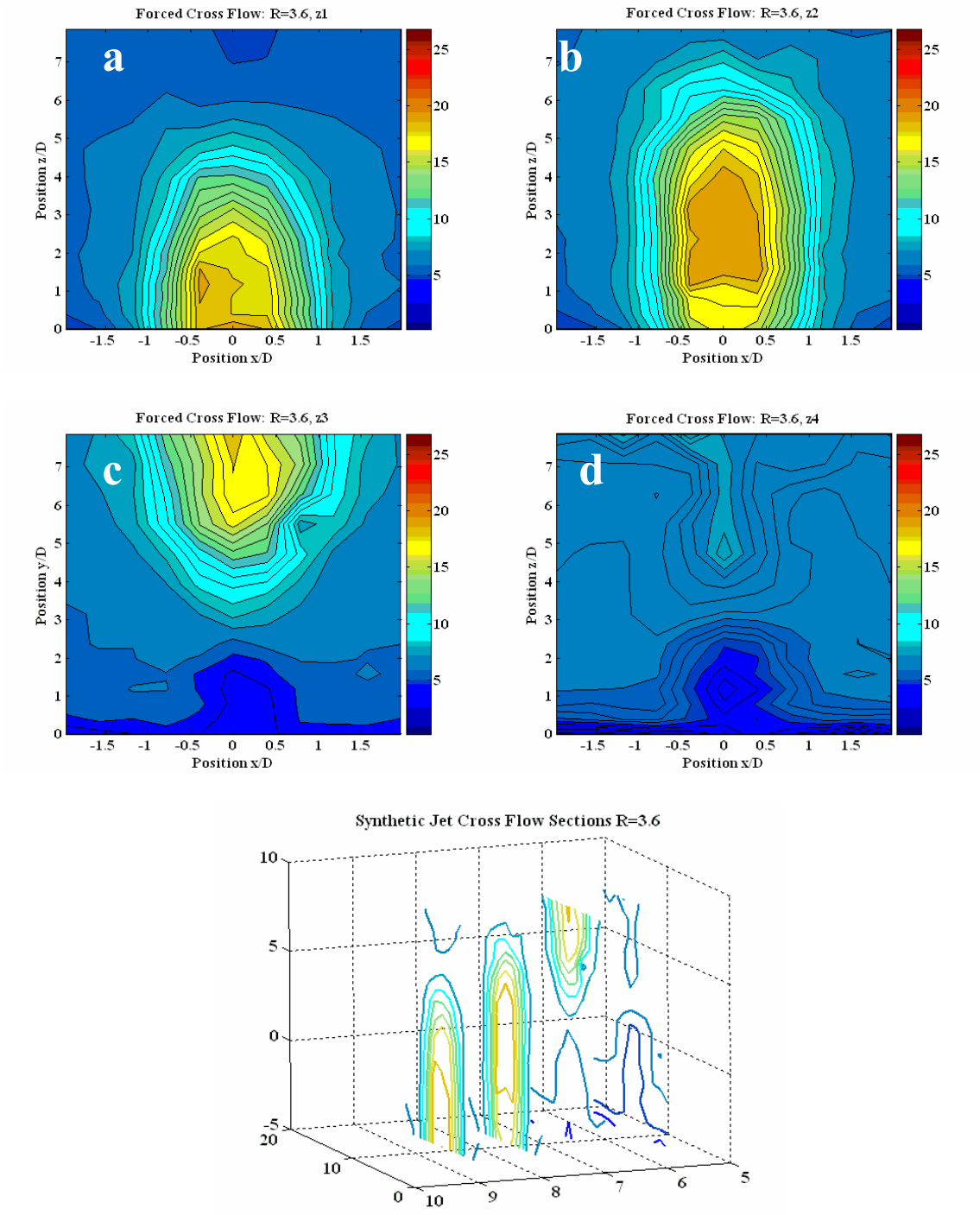

Figure 4.8 Cross sectional slices of the jet presented in a 3D frame at the jet to free stream velocity ratio of 3.6 a) x=0, b) x=0.5D, c) x= 1D, d) x=2D.

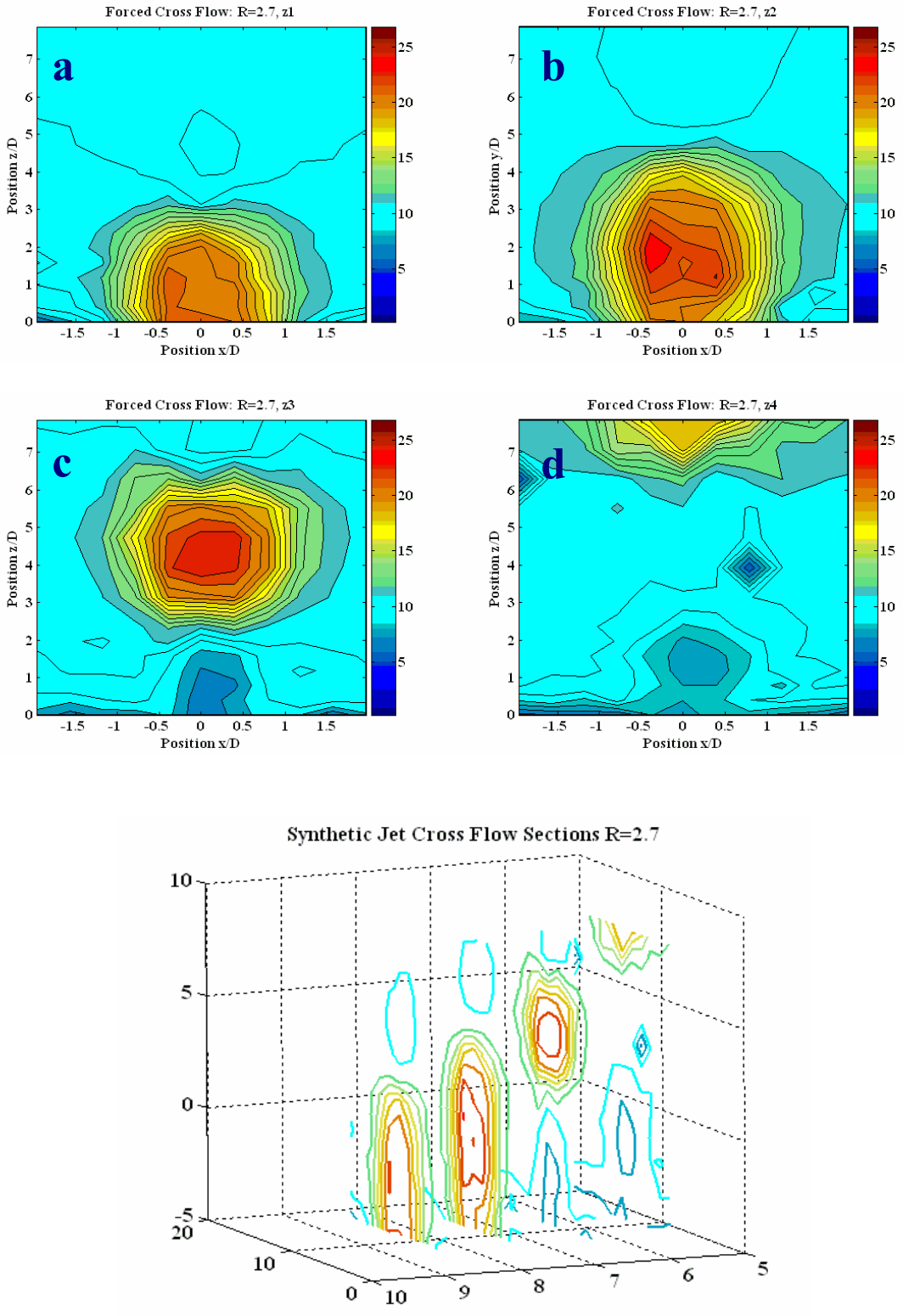

Figure 4.9 Cross sectional slices of the jet presented in a 3D frame at the jet to free stream velocity ratio of 2.7 **a)** x=0, **b)** x=0.5D, **c)** x= 2D, **d)** x=3D

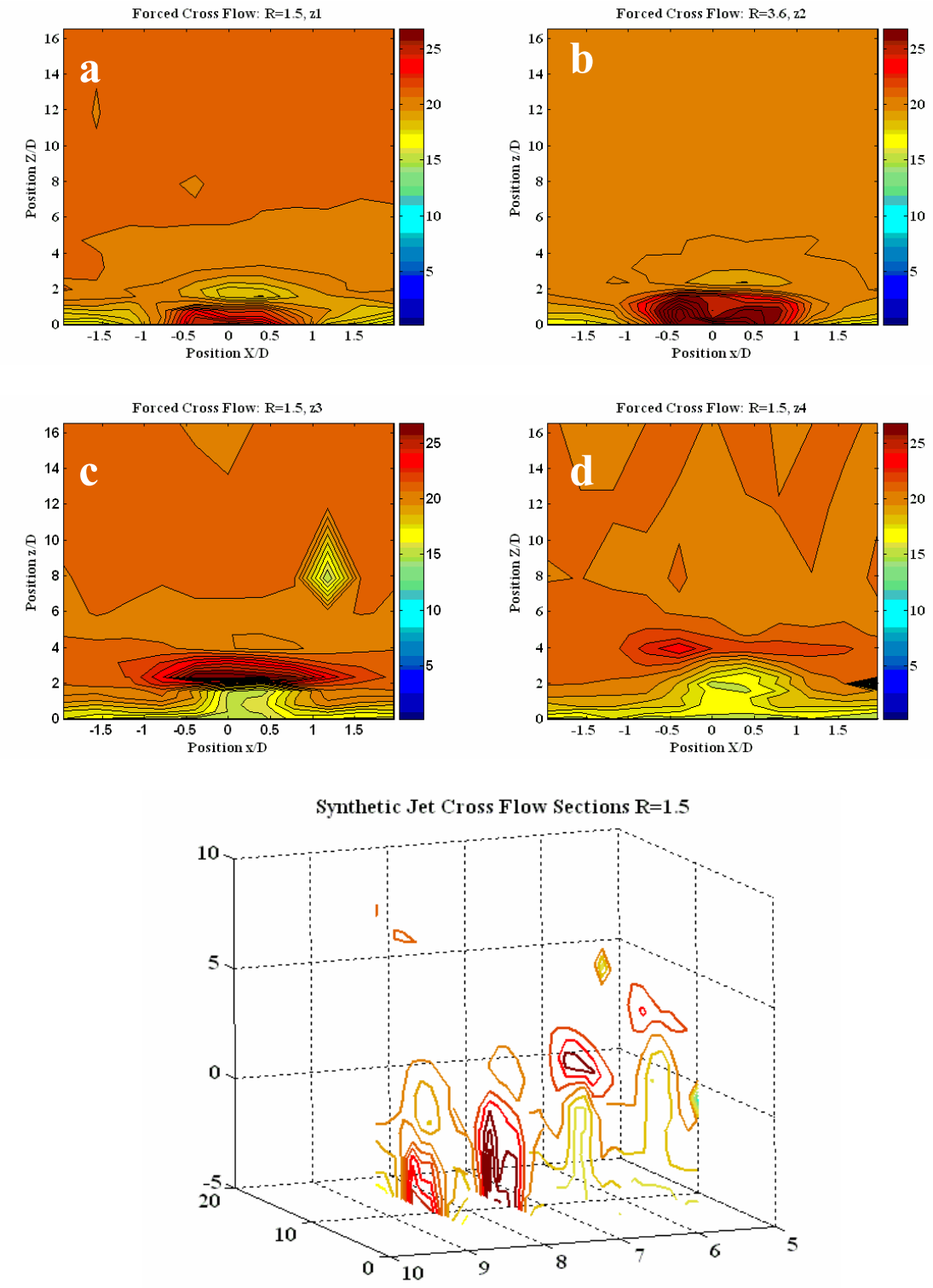

Figure 4.10 Cross sectional slices of the jet presented in a 3D frame at the jet to free stream velocity ratio of 1.5 **a)** x=0, **b)**x=0.5D **c)** x= 2D **d)** x=3D.

4.6 Velocity Spectrum

Velocity spectrum of the unforced flow includes no spectral peaks at lower frequencies. It is a fully attached flow and the velocity frequency response should be very low broadband i.e. with no significant peaks (Figure 4.11.a). The spectral peaks would be more distinct in the case of a separated flow in which case they would represent the natural shedding frequency of the flow. When the fully attached flow is forced at 2200 Hz, the velocity spectrum exhibits a pronounced peak at the forcing frequency and smaller peaks at several higher harmonics (Figure 4.11.b).

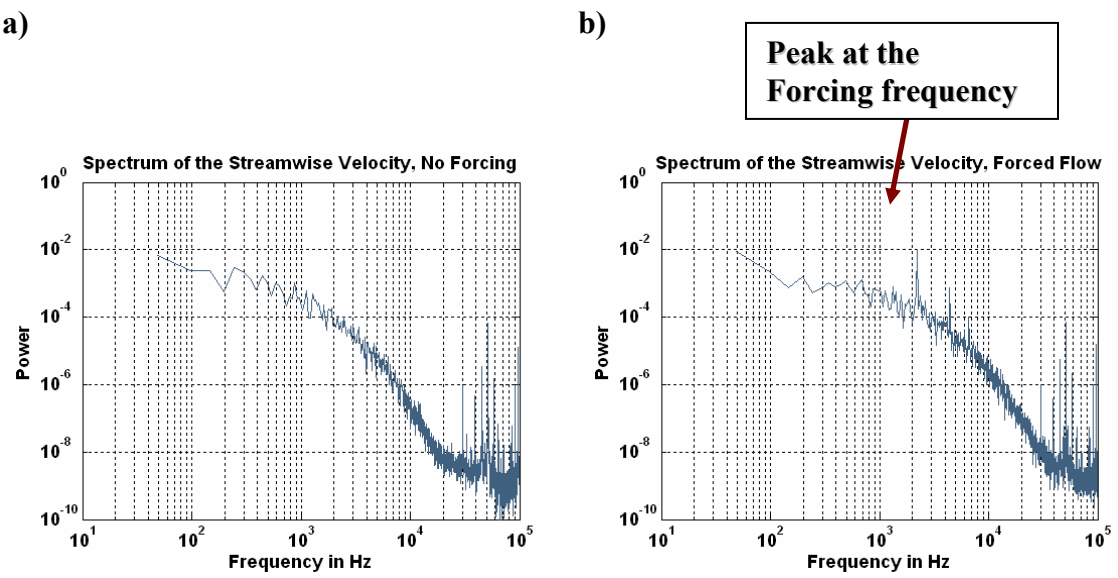

Figure 4.11 Velocity Spectrum of the a) unforced and b) forced flows.

4.7 Conclusion

High frequency synthetic jet actuators were embedded in an "infinite" flat plate oriented at zero angle of attack. Various jet-to-free stream velocity ratio case studies were analyzed to find the thresholds that would allow this jet to penetrate boundary layers of different thicknesses. The critical jet-to-free stream velocity ratio was one for this to occur in the flow field topologies studied. Below one, the jet was contained inside the boundary layer barely shuffling the surrounding flow and never making its way to the potential flow regions. Above $R=1$ however, the jet had enough momentum to break through the boundary layer and exit well above the boundary layer edges.

An attempt was made to find the regions of the recirculating flow that have been hypothesized to exist at high velocity ratios. Clean regions of recirculating flow as depicted by Mittal et al. were not identified. However, thickening of the boundary layer was observed in the low velocity ratio cases. From the available experimental data it appeared as though these recirculating flow regions should exist somewhere between R=1 and R=0.5. Better information on the formation of these regions may be found once array of closely spaced actuators can be analyzed. An array of actuators would alleviate the leakage of the flow around the individual circular type jet as the actuator array would provide the equivalent of a blocking sheet rather than an isolated fluid pole.

Further investigations demonstrated that an increased orifice diameter reduced the penetration length of the synthetic jet. Even though synthetic jet velocity was kept the same it was seen that at larger orifice diameters the jet had more difficulties in controlling

the boundary layer. This was tied to the Strouhal number effects, since the increase of the diameter caused a higher Strouhal number which, as a result, lowered the synthetic jet performance even though the mean velocity was the same. Finally, the change of the trajectory and the cross section area and shape of the jet at several distances downstream were measured. This essential information will be used for determination of empirical entrainment constants and for validation of the jet trajectory predictions to be developed in the next chapter.

Chapter 5

Modeling of Synthetic Jets in Cross Flow

5.1 Introduction

This part of the research focused on development of an analytical model capable of predicting synthetic jet-cross flow interactions as a function of the jet-to-free stream velocity ratio and boundary layer thickness-to-orifice diameter ratios. The shift from experimental to analytical analysis for this portion of the dissertation was a result of the challenges associated with design of an experimental matrix for optimization of synthetic jet actuator arrays for flow control applications (an example of such an experimental approach is discussed in Appendix B).

The effectiveness of synthetic jet actuators in various external conditions is a function of a number of parameters. It depends on the operational mode of the actuators (actuation frequency, jet momentum coefficient, orifice orientation) and on their particular location in the operating fluid. Synthetic jet actuators will rarely act as independent units. They will be combined to act in arrays designating the intelligent control of their mutual interaction as another critical element governing the synthetic jet

full potential benefits. Their placement in the flow and fine tuning through excitation of adjacent actuators at different relative phase angles has to be optimized.

Investigating the sensitivity of the influence of the actuator location and operational mode on the global aerodynamic flowfield and studying parameter optimization through experimental and numerical work has shown practical limitations. The experimental test matrix was prohibitively large and numerical simulations are computationally expensive and time consuming. An alternative approach, taken in this dissertation involves the development of a simplified model based on integral methods and the control volume concept. The model provides information on the direction of the jet trajectory and the variation in jet diameter and shape, as well as velocity as the jet is deflected by cross flows of varied strength. The model was developed with the goal of using predicted changes in flow field velocity with an appropriate lifting surface theory model to estimate synthetic jet actuator induced forces on a given surface. This work concentrated on developing and validating a model of a single jet in cross flows. The model, however, has the flexibility for being expanded to allow study of the more complex flow structures associated with interaction of multiple synthetic jet actuators and various actuation frequencies.

5.2 Previous analytical analysis of synthetic jet-cross flow interactions

Just recently has there been an attempt to use a reduced order model to investigate the influence of synthetic jet actuators on aerodynamic forces and moments **[Schober2006]**.

Theodorsen theory was applied and extended to model the synthetic jet cycle. This model neglected the interactions with the boundary layer but it captured the circulation changes due to the presence of jet momentum. The model was used to predict lift curves for a NACA 0012 airfoil in pre-stall conditions as a function of synthetic jet actuators locations and actuation frequency. The rest of the published approaches to simulate synthetic jet-cross flow interaction were limited to complex computational fluid dynamics solvers.

5.3 Different Types of Modeling Approaches

The search for a modeling technique that could capture synthetic jet-cross flow interaction lead to a recognition that, although created with a novel oscillating zero-net-mass flux device, the resultant jet resembles conventional turbulent discharge flows. Several different techniques have been taken on by researchers and scientists, particularly in the environmental engineering field, to model conventional turbulent jets in cross flow. Chimney gases discharged into the atmosphere are just an example of such flow interfaces that have existed for a long time and, in return, have stimulated a development of a chain of methods to predict these flow phenomena.

Empirical models present the most simplified way of predicting major properties of jets in cross flow. They generally just correlate experimental data and are capable of providing information on the jet trajectory only **[Abramovich1963, Schetz1980]**. Perturbation models study the physics of flow in very specific regimes (either near field

or far field). They require small parameters and restrictive assumptions such as very strong jets in very weak cross flows **[Needham1988]**. Numerical models include the solution of a form of partial differential equations. It is the most accurate approach, applicable to a wide range of flow conditions requiring the least amount of empirical data **[Baker1987, Demuren1992]**. However, this method is also very time consuming, requires strong computational resources and as such is not the best method for optimization or real time feedback control applications.

The integral method is a semi-empirical approach that stood out from this set of available models as potentially well suited for synthetic jet-in-cross flow calculations. This model is founded on conservation laws applied to a control volume and expressed through a set of ordinary differential equations **[Rajaratnam1976]**. This particular approach tremendously simplifies the prediction problem. The method, however, requires development of an empirical function, which represents a drawback of this method and is also why this approach is often discarded as inconvenient and/or inadequate for systems where the requisite empirical relationship is difficult to determine. Nevertheless, with proper empirical correlations, integral models provide an abundance of information. In the following discussion, this method will be shown to be a very useful approach for predicting the behavior of synthetic jets in cross flow.

5.4. Synthetic vs. Conventional Steady Jets

The applicability of integral methods developed for continuous jets to synthetic jets was highly dependent on the resemblance level of these two types of flows. To make use of the extensive work done on modeling of continuous jets in cross flow it was necessary to establish the relationship between continuous and synthetic jets.

The difference between these two types of flows is most obvious in the near field. Continuous jets are observed to develop a potential core along which entrainment increases. At the end of the potential core instabilities occur after which the modes settle and the entrainment reaches a steady value **[Pratte1967, Cater, Soria2002]**. Synthetic jets, on the other hand, have been described as jets with no potential core. They are synthesized by the interactions of vortex rings that quickly lose their identity suggesting a constant entrainment throughout the entire jet trajectory. Another hypothesis states that since synthetic jets mandate ambient flow for their existence, they are capturing most of the flow in these initial stages of formation and (at least in the near field) they may entrain more fluid than continuous jet elements do **[Jamesand1996, Sauerwein1999, Gordon2002].**

In the far field, the effects of the suction part of the cycle diminish and the time averaged synthetic jet mean flow appears to be very much like the continuous turbulent jet **[Smith, Swift2003]**. Turbulent diffusion damaged the clear vortex cores that were present in the near field of the synthetic jets.

Glezer et al. contributed to the synthetic jet-continuous jet comparison by providing empirically determined best fit to the mass flow rate from experimental data for both flows. For synthetic jets $\frac{Q}{Q_0} = 1.11\left(\frac{z}{d_0}\right)^{0.85}$ and for continuous jets $\frac{Q}{Q_0} = 0.32\left(\frac{z}{d_0}\right)$, where $Q = 2\pi\int Udr$, Q_0 is taken at the maximum centerline velocity, d_0 is the diameter of the orifice and z is the distance above the orifice. These relations show that the entrainment rate for the synthetic jet is by almost three times larger than that of a continuous jet and that its variation is not as linear. Gordon and Johari showed that pulsed excitation causes an increase in the entrainment of ambient fluid into the jet which in turn leads to a greater mass flow rate. The pulsatile nature of the synthetic jet would suggest having the same effect **[Gordon2002, Johari2002]**. In summary synthetic jets spread differently than continuous jets due to the differences in their near field. Their width and volume flux grows more rapidly than those of continuous jets **[Gordon2004]**.

Continuous turbulent jets are self-similar **[Keffer1968]**. Synthetic jets are also considered to be self-similar and Figures 5.1 and 5.2 demonstrate the self-similarity of synthetic jets studied in this research. In general, self similarity is demonstrated when a cluster of empirical points can be reduced into a single curve using self similar variables. Figures 5.1 and 5.2 demonstrate that features of synthetic jet profiles remain the same once velocity or turbulence scales were multiplied by a common factor. The spanwise distribution of the streamwise velocity component measured at ten equally spaced stations was normalized by the mean centerline velocity and the orifice diameter. All the curves coincided (Figure 5.1) showing that in the range studied the synthetic jet velocity

attributes are self similar. Likewise, turbulence intensity, plotted in the same similarity coordinates, exhibited self similar profiles (Figure 5.2). Therefore, similarity parameters for conventional jets also apply to synthetic jets, demonstrating the resemblance of the two flows.

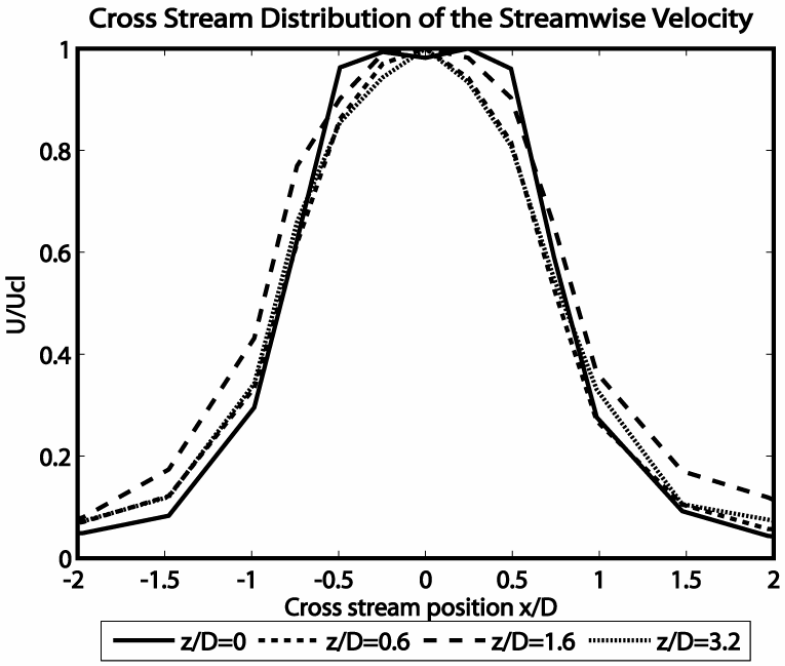

Figure 5.1 Collapse of the normalized synthetic jet cross stream velocity, an evidence of self similarity of synthetic jets.

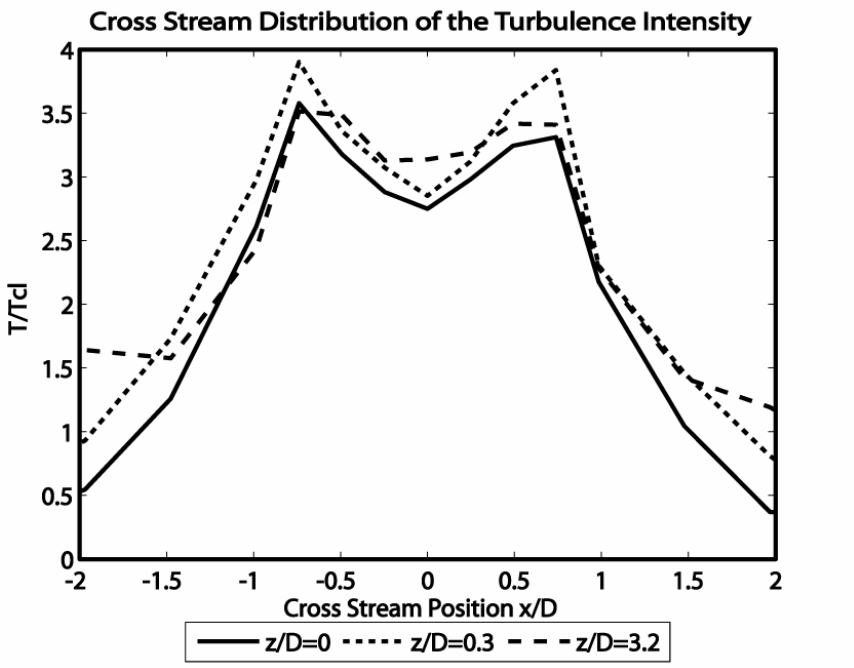

Figure 5.2 Collapse of the synthetic jet normalized turbulence intensity profiles, an evidence of self similarity of synthetic jets.

5.5 Governing mechanism in transverse synthetic jets

The degree of deflection of the jet into the cross flow is determined by two major mechanisms: entrainment of the cross flow by the jet and the pressure exerted on the jet by the cross flow **[Demuren1985]**. The presence of the jet blocking the naturally developing path of the cross flow streamlines is known as the blockage effect. The jet also captures some of the cross flow through the entrainment process (entrainment effects) causing a low energy region to form downstream of the jet (wake region) **[McMahon1968, Moussa1977]**. Formation of the wake behind the jet increases pressure drag. A strong pressure gradient is created on the downstream side that forces the cross

flow fluid inwards into the jet, additionally increasing entrainment and causing deformation of the jet cross section **[Crabb1981, Muppidi2006].** Shear forces created in these flows add to the jet deformation effect by stretching the jet vortex rings towards its side.

The literature on modeling continuous jets in cross flow has raised some controversy in explaining the relative magnitude of the effects of pressure drag as compared to the rate of entrainment on jet deflection **[Yuan1998]**. Various combinations of entrainment functions and drag coefficients demonstrated satisfactory predictions of the trajectory of the jet, regardless of which of those two mechanisms was considered to be the dominating one. It will be the task of the next few sections to determine, which one of these two mechanisms (entrainment and pressure), prevail in the synthetic jet-cross flow interactions.

5.6 Entrainment coefficients

Two streams of fluid with the relative motion between them have to exist for the entrainment process to occur. Vertical motion of the jet and the horizontal motion of the cross flow imply that advancements of synthetic jets in cross flow are heavily managed by entrainment. For transverse jet cases entrainment is most easily defined as a rate of change of mass flux with downstream distance.

It was primarily expected that this inflow of fluid be proportional to the local difference between jet velocity and cross flow velocity. An increase in entrained fluid is consistent with a loss of momentum and with an increase of the effective jet diameter. Since the control volume changes its cross sectional area and circumference as it travels along the trajectory, entrainment rate will be affected accordingly. A jet *shape factor* (*A/C,* where *A* is the local area of the jet column and *C* its circumference) was introduced and determined by matching it to an ellipse of a certain aspect ratio. The local *ratio of the major and minor axes* of the jet cross section and its *orientation* or *Θ,* are elementary parameters influencing the entrainment rate **[Keffer1962]**. The entrainment rate is, therefore, mainly a function of the velocity change across the "ellipse" of the jet and can be expressed as: $E = \frac{A}{C}\rho_\infty E^*\left(U_j - U\right)$ as derived by Campbell and Schetz **[Campbell1972]**, where the entrainment coefficient E^* was obtained from measurements of mass flux along the conventional jet axis provided by Keffer et al. Using experimental data, they derived an expression for this coefficient in terms of the position along the axis and jet to free stream velocity ratio **[Keffer1962]**:

$$E^* = a\frac{\left(\frac{s}{d_j}\right)^b}{\left(\frac{U_j}{U}\right)^c} \tag{5.2}$$

For a conventional turbulent jet a = 0.2, b = 1.37 and c = 0.6. These empirical entrainment coefficients will be different for synthetic jets. A way of estimating these coefficients is by analyzing the experimentally obtained jet trajectory. More deflection

implies higher cross flow entrainment. The distribution of these coefficients and exponents for our synthetic jets were, therefore, obtained by matching the experimental data to the theoretical curves satisfying simultaneously the jet deflection curves and the jet velocity deficit curves. Using this technique, the entrainment coefficient for synthetic jet was found to be equivalent to:

$$E_{SJ}{}^{*} = 0.6 \frac{\left(\frac{s}{d_j}\right)^{1.5}}{\left(\frac{U_j}{U}\right)^{0.5}} \tag{5.3}$$

The magnitude of these coefficients (a_{SJ} = 3a) is consistent with Glezer's comparison of entrainment rates for synthetic and continuous jets. Glezer's evidence that the entrainment rate for synthetic jets is increased by almost three times when compared to conventional jets was supported by this analysis.

5.7 Details of the synthetic jets in cross flow model using integral methods

Predictions to be presented were based on the model developed by Campbell and Schetz in 1972 **[Campbell1972]**. A slug of jet fluid was used as a control volume and was followed from the origin (center of the orifice exit plane) to a position downstream where it was completely mixed with the cross stream. Figure 5.3 presents the slug of fluid with a coordinate system along and perpendicular to the trajectory (labeled *s* and *n* respectively).

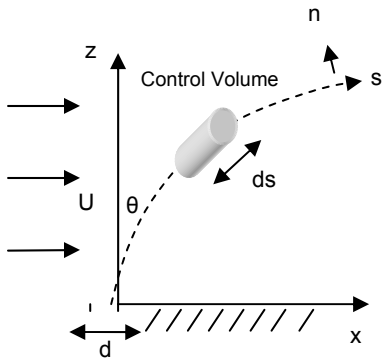

Figure 5.3 Slug of a jet fluid along the trajectory used as a control volume.

5.7.1 Continuity equation

The amount of free stream flow per unit length entrained in the control volume is expressed using the continuity equation **[Cater, Soria2002]**.

$$\rho\left(\frac{d}{ds}\right)\left(A_j U_j\right) = E \tag{5.1}$$

The natural "*s*-*n*" coordinate system of the transverse jets was for simplicity replaced with an *"Z-X"* coordinate system by introducing the transformation expression: $\frac{d}{ds} = \cos\theta\left(\frac{d}{dZ}\right)$. X represents the horizontal distance and θ is the angle of the jet with respect to the Z-axis. Part of the challenge of modeling a jet in cross flow with this technique is in determining a valid representation of *"E"* (difficulties associated with predicting these entrainment functions are discussed in Section 5.6).

5.7.2. Momentum equations

Cross flow has momentum that gets enforced on the jet causing it to slowly change its direction from vertical, in the near wall region, to the direction of the cross flow in the far field region. The jet has its own momentum resisting these changes. At the injection point the momentum of the jet in the *Z* direction can be equated to the *s* momentum. As the jet axis asymptotes to the direction of the cross flow, the *Z* momentum of the jet approaches zero and the *X* momentum or the momentum of the cross flow becomes synonymous to the *s* momentum. This exchange of flow effects (a function of the velocity ratios) leads to a constant adjustment of momentum along the jet's path resulting in different trajectory curvatures.

5.7.2.1 *n*-momentum equation

n-components (perpendicular to the trajectory) of the balance of net flux of momentum into the control volume and the sum of forces acting on the control volume is represented by:

$$\frac{A_j U_j^2}{\widetilde{R}} = \frac{A_j U_j^2 X''}{\left(1 + \left(X'\right)^2\right)^{\frac{3}{2}}} = EU\cos\Theta + C_D \frac{1}{2}\rho U^2(\cos^2\Theta)d \qquad (5.4)$$

where $\widetilde{R}$ is the radius of the curvature, C_D is the drag coefficient and *d* the local jet diameter. Expression on the left side of the equation represents the centrifugal force caused by the curvature of the jet trajectory. The first expression, on the right side, stands

for the rate at which mass enters the sides of the control volume multiplied by the free stream velocity component in the *n* direction $(U\cos\Theta)$. The non-uniform free stream velocity profile (boundary layer type velocity distribution) was easily integrated into this expression. The last term in the *n*-momentum equation includes the blockage effects of the free stream flow. In the case of continuous jets, the force resulting from this blockage effect is often taken to be equivalent to the drag on a "solid" cylinder inclined at an angle θ to the free stream flow. This coefficient has been measured before and it was approximated to be anywhere between 1.2 and 3 **[Campbell1972, Wooler1968, Abramovich1963]**. Results from Chapter 4 experiments suggest that synthetic jets are not well represented using this assumption. (Crabb also agreed that the flow behind a turbulent jet is very different than the one associated with the wake from a solid body **[Crabb1981])**. External flow around a flow jet is more likely to be represented by a type of a streamline pattern equivalent to characteristics of a flow around a circular cylinder with suction **[Keffer1968, Coelho1989]**.

5.7.2.2 *s*-momentum equation

The *s*-momentum equation was introduced to enable the solutions for the cross sectional area of the jet. It expresses the balance between the rate of change of jet momentum and the forces acting along the trajectory (entrainment of ambient fluid into the jet, pressure and the shear stress):

$$\frac{d}{ds}\left(A_j U_j^2\right) = EU\sin\Theta + \frac{1}{2}\rho U^2 A\sin\Theta\cos\Theta\frac{d\Theta}{ds} + \pi d\beta(U_j - U\sin\Theta)^2 \qquad (5.5)$$

where β is an empirical constant to be discussed shortly **[Schlichting1968]**.

5.8.2.2.a Pressure term

Second term in the *s*-momentum expression represents the pressure gradient along the trajectory. Static pressure variation around the perimeter of a circular cylinder relative to the dynamic pressure $q_\infty = \frac{1}{2}\rho U^2$ is assumed to be: $C_p = 1 - 4\sin^2\theta$, for $0 \le \theta \le \frac{\pi}{2}$ and $C_p = 0$ in the wake behind the cylinder. Mean pressure is expressed as $\overline{p} = \frac{\int_0^\pi p d\theta}{\int_0^\pi d\theta}$ (where the local surface pressure is given by $p = C_p q_{\infty_n} + p_\infty$) or as $\overline{p} = p_\infty - \frac{1}{2} q_{\infty_n}$ (after integration), **[Campbell1972]**. The jet flow pressure can then be differentiated with respect to the trajectory unit length (*s*) to obtain the expression represented in the *s*-momentum equation: $\frac{\partial \overline{p}}{\partial s} = -q_\infty \sin\theta\cos\theta \frac{d\theta}{ds}$.

5.7.2.2.b Shear stress term

Shear stress is proportional to the differences between the jet velocity and the free stream velocity (component tangent to the jet flow). The shear stress term in the *s*-momentum equation is an extended form of its usual representation: $\tau = \rho(\nu + \varepsilon)\frac{\partial U}{\partial n}$. The velocity

gradient is approximated by: $\frac{\partial U}{\partial n} = \frac{U_{\max} - U_{\min}}{b} = \frac{U_j - U_\infty \sin\theta}{b}$, where U_{min} is the free stream velocity component tangent to the direction of the jet flow and the maximum velocity is replaced by the mean jet velocity **[Rajaratnam1976]**. Kinematic viscosity (ν) for turbulent mixing flows is considered small and thereby ignored. Eddy viscosity has been estimated using Prandtl's mixing length hypothesis valid only for turbulent flows: $\varepsilon = \beta b\left(U_{\max} - U_{\min}\right)$, where b is the width of the mixing zone **[Schlichting1968]**. Schlichting's description of a free jet boundary is used to obtain the expression: $\beta = \frac{0.00217}{\tilde{c}}$ where $\tilde{c}$ is the rate of spread of the jet flow. Although $\tilde{c}$ might be expected to be a function of distance along the trajectory it is taken to be a constant value of 1.11 from Glezer's previously mentioned observations. The final expression for the shear stress was then written as $\tau = \rho\beta\left(U_j - U\sin\theta\right)^2$.

5.7.3 Equations of motion

The above coefficients and expressions, when factored together, result in a final set of ordinary differential equations with three main unknowns to be solved for: the velocity of the jet, the diameter of the jet and the jet trajectory coordinates (all a function of *Z*).

$$\frac{dU_j}{dZ} = \frac{1}{A_j U_j}\left(EU\sin\Theta + 0.5\rho U^2 \sin\Theta\cos^2\Theta\frac{d\Theta}{dZ} + \tau\beta d(U_j - U\sin\Theta)^2 - EU_j\right)\frac{1}{\cos\Theta}$$

$$\frac{dA_j}{dZ} = \frac{1}{U_j}\left(\frac{E}{\cos\Theta} - A_j\frac{dU_j}{dZ}\right)$$

$$\frac{d^2X}{dZ^2} = \frac{\left(1+X'^2\right)^{3/2}}{A_j U_j}\left(EU\cos\Theta + C_D\frac{1}{2}U^2\cos^2\Theta d\right) \tag{5.6}$$

In order to be able to solve for these equations a specific relationship between the area/circumference of the jet was assumed. The assumptions were based on the experimentally obtained jet cross sections. Cross sectional area and circumference undergo both size and shape changes as the jet entrains fluid from the external stream. It was observed from the experimental snapshots presented in *Chapter 4* that the jet stretched in the spanwise direction. The shape of the jet continuously changed from circular to an ellipse (labeled as first region) up to a certain location downstream beyond which the shape of the jet remained relatively the same (second region). These transformations were found to be highly dependent on the jet velocity ratio. Experimental data indicated that the extent of the first region ended at a downstream distance of approximately 2.5 times the magnitude of the jet to freestream velocity ratio. For example, if the velocity ratio was 3, experimental data show that the jet was changing its shape from circular to an ellipse up to the streamwise distance of 7.5 diameters. At this point the jet cross section reached a shape equivalent to an ellipse of an aspect ratio of 3:1. This shape was maintained throughout the second region. Therefore, there is a region in which the jet has a cross section whose minor-to-major axis ratio decreases linearly from 1 at $\frac{Z}{d_0} = 0$ to $\frac{1}{3}$ for $\frac{Z}{d_0} = 2.5\frac{Uj}{U}$. General expressions for the circumference and the area of the jet cross section were modified accordingly:

$$\textit{Minor axis /major axis} = 1 - \left[\frac{4}{15}\left(\frac{Z}{d_0}\right)\left(\frac{U}{Uj}\right)\right] \tag{5.7}$$

$$C = \pi d \left(\frac{1 + \left[1 - \frac{4}{15} \left(\frac{Z}{d_0} \right) \left(\frac{U}{U_{j0}} \right)^2 \right]}{2} \right)^{\frac{1}{2}}, \quad A_j = \pi \left(1 - \frac{4}{15} \frac{Z}{d_0} \frac{U}{U_j} \right) \frac{d^2}{4} \tag{5.8.a}$$

In the second region, in which a jet maintains an elliptical cross section with the ratio of the minor to major axis of 1/3 (equivalent to the cross section at the end of first region) the circumference and the jet area are expressed as:

$$C = 2.34d, \; A_j = \frac{\pi d^2}{12} \tag{5.8.b}$$

These estimated geometric parameters were substituted in the predetermined set of ordinary differential equations and were then integrated numerically. The incremental values for Z were assigned. The continuity equation was used to provide updates on the velocity of the jet while the *s*-momentum equation was used to continuously update the information on the diameter of the jet. Those properties were then used in the elements of the *n*-momentum equation to get information on the curvature of the trajectory $\left(\frac{d\Theta}{dZ} \right)$.

5.8 Results and discussion

5.8.1 Entrainment and drag contribution predictions

Comparison of the experimental data to the integral model results showed that the jet velocity deficit prediction, jet growth and the trajectory can only be accurately presented if both entrainment and pressure drag mechanisms were equally included. Pressure drag and the entrainment rate will be shown to be of the same order of magnitude.

Presented in Figure 5.4 and Figure 5.5 are entrainment and drag contributions that were used to successfully simulate the jet trajectories and velocity profiles for three different velocity ratios: 6, 3.5 and 2.7. For the jet to free stream velocity ratio of 6, the jet velocity was 18 m/s and the cross stream velocity was 3 m/s. For the other two cases the jet velocity and the cross flow velocities were higher but the total ratios of the two were smaller. The smallest jet velocities in the first case (R=6) imply a highest entrainment rate as demonstrated in Figure 5.4 (loss of momentum causes an increase in entrainment). The drag coefficient for all cases was assumed to be 0.1 which is significantly smaller than what was used in predicting continuous transverse jet trajectories. Larger drag coefficients would have required lower entrainment rates for accurate jet trajectory predictions. Lower entrainment rates, however, didn't seem appropriate as they affect the jet velocity decay and at such rates they were not correctly predicting the velocity distribution. This suggested that the pressure drag effects had to be smaller, i.e. of the same order of magnitude as the entrainment rate. The ratio of entrainment rates and drag forces, needed to obtain representative prediction of the

Chapter 4 synthetic jets in cross flow test cases, were determined by comparison of the measured flow properties with the predictions obtained using various entrainment/pressure drag influence functions.

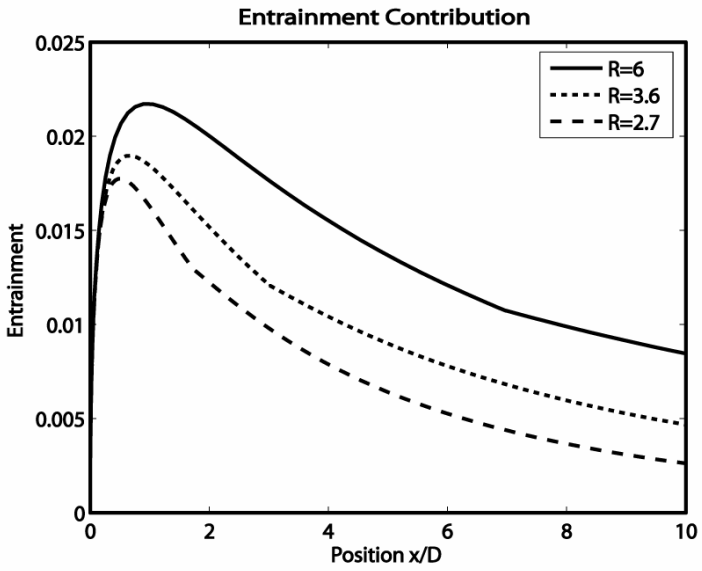

Figure 5.4 Entrainment rates predicted for different jet to free stream velocity ratios.

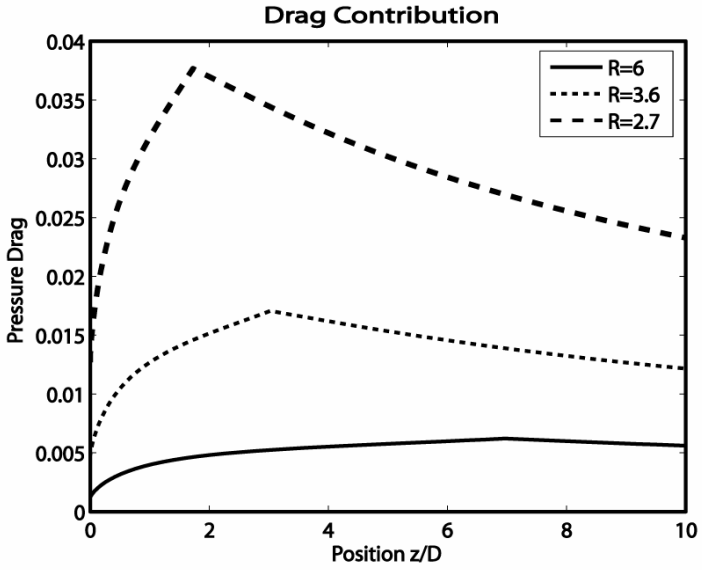

Figure 5.5 Drag forces predicted for different jet to free stream velocity ratios.

Some researchers assumed there were no significant changes in the entrainment rate along the synthetic jets development region. Entrainment rate was assumed to be constant. Others assumed that the synthetic and continuous jets were similar enough and with proper "coefficient" adjustments, the same entrainment rate laws could be used for both types of flows. Both assumptions have been investigated and they both seem sufficient for a good representation. Their similarity and differences will be presented shortly.

5.8.2 Jet cross section area and velocity decay prediction

The width of the jet trajectory is a function of a downstream distance and momentum. The cross sectional area of the jet continually increases as the jet flow moves along the trajectory. Figure 5.6 shows the change in the area of the synthetic jet with respect to its initial area. The initial area for all three inspected cases was the same. In the first region (near orifice region) the area increases almost linearly and in the second region the rate of change slowed down.

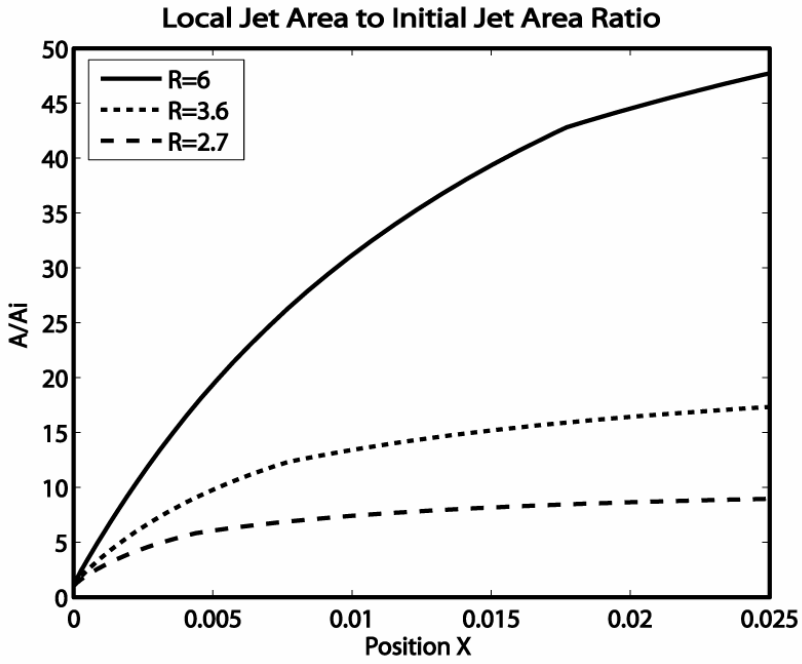

Figure 5.6 Change of the area of the jet with respect to its initial area as the downstream distance increased for velocity ratio R=6, 3.5 and 2.7.

Since the diameter of the jet increases with the downstream distance, the jet velocity will continuously decrease until it reaches the free stream velocity. Figure 5.7.a-d shows the trend for the velocity decay was similar for all injection velocities (velocity ratios of 6, 3.5, 2.7 and 1.5).

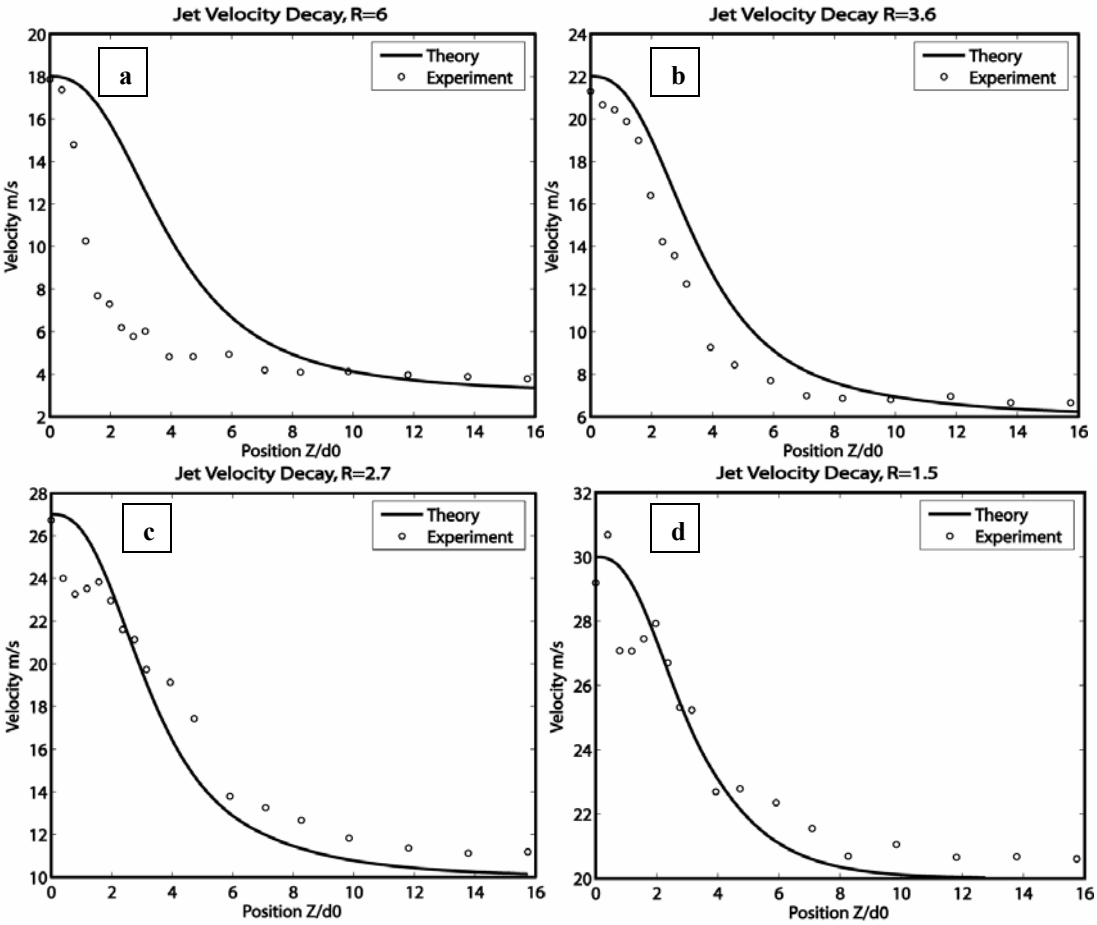

Figure 5.7 Prediction of the jet velocity decay at different velocity ratios. a) R=6, b) R=3.5, c) R=2.7, d) R=1.5.

5.8.3 Jet trajectory predictions

Jet trajectory is strongly influenced by the near field conditions. The jet velocity profile and the cross flow boundary layer govern the deflection of the jet into the cross flow (jet trajectory displayed more deflection at lower jet to free stream velocity ratios). Experimental trajectory data was obtained from hot wire measurements and represent the

locus of maximum velocity in the jet flow. These were used to validate the model trajectory predictions, demonstrating good agreement throughout a limited range of the injection velocities. Experimental and simulated jet trajectories for all four cases (velocity ratios of 6, 3.5, 2.7 and 1.5) are presented in Figure 5.8.a-d, respectively.

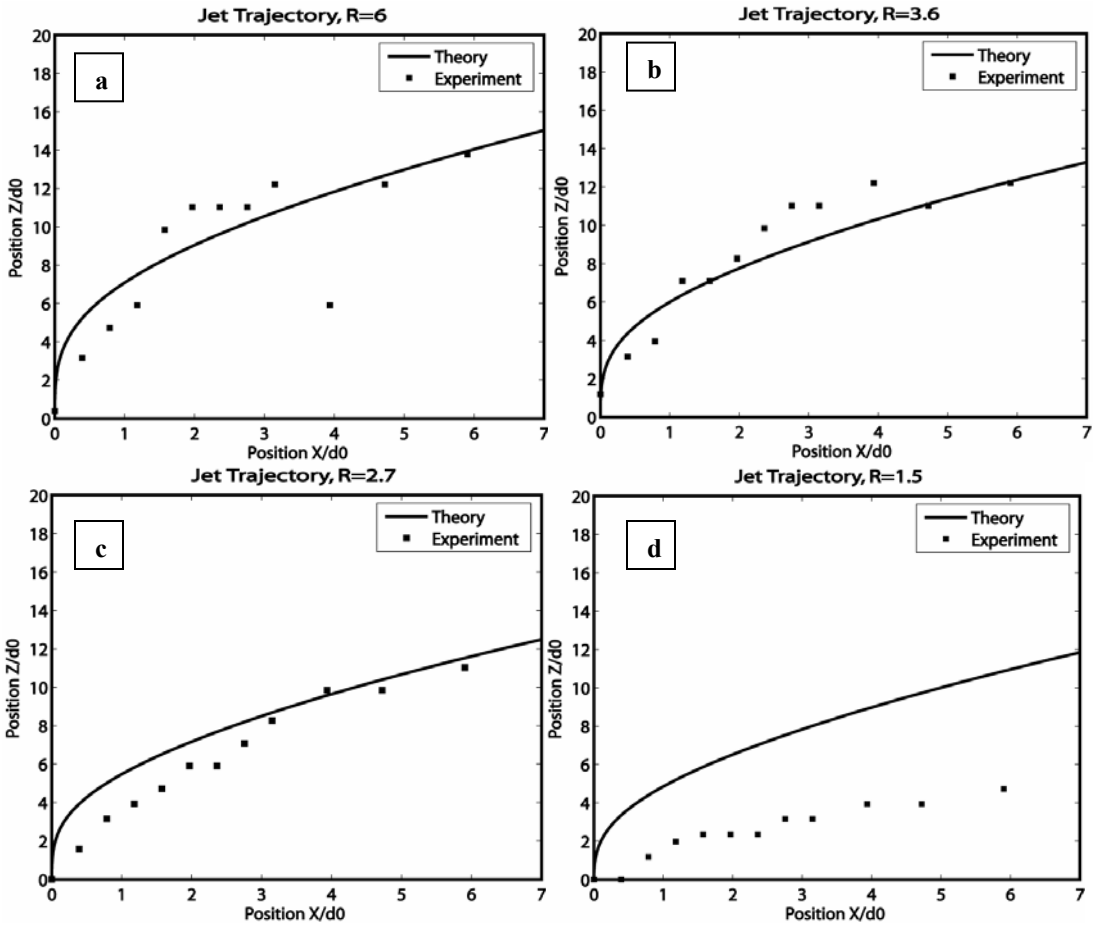

Figure 5.8 Comparison of experimental and predicted jet trajectories for jet to velocity ratios of a) R=6, b) R=3.5, c) R= 2.7, d) R= 1.5.

A significant over prediction was evident for the smallest velocity ratio case even though the velocity decay for this case was well captured. Modeling jets in cross flow at such small velocity ratios may require additional terms in the model due to the different mechanisms controlling such flows. It is known that the deflection of the jet depends on its vertical momentum. In the first two cases, for larger velocity ratios, the jet was allowed a certain region of development before deflection began. In the last two cases, the jet had a very low momentum in comparison to the free stream (not enough to achieve a dominating appearance in the existing flow). This is particularly evident for the jet-to-free stream velocity ratio of 1.5 where the jet was deflected by a strong pressure field set up around the jet by the cross flow. Experimental data gives rise to an apparent shift in the jets origin. The virtual origin of a synthetic jet, at these low velocity ratios, lies downstream of the true synthetic jet position. It was shifted to approximately 0.5 diameters. The jet was deflected before it even had an opportunity to properly exit the orifice which may have changed its angle of ejection from 90 degrees to lower angles. This implies that this particular set of assumed pressure and entrainment coefficients is not valid for velocity ratios of ~2 and lower. A higher pressure-drag coefficient, equivalent to 1.2 as used in continuous turbulent jets, better predicted the deflection with little or no compromise in the velocity decay plots. Trajectory prediction for the jet to velocity ratio of 1.5 with the new assumed coefficients is presented in Figure 5.9.

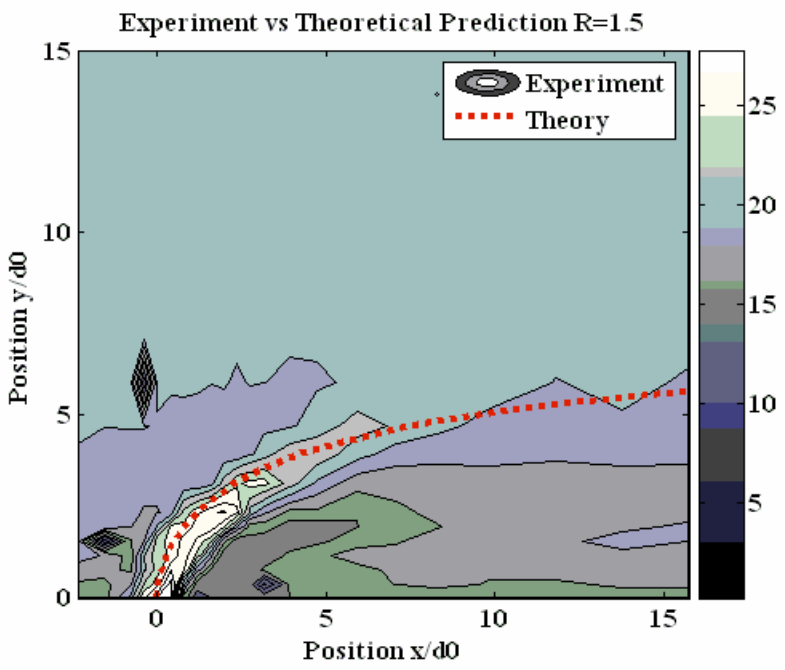

Figure 5.9 Comparison of experimental and predicted jet trajectories for jet to velocity ratios of 1.5 at a modified pressure drag coefficient.

To better visualize the validity of the model, Figure 5.10 presents the superposition of the two sets of data (experimental and theoretical) for the case of the jet to free stream velocity ratio of 2.7. We notice a slight over prediction of the trajectory in the near field region.

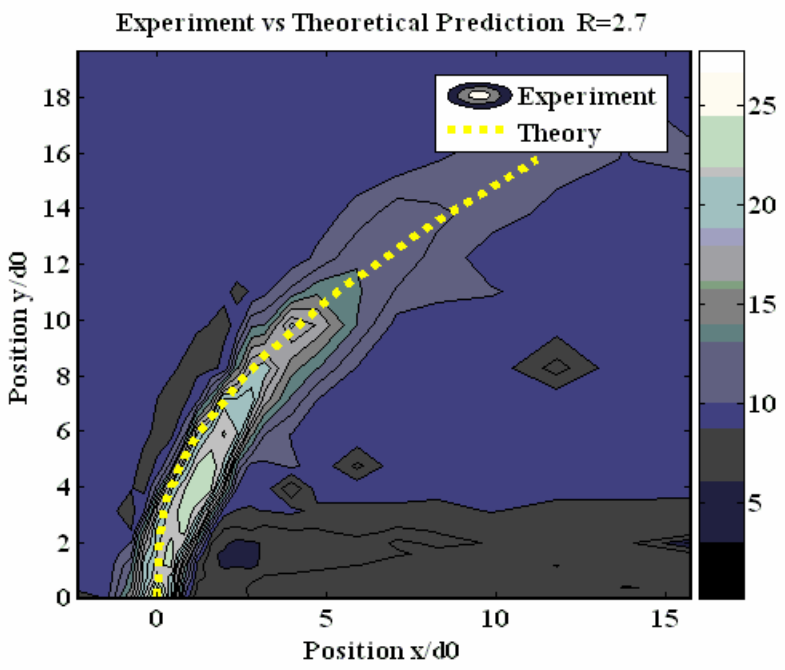

Figure 5.10 Comparison of experimental and predicted jet trajectories for jet to velocity ratios of 2.7.

5.8.4 Jet simulations assuming a constant entrainment rate

For comparison, predictions obtained assuming a constant entrainment rate (along the entire region of jet development) will be presented next to the simulation results that assumed the entrainment rate changing according to the conventional jet laws. For constant entrainment cases, the growth prediction of the jet began much closer to the exit plane which is generally true for a synthetic jet (a synthetic jet is developed from the working fluid in which it is embedded, implying that the entrainment rate in this near field region must be very high). The entrainment rate used in the first set of simulations was defined by an expression for which entrainment was continuously increasing from zero (at the origin) to a certain point (at the end of the hypothetical potential core) after

which the entrainment rate settled. Figures 5.11 and 5.12 compare the jet trajectory and velocity predictions for the two different entrainment rate assumptions. It seems that the constant entrainment rate gives us a better prediction of both the jet trajectory and the diameter growth (especially in the near field region). The velocity decay however, is arguably better represented with the functional entrainment rate but the differences are very small relative to the scatter in the data for both of the approaches.

Figure 5.12 present the predictions of the velocity decay for the two different entrainment rate conditions. The entrainment rate for these cases was obtained from the mean of the functional values used from the modified conventional jet entrainment law.

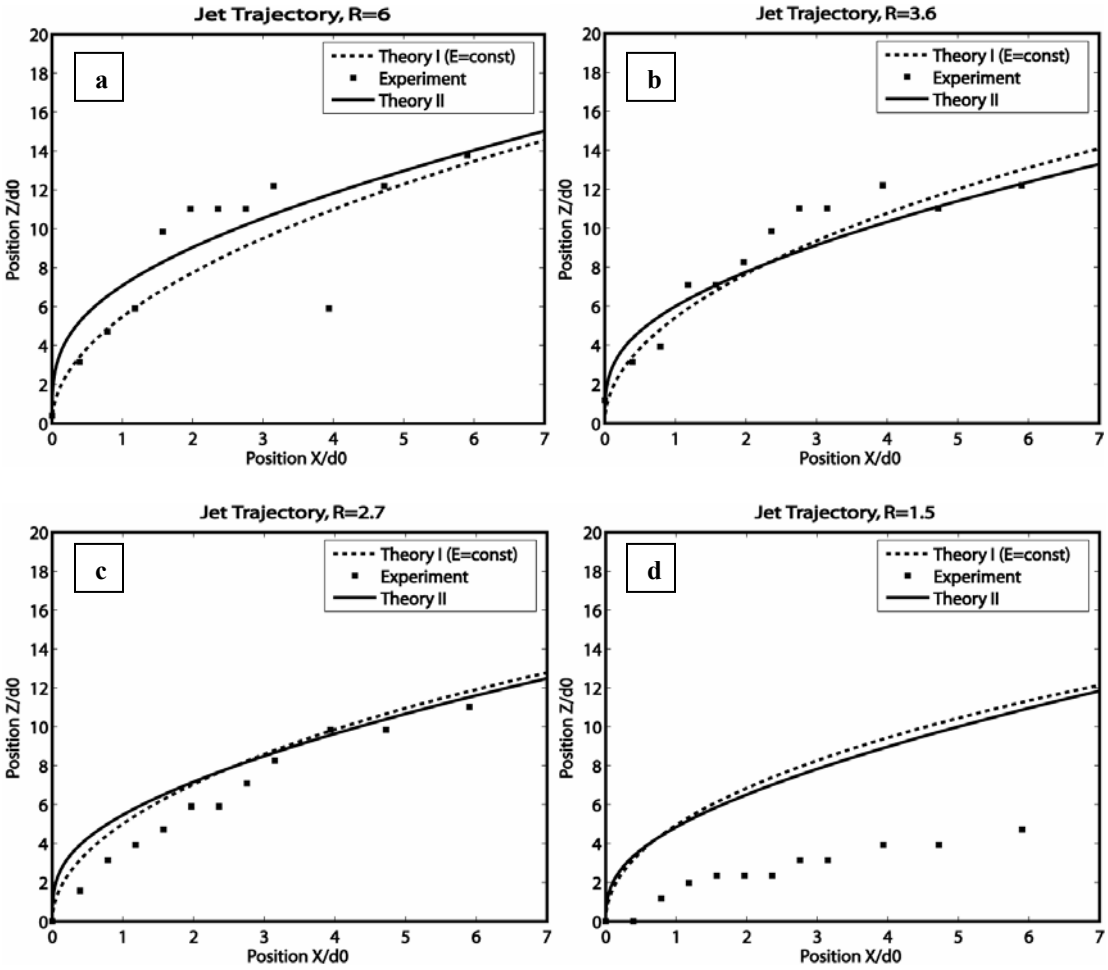

Figure 5.11 Comparison of experimental and predicted jet trajectories for jet to velocity ratios of a) R=6, b) R= 3.5, c) R=2.7, d) 1.5.

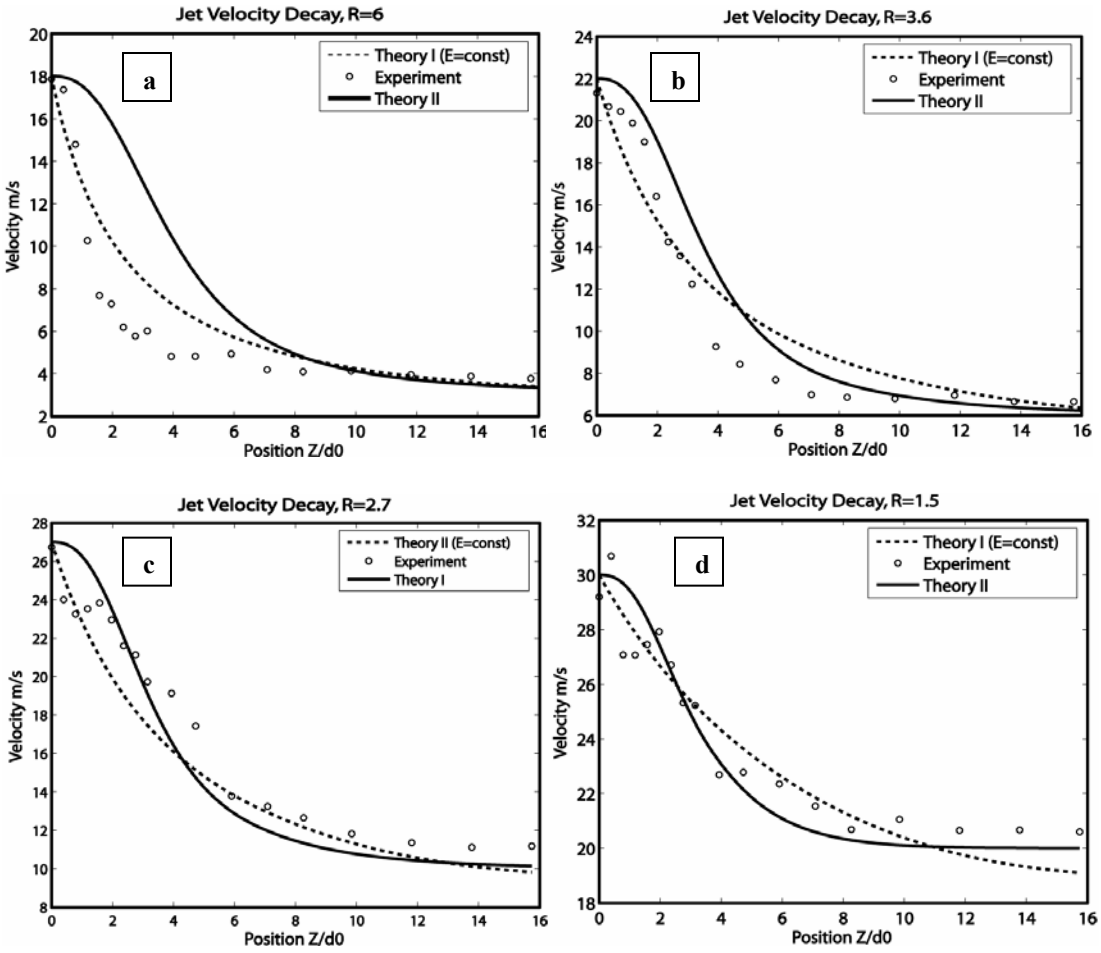

Figure 5.12 Comparison of experimental and predicted velocity decays for jet to velocity ratios of a) R=6, b) R= 3.5, c) R= 2.7 and d) 1.5.

5.8.5 Jet stream tube predictions

Differences in entrainment rate assumptions were evident in the 3D plots of the simulated transverse synthetic jets. Figure 5.13.a and Figure 5.13.c present the jet development prediction for velocity ratios of 6 and 3.6 respectively when assuming that the entrainment changed along the jet with the law similar to the one of continuous turbulent

jets. Figures 5.13.b and 5.13.d. present these jets under the same conditions but assuming an entrainment function that is constant along the jet trajectory. The main difference between these two sets of predictions can be noticed in the near field. The synthetic jet develops faster in this region if the entrainment function is assumed to be constant along the entire path. This agrees better with the typical description of synthetic jets in the near field. They form faster in this region than conventional jets **[Smith, Swift2003]**.

Analyzing the change of the synthetic jet cross section, it was observed that more jet momentum keeps the jet width closer to the original orifice diameter. More momentum also implies less entrainment required by continuity. The jet will, therefore, be wider at increased entrainment or lower momentum. This was verified with our jet stream tube plots presented in Figure 5.13. The jet's width was the highest in the first case (Figure 5.13.a or Figure 5.13.c), the case where the jet had the lowest overall momentum out of all the examples tested.

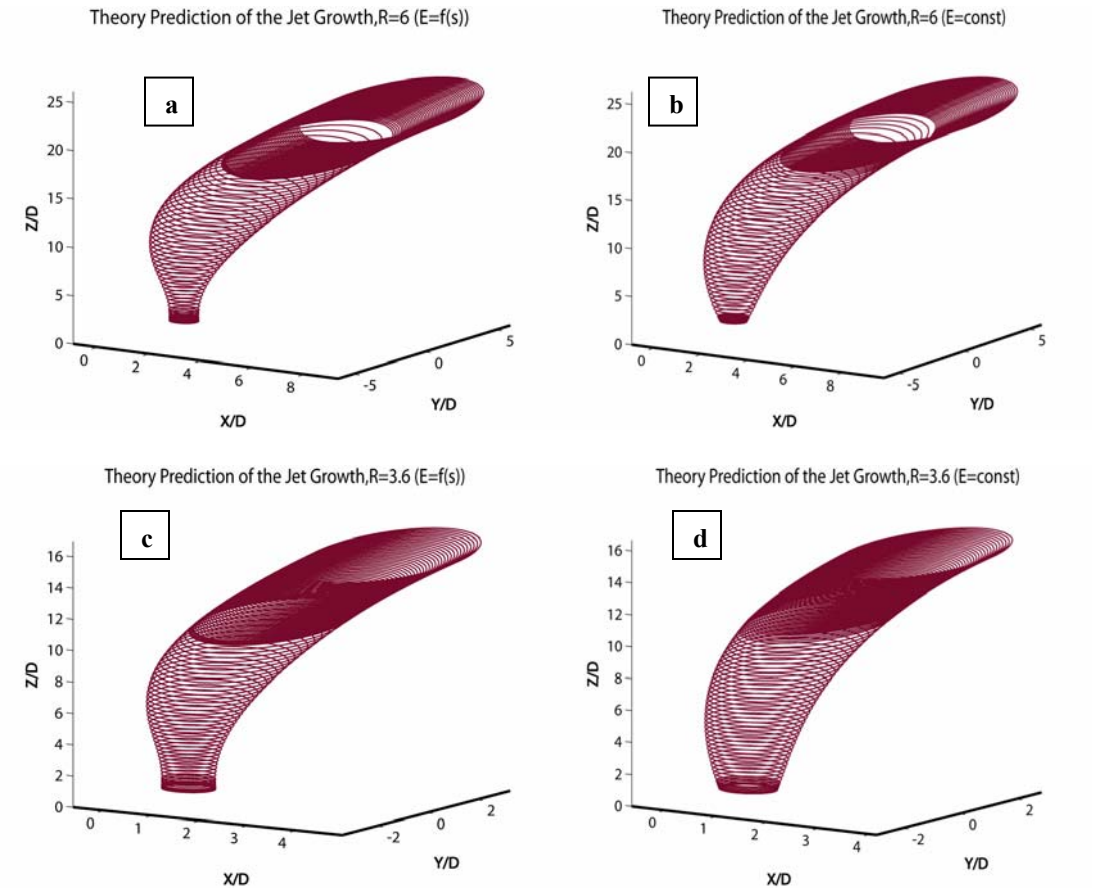

Figure 5.13 Comparison of the jet stream tubes for jet-to-free stream velocity ratios of a) R=6, b) R= 6 (constant entrainment) c) R=3.5, d) R=3.5 (constant entrainment).

5.9 Conclusion

An analytical investigation has been conducted to determine the key parameters affecting the trajectory and flow properties of a synthetic jet discharging into a cross flow of different velocities. The theory was developed using an integral method. Natural fluid mechanisms such as mixing, shear, entrainment and imposed pressure were used to obtain the conservation equations of the jet flow. The suggested model required

information on the entrainment of the cross flow and jet cross section shape. Suitable assumptions based on experimental observation of the jet geometry had to be made. Solving these equations simultaneously yielded predictions of jet trajectory, jet velocity and area growth that agreed well with experimental results. The model was suitable for estimating the location and size of the jet with respect to the orifice location for jet-to-free stream velocity ratios of ~2 and higher. Difficulties occurred in predicting trends for transverse synthetic jets at very low velocity ratios, suggesting different dominating mechanisms influence the jet character.

Results of this investigation show that this analytical approach provides a sound basis for capturing synthetic jet-cross flow interaction. It provided information on direction of motion of a single jet and changes in the jet shape as it was proceeding downstream into the cross flow. This information provides the basis for the model developed in the next Chapter that predicts the loads on a surface due to the jet presence in the flow.

Chapter 6

Prediction of the Induced Pressure Distribution on a Flat Plate due to Synthetic Jet Actuation

6.1 Introduction

This chapter presents a model for calculating the aerodynamic loads induced on a flat plate due to synthetic jet actuation. Prediction tools from Chapter 5 that describe the jet deflection, velocity and cross section as the jet interacts with cross flow were expanded in this chapter to predict the pressure distribution on an aerodynamic surface.

A synthetic jet issuing from a lifting surface was represented using elementary potential flow elements. Sinks and doublets were strategically placed on the theoretically developed jet stream tube. Sinks and doublets symbolize the jet entrainment and blockage effects. Distribution of the velocity, induced by these potential elements, was estimated using the Biot Savart Law. The induced velocity was then used to predict the changes in pressure distribution on the lifting surface produced by the jet. This analysis was based on the model for conventional turbulent jet acting on a rectangular wing developed by Wooler et al. in 1967 **[Wooler1967]**. Considering the approximation constraints, the

validity of using such simplified models to approximate gross changes in loads and moments due to a single synthetic jet actuation will be assessed.

6.2 Elementary Ideal Flows

Uniform flow, source (or sink) flow, doublet flow and vortex flow are four elementary flows that can be superimposed to create more complex flows. Although these represent ideal flows (that are rarely encountered) they are very useful for simulating a variety of fluid motions. The first three will be used for modeling in this chapter and a brief review of their properties is presented next.

1. Uniform Flow- is the simplest possible potential flow. It is a flow with constant velocity and magnitude. Figure 6.1 shows the uniform flow of magnitude V_∞ directed at an angle α to the x axis. Uniform flow can be expressed as: $W(z) = u - iv = V = \sqrt{u^2 + v^2} = const$, where u and v are the velocity components in the x and y direction:

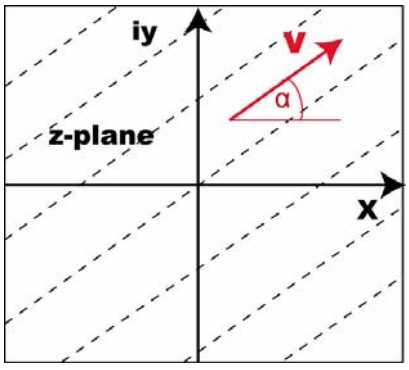

Figure 6.1 Uniform flow

2. Source Flow- is represented by a point of continuous outward flow. Figure 6.2 shows the streamlines directed radially away from the origin which is characteristic of a typical source flow field.

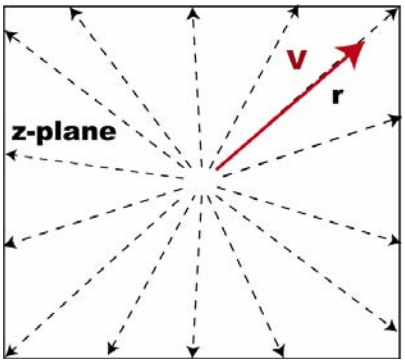

Figure 6.2 Source Flow.

If the source is negative the flow is reversed and the flow field is then called a sink flow field. Strength of a sink flow is defined as the rate of volume of flow into the origin per unit depth and it can be expressed in terms of the radial velocity and the radial distance as $V = \frac{m}{2\pi r}$, where m is the strength of the sink **[Plotkin2001]**. Units for the strength of either a source or a sink are square meters per second, and a strength value can be either positive (for the source) or negative (for the sink).

3. Doublet Flow- is a singularity developed by merging a source and a sink to the same point. As the distance between a source and a sink becomes infinitely small a specific flow pattern, shown in Figure 6.3, is produced. Double lobed circular streamlines

are representative of a typical doublet flow of strength μ. Doublet can be mathematically expressed as: $W(z) = \frac{\mu}{2\pi z^2}$.

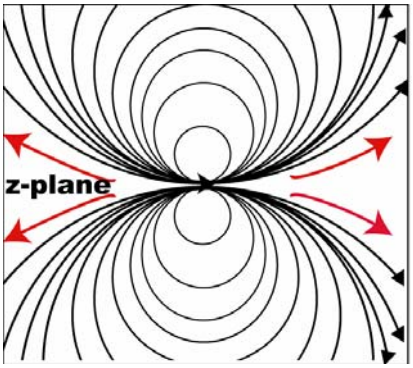

Figure 6.3 Doublet flow pattern.

3.a. Flow over a circular cylinder- a doublet flow can be superimposed on a uniform flow to simulate flow past a cylinder. This type of flow superposition is of particular interest for modeling jets in cross flow because, as was shown in Chapter 5, pressure imposed on the jets boundary can be roughly approximated by modeling the jet as a cylinder obstructing the path of oncoming crossflow. Figure 6.4 illustrates the practicality of adding elementary flows to obtain a more complex flow over a body of interest **[mit.edu]**. The right image in Figure 6.4 shows the flow closing behind the body implying that viscous effects are not included in this analysis. As a result the flow doesn't separate behind the cylinder and the simulation doesn't predict any wakes.

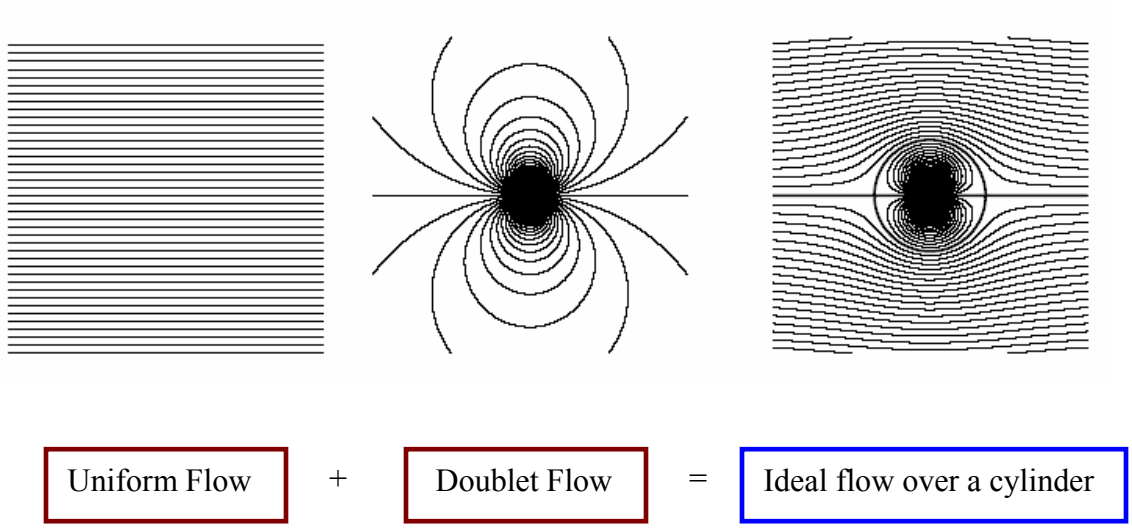

Figure 6.4 Superposition of uniform and doublet flows **[mit.edu]**.

6.3 Blockage- Sink Representation of the Transverse Synthetic Jet

The influence of a synthetic jet on a lifting surface is discussed in terms of the velocities induced by the distribution of sink and doublet flow singularities placed along a surface encompassing the synthetic jet (*S*). The entrainment of the cross flow into the jet was represented by a sink distribution along the jet axis perpendicular to the cross flow. Length of a synthetic jet element was labeled as δs and its sink strength per unit distance in the η direction (direction of the jet width) was given by $\overline{m} = E\frac{\delta s}{d}$ (E is the entrainment function discussed in Chapter 5 and d is the local diameter of the jet) **[Wooler1967, Wu1968]**. Doublets were spaced along the jet trajectory with their axis normal to the jet trajectory in the plane of the paper (see Figure 6.5). Their strengths were defined using

the coefficient in the velocity potential expansion *W(z)* for the two dimensional flow past an ellipse **[Milne-Thompson1968]**. *μ(s)* was labeled the doublet strength. Each of these sinks and doublets contributes to the entrainment-induced and blockage-induced velocity adding up to the total interference velocity. An expression for the velocity components that each of these elements (positioned along the jet boundaries) would induce at a given point on the lifting surface was developed and is presented in the next section.

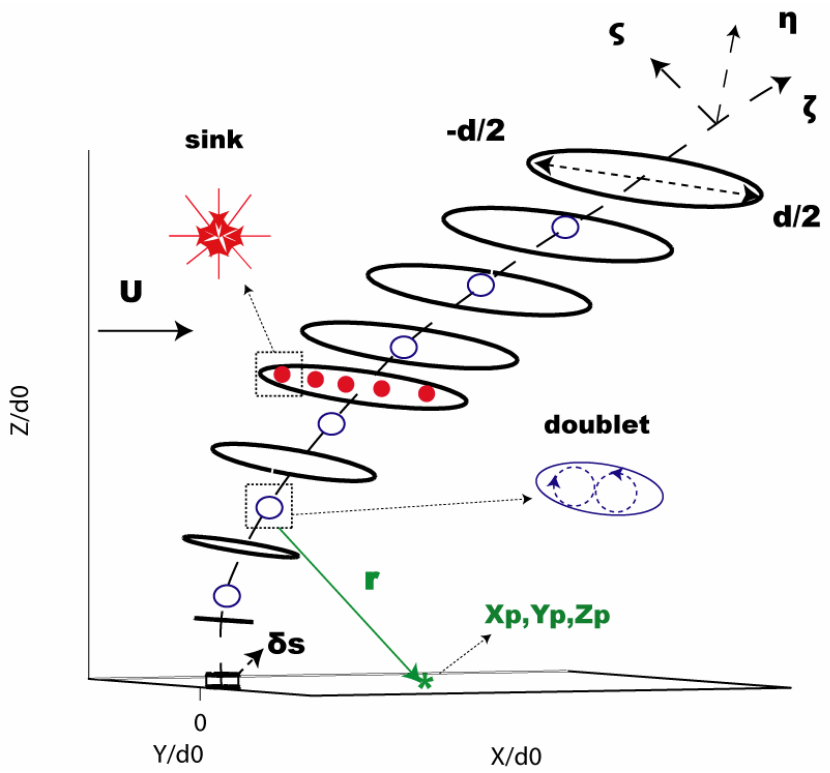

Figure 6.5 Distribution of discrete sinks and doublets along the jet trajectory (d_0 is the initial jet diameter).

6.3.1 Sink Induced Velocity

An *X,Y* and *Z* coordinate system was selected as the orthogonal system for the model axes. The *X*-axis was oriented to coincide with the direction of the cross flow, the *Y*-axis was in the direction of the width of the jet stream tube and the *Z*-axis pointed upwards, perpendicular to the plane of the lifting surface. At a chosen control point $P(X_P, Y_P, Z_P)$, the normal velocity induced by the sink elements was obtained from the Biot Savart Law. The distance vector (shown in Figure 6.5) from the discrete doublet (or sink) located at (*X,η,Z*) to the point of control is expressed as:

$r = \sqrt{(Z - Z_p)^2 + (X - X_p)^2 + (Y_p + \eta)^2}$. The induced infinitesimally small velocity at the chosen point due to the sink element of strength $\overline{m}d\eta$ can be expressed as **[Robinson1956]**:

$$dV = \frac{\overline{m}d\eta}{4\pi\left[(Z - Z_p)^2 + (X - X_p)^2 + (Y_p + \eta)^2\right]} \tag{6.1}$$

Accordingly, three components of this velocity in the direction of the *X,Y,Z* axes are expressed as:

$$\delta u_{s1} = \frac{\overline{m}d\eta(X - X_p)}{4\pi\left[(Z - Z_p)^2 + (X - X_p)^2 + (Y_p + \eta)^2\right]^{\frac{3}{2}}}$$

$$\delta v_{s1} = \frac{\overline{m}d\eta(Y_p + \eta)}{4\pi\left[(Z - Z_p)^2 + (X - X_p)^2 + (Y_p + \eta)^2\right]^{\frac{3}{2}}}$$

$$\delta w_{s1} = \frac{\overline{m} d\eta (Z - Z_p)}{4\pi \left[(Z - Z_p)^2 + (X - X_p)^2 + (Y_p + \eta)^2 \right]^{\frac{3}{2}}} \tag{6.2}$$

Sum of the individual sink effects of the jet element is obtained by integrating these velocity component expressions over the range of the local width of the jet $-\frac{d}{2} \le \eta \le \frac{d}{2}$ resulting in the total induced velocity components $\delta u_s , \delta v_s , \delta w_s$ **[Robinson1956]**:

$$\delta u_s = \frac{-\overline{m}}{4\pi} \frac{X - X_p}{(Z - Z_p)^2 + (X - X_p)^2} \times$$

$$\left[\frac{Y_p - \left(\frac{d}{2}\right)}{\left[(Z - Z_p)^2 + (X - X_p)^2 + \left(Y_p - \left(\frac{d}{2}\right)^2 \right) \right]^{\frac{1}{2}}} - \frac{Y_p + \left(\frac{d}{2}\right)}{\left[(Z - Z_p)^2 + (X - X_p)^2 + \left(Y_p + \left(\frac{d}{2}\right)^2 \right) \right]^{\frac{1}{2}}} \right]$$

$$\delta v_s = \frac{-\overline{m}}{4\pi} \left[\frac{1}{\left((Z - Z_p)^2 + (X - X_p)^2 + (Y_p - (d/2))^2 \right)^{1/2}} - \frac{1}{\left((Z - Z_p)^2 + (X - X_p)^2 + (Y_p + (d/2))^2 \right)^{1/2}} \right]$$

$$\delta w_s = \frac{-\overline{m}}{4\pi}\frac{Z-Z_p}{(Z-Z_p)^2+(X-X_p)^2}\times$$

$$\left[\frac{Y_p-\left(\frac{d}{2}\right)}{\left[(Z-Z_p)^2+(X-X_p)^2+\left(Y_p-\left(\frac{d}{2}\right)^2\right)\right]^{\frac{1}{2}}}-\frac{Y_p+\left(\frac{d}{2}\right)}{\left[(Z-Z_p)^2+(X-X_p)^2+\left(Y_p+\left(\frac{d}{2}\right)^2\right)\right]^{\frac{1}{2}}}\right]$$

(6.3)

6.3.2 Doublet Induced Velocity

The next step required the definition of the induced velocity due to the doublet distribution. Due to the circle to ellipse transformation of the jet cross section as it deflects into the cross flow, the strength of the doublets is given by:

$$\mu = \frac{\pi U d^2}{2}\cos\Theta\left(1-\frac{4}{15}\frac{Z}{d_0}\frac{U}{U_j}\right),\ 0\le\frac{Z}{d_0}\frac{U}{U_j}\le 2.5$$

$$\mu = \frac{\pi U d^2\cos\Theta}{6},\ \frac{Z}{d_0}\frac{U}{U_j}\ge 2.5 \qquad (6.4)$$

Interference velocity at a point due to the presence of a synthetic jet and its blockage effects may be determined by integrating the induced velocity equations over the entire extent of the jet giving the total doublet component velocities. Using the Biot- Savart

Law the induced velocity field at a point *P* due to a doublet of strength μ is given by the velocity components:

$$u_{D1} = -\frac{6\xi\varsigma\mu}{4\pi\left(\xi^2+\eta^2+\varsigma^2\right)^{\frac{3}{2}}}, v_{D1} = -\frac{6\eta\varsigma\mu}{4\pi\left(\xi^2+\eta^2+\varsigma^2\right)^{\frac{3}{2}}},$$

$$w_{D1} = \frac{2\mu}{4\pi\left(\xi^2+\eta^2+\varsigma^2\right)^{\frac{3}{2}}} - \frac{6\mu\varsigma\varsigma}{4\pi\left(\xi^2+\eta^2+\zeta^2\right)^{\frac{5}{2}}} \tag{6.5}$$

$u_{D1,}$ v_{D1} and w_{D1} are the velocities in the jet coordinate direction (ξ,η,ς). Transformation coordinates are given by: $\xi = (X_P - X)\sin\Theta - (Z - Z_p)\cos\Theta$, $\eta = -Y_P$ and $\zeta = (X_P - X)\cos\Theta + (Z - Z_p)\sin\Theta$. The induced velocities δu_D in the *X,Y,Z* directions at a point *P* will then be:

$$\delta u_D = u_{D1}\sin\Theta + w_{D1}\cos\Theta$$

$$\delta v_D = -v_{D1}$$

$$\delta u_D = u_{D1}\cos\Theta - w_{D1}\sin\Theta \tag{6.6}$$

The total interference velocity at a point was obtained by integrating and summing the induced velocity components due to both the sink and doublets over the surface boundary of the jet, giving the total induced velocity components due to synthetic jet activation in cross flow.

6.4 Results and discussion

Experimental results of velocity flow fields induced by several synthetic jet-cross flow interactions presented in Chapter 4 were used to validate the model developed in Chapter 5. This model information was extended in this chapter to predict changes in aerodynamic load distribution stimulated by synthetic jets.

Induced velocity predictions for synthetic jets operating with a jet to cross flow velocity ratio of 6, 3.6 and 2.7 will be presented for flows over a flat plate with a 3 inch chord length, a span of 12 inches and 0.1 of the chord thickness. The model allows the jets to be placed anywhere on the flat plate with respect to the leading and trailing edges, including the top or bottom surfaces. The exit diameter for all the jets considered in this study was the same and was equal to 0.1 inches. Figure 6.6 depicts the induced velocities due to sinks and doublets and the total velocity on a flat plate at three different velocity ratios (R=6 (a), R=3.5 (b) and R=2.7 (c)). In all cases the jet was placed in the middle of the plate (0.5 chord length) on the lower surface. The model predictions show that the jet with the higher velocity ratio induced more downwash. A simplified version of the lifting surface theory will help convert these results into induced loads, a more meaningful indication of synthetic jet potential performance benefits.

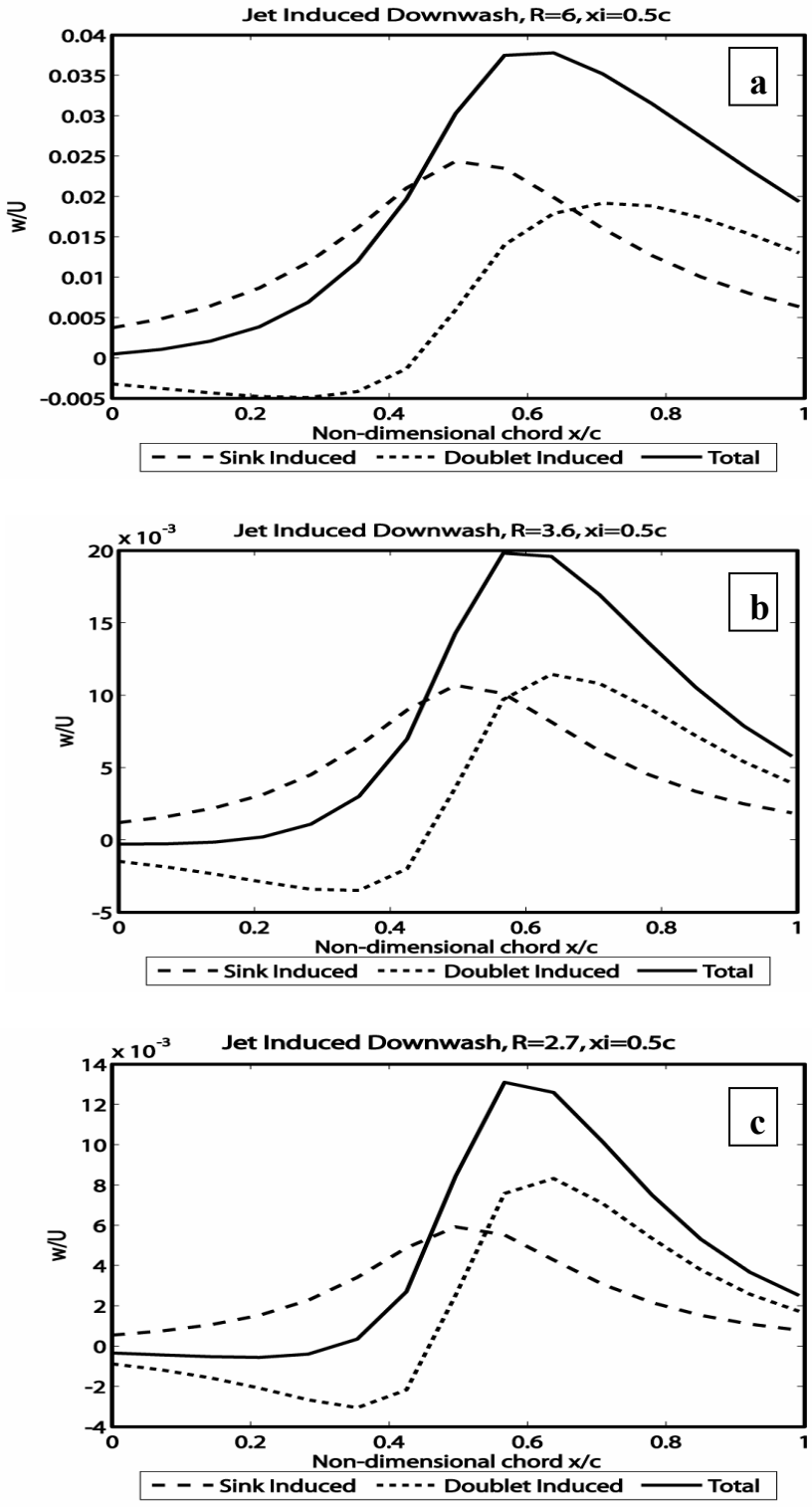

Figure 6.6 Jet induced downwash for a jet placed at the 0.5 chord at three different jet-to-free stream velocity ratios. a) R=6, b) R=3.6, c) R=2.7.

Figure 6.7 shows the total induced velocity at three spanwise locations b/2=0, 0.2 and 0.7 (i.e. at 0, 1.2 and 4.2 inches) on the 12-inch long flat plate due to the presence of a single synthetic jet located at b/2=0. In Fig. 6.7a, the jet is acting at the leading edge and in Fig. 6.7b the jet is at the 0.5 chord length position. The jet to free stream velocity ratio of 6 was used in both cases. As expected in both cases this velocity distribution decreases in strength moving away from the orifice in the streamwise direction and in the spanwise direction.

An interesting phenomenon to observe would be the change of this distribution as two or more synthetic jets were positioned on the flat plate, either aligned or placed at an angle to the synthetic jet observed. The spanwise distribution of such synthetic jet arrays would be much different and much more authoritative than a single jet. This is considered an important part of the future work that can readily be investigated through application of the current model.

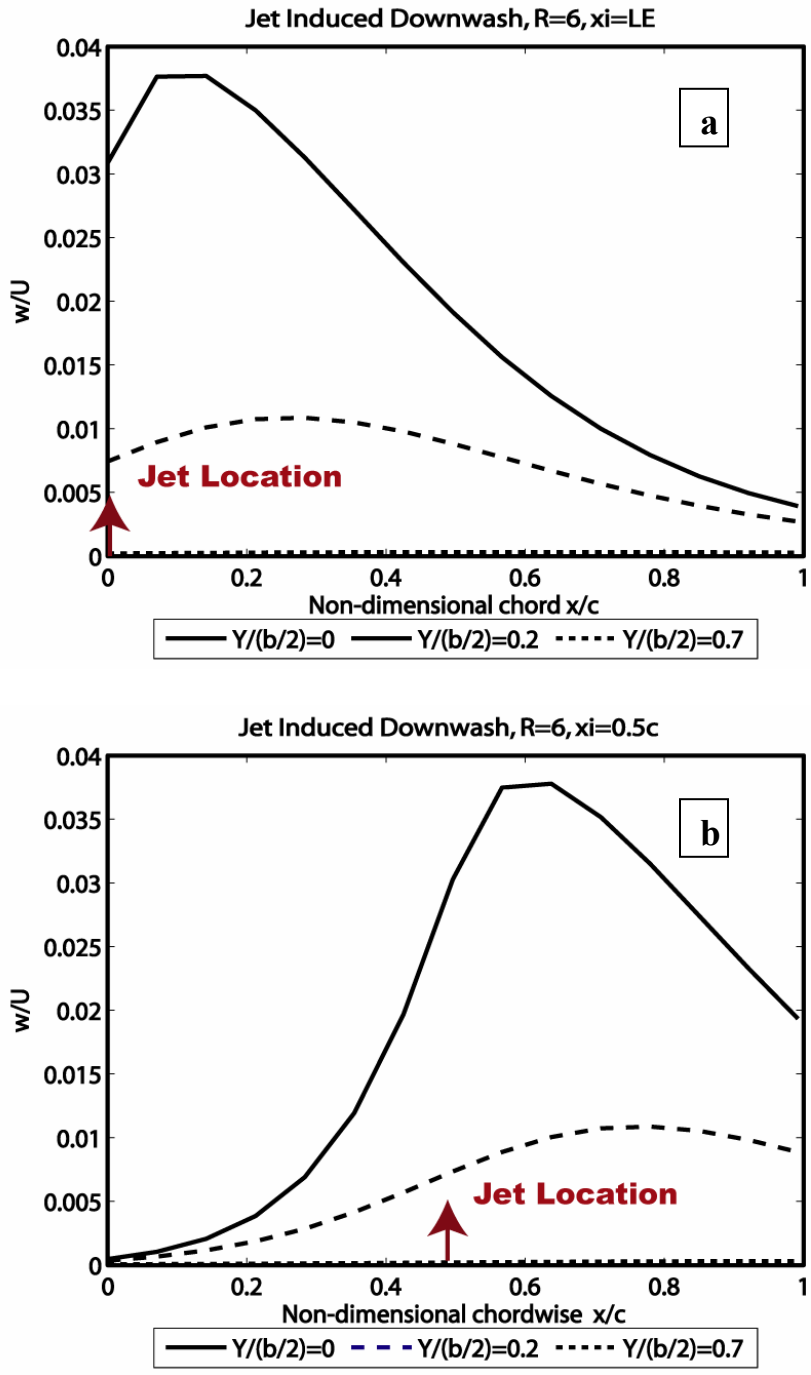

Figure 6.7 Jet induced downwash for a jet placed at the leading edge (a) and 0.5 chord (b) at three different spanwise locations (b/2=0, b/2 = 0.2 and b/2 =0.7).

6.5 Lifting surface theory

The objective of this section is to demonstrate the effectiveness of representing a transverse synthetic jet with elementary potential flow elements, providing induced velocity information that can be used as input to surface lifting theory programs. Using a simplified version of the lifting surface theory (a single chordwise control point), jet induced velocity (acting as an effective change in camber) will be used to relate the jet-induced virtual wing surface to the pressure distribution. It was assumed that the induced velocity due to the activation of the jet acted to modify the local incidence angle. Downwash at a point on a surface was then equated to the wing loading. The method used here to determine the loading distribution was the subsonic lifting surface theory developed by H. Multhopp **[Multhopp1950]**. Section 6.6 and Section 6.7 present the highlights of this method. Key features that are needed for application to predicting the influence of a single jet on the flat plate used in Section 6.4 will be summarized.

A full pressure distribution induced by multiple jets would require a lifting surface program that includes several chordwise and spanwise modes. Once synthetic jet array interactions are reasonably well modeled, predicting the induced aerodynamic loads should be trivial. A variety of commercially available programs that tackle similar and even more complex problems already exist.

6.6 The integral equation of the lifting surface

The downwash integral is presented as follows:

$$\alpha(x,y)=\frac{-1}{8\pi}\iint_S \frac{l(x_0,y_0)}{(y-y_0)^2}\left(1+\frac{x-x_0}{\sqrt{(x-x_0)^2+(y-y_0)^2}}\right)dx_0dy_0 \qquad (6.7)$$

This relationship explains the connection between the velocity field and the pressure field around a body. It was obtained by combining the continuity equation with an appropriate form of Euler's equations of motion. The pressure field was equated to the enthalpy field (*I*). Equations were differentiated such that continuity could be represented in the regular Laplace's form (aerodynamic loading for thin wings is described with a sheet of doublets representing a discontinuity surface in the enthalpy potential field which satisfies the Laplace equation) **[Multhopp1950]**. An approximation of the elementary field is obtained, which enabled the replacement of the curved sheet of the wing by its projection on the plane z=0: $I(x,y,z)=\frac{-zU^2}{8\pi}\iint_S \frac{l(x_0,y_0)dx_0dy_0}{\left[(x-x_0)^2+(y-y_0)^2+z^2\right]^{\frac{3}{2}}}$. The flow at a point *z=0* must be the same as the actual flow at the same point on the wing **[Anderson1991]**. If the local incidence $-\frac{\partial z}{\partial x}$ of the surface at this point is α then the following relationship holds: $\alpha=\frac{-w}{U}$. Integrating a component of the Euler's equation: $w(x,y,z)=\frac{-1}{U}\int_{-\infty}^{\infty}\frac{\partial I}{\partial z}(x',y,z)dx'$, provides the final expression for the downwash as given

at the beginning of this section. It is an equation that, once solved, provides a total downwash distribution (α) of the wing for a given load distribution $l(x_0, y_0)$. For a known downwash distribution, Muthopp developed a method to solve for the load distribution by reducing the above integral to a set of linear equations.

6.7 Multhopp's method for solving the downwash velocity integral

The surface of a wing is divided into predetermined spanwise and chordwise sections. Aerodynamic loads and moments are calculated from a set of linear equations satisfying the downwash conditions at the user specified control points in each of those sections. The choice of control points on the wing surface at which the boundary conditions of the integral equations had to be satisfied is important. Based on lifting line theory, the optimized spanwise distribution of the control stations is attained by equally dividing a semi circle over the wing span (Figure 6.9).

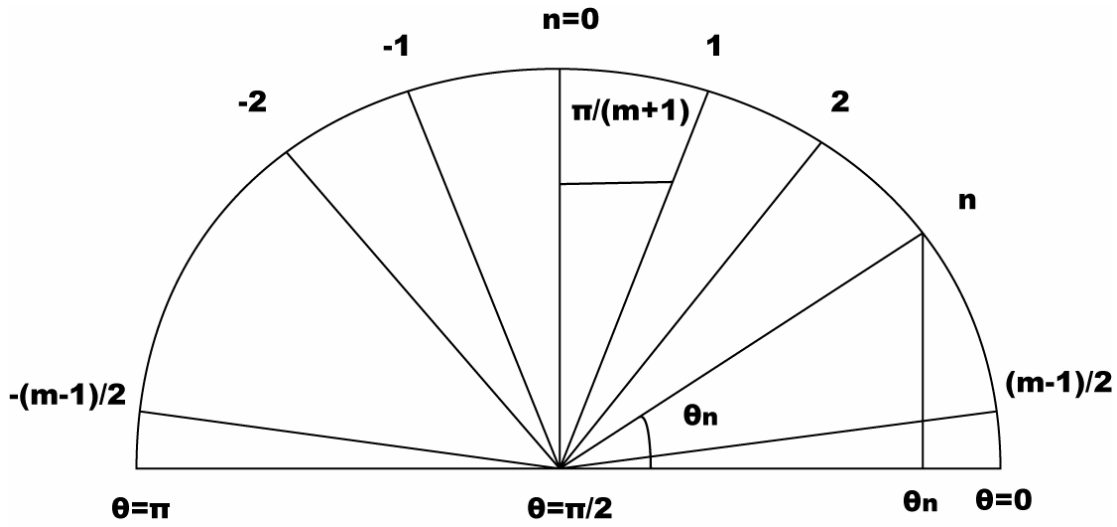

Figure 6.9 Equidistant subdivision of the angular co-ordinate range

As for the chordwise stations, it was established that if only one point was used it would be best to place it in the rear part of the wing as this section counts more than the front parts **[Muthopp1950]**. A more detailed load description would require more than one chordwise control point and in such cases the distribution of these points would have to be considered more carefully.

Muthopp suggested performing the chordwise integration first in order to bring the final integral closer to the well known form of the downwash integral of the lifting line theory. As in the two-dimensional airfoil theory, a Fourier series representation was assumed for the chordwise load distribution: $l = a_0 \cot\frac{\varphi}{2} + \sum_1^\infty a_n \sin(n\varphi)$, where φ is the angular chordwise coordinate ($\varphi = \cos^{-1}(1-2X)$). For the case of a single control point, the chordwise load distribution was expressed as $l_0 = a_0 \cot\left(\frac{\varphi}{2}\right)$, giving the lift coefficient $C_L = a_0 \frac{\pi}{2}$. An influence function *i* was obtained by relating the chordwise part of the downwash integral (with the load distribution l_0) to the lift coefficient value at y_0:

$$i(x, y, y_0) = \frac{1}{C_L c} \int_{x_{0L}}^{x_{0Y}} l(x_0, y_0) \left(1 + \frac{x - x_0}{\sqrt{(x-x_0)^2 + (y-y_0)^2}} \right) dx_0 \qquad (6.8)$$

(In order to be able to determine the pitching moment along with the lift coefficient, naturally at least two chordwise points were needed.) The influence function was

calculated numerically and graphically and the results of these calculations were given by Multhopp in a series of diagrams and tables **[Multhopp1950]**. Using these influence functions the downwash integral was transformed into a more familiar form, the one of lifting line theory. A non-dimensional lift per unit span (circulation) was defined: $\gamma = \frac{C_L c}{2b}$ and along with the new above defined influence functions the downwash integral was re-written in non-dimensional units. Different interpolation functions ($g_n(\theta)$) were used to find the non-dimensional lift per unit span $(\gamma \cdot i)$ between the limited control stations. The non-dimensional lift per unit span was finally written as: $(\gamma \cdot i) = \sum_{-\frac{m-1}{2}}^{\frac{m-1}{2}} (\gamma \cdot i)_n g_n(\theta)$. $(\gamma \cdot i)_n$ is the value of $(\gamma \cdot i)$ at the interpolation station and $g_n(\theta)$ the interpolation function belonging to the same station. With some manipulations and in agreement with the lifting line theory the downwash at one of the spanwise stations (v) was written:

$\alpha_v = b_{vv}(\gamma \cdot i)_v - \sum_{-\frac{m-1}{2}}^{\frac{m-1}{2}} b_{vn}(\gamma \cdot i)_n$, where $b_{vv} = \frac{m+1}{4\cos\frac{v\pi}{m+1}}$ and $b_{vn} = \frac{\sin\theta_n}{(m+1)(\cos\theta_n - \cos\theta_v)^2}$,

m is the number of spanwise control points.

With this method the integral equation of the lifting surface was satisfied at a limited number of control stations. The above equations were taken as systems of equations to determine the non-dimensional lift per unit span with the downwash

α_v being equal to the given local incidence angle. In this case the local incidence angle was the one obtained from Biot Savart Law in the first part of this model.

This technique was applied to determine the gross value of the change of the lift coefficient with the angle of attack $\left(\frac{dC_L}{d\alpha}\right)$ of a 3 inch chord and 12 inch span flat plate. This coefficient was estimated to be about 5 per radian. If the effects of the synthetic jet presence were taken into consideration by considering the jet induced downwash plots at the given chordwise station, this coefficient increased to 5.18 per radian. While a relatively crude approximation, these results demonstrates the usefulness of such an analytical approach. Clearly a more detailed lifting surface program with significantly more chordwise stations would better capture the downwash distribution and its effects.

This modeling approach can readily be extended to include the effects of multiple synthetic jets and their interactions with one-another and their influence on the total downwash induced on such surfaces. Once these issues are incorporated, phenomena like antisymmetric loading including rolling moments due to a sequence of synthetic jet actuation could be predicted.

6.8 Conclusion

Analytical advancements that will facilitate the optimization of synthetic jet actuation operational levels, their placements and sequence of actuation are of significant

technological importance. The method developed in this chapter is the first step towards realizing such an optimization tool for maximizing the benefits of the synthetic jet actuator technology.

Elementary two dimensional flows were used to represent a transverse synthetic jet. A set of discrete sinks and doublets was strategically positioned along the jet trajectory to account for the entrainment and pressure effects due to the activation of the synthetic jets in uniform cross flows. The strength of these elements was deduced from the experimental data. Using the Biot Savart Law and these abstract flow concepts, the interference velocity induced by synthetic jets was predicted and presented. A general and convenient method developed by Multhopp was then used to explain the significance of these jet-induced velocities. By treating the downwash distribution as an effective surface camber, lifting surface theory was effectively used to predict the induced pressure distribution on the wing and thereby allow for prediction of aerodynamic loads and moments. The foundation of the lifting surface theory is the downwash integral. Multhopp treated this integral in two stages: chordwise integration (performed first) and spanwise integration. The end-result was a linear system of equations with the lifts and moments per unit span at certain spanwise stations left as unknowns. The coefficients of this system, depending partially on the geometrical data and the arrangement of user specified control points, were then easily calculated. A small but significant percentage in increase in lift was demonstrated by using the most simplified version of the lifting surface theory. Future work lies in predicting the jet induced downwash for a series of jets and using a more involved lifting surface theory that will better capture the details of

these induced velocity distributions. The flow in the wake hasn't, in this particular work, been given the deserved attention although the elementary flows could potentially be placed in the region behind the jet to model these effects as well.

Chapter 7

Conclusions

Synthetic jet actuators are simple devices. They consist of an enclosed cavity with a moving surface replacing one or more of the cavity walls. When properly excited, the wall motion creates pressure changes that continuously push air in and out of the cavity through an orifice located on one of the chamber walls. Synthetic jet formation and evolution is very dependent on the relative strength of the flow into and ejected from the cavity during each cycle. Synthetic jets studied in the literature usually operate at a relatively high Reynolds and low Strouhal numbers, a combination important for generating jets with high directivity and high momentum flux (i.e. good for dynamic virtual shaping). For near wall control, a different operational mode appears to be required. For example, for turbulent boundary layer control, actuators with low Reynolds numbers and high Strouhal number, i.e. velocities on the order of the turbulent friction velocity, may be needed to keep the jet from blowing through the boundary layer.

The strength and the overall character of a synthetic jet will highly depend on the capabilities of the actuator driver. The size of the cavity and the ratio of its geometry to the orifice diameter also play a significant role in the synthetic jet dynamics. Finally, as

the air is pushed periodically through an orifice, the size and shape of the specific opening can induce unsteadiness and compressibility effects adding to the complex behavior of these devices. The importance of the adequate actuator design for the formation of a synthetic jet has therefore been a very important issue and most of the published work to optimize synthetic jets has been directed towards the comprehension and modeling of the dynamics of this coupled fluid-structural behavior.

Current and past research on synthetic jets typically involved three broad research areas: (i) improving the capabilities of different types of drivers used as the active part of the actuator, (ii) understanding the effect of scaling and geometry parameter ratios on synthetic jet formation and (iii) understanding the operational conditions and location of these actuators for beneficially modifying flows over arbitrary lifting surfaces. The contribution of the research presented in this dissertation focused on the last two research areas. Experimental and analytical approaches have been developed to advance the understanding of miniature high frequency synthetic jet actuators on fully attached flows.

Previous work has demonstrated that synthetic jets operating at frequencies of approximately the same order as the frequency of flow instabilities in a flow field and placed closely to the point of separation would have the highest effect on delaying and/or preventing separation. Fewer publications have been found on the effectiveness of using synthetic jets for adaptive lifting surfaces. For that reason, the main question motivating the issues addressed in this work is: can synthetic jets, when placed strategically on a

lifting surface, produce an effect equivalent to that of control surfaces thereby produce an effective shape change in an aerodynamic surface?

Investigation of the design performance of synthetic jet actuators needed to manipulate fully attached flows and to change the load distribution on an arbitrary lifting surface at low angles of attack was the focus of Chapters 2, 3 and 4 of this dissertation. Development of modeling tools needed for assessing synthetic jet influence on aerodynamic lifting surface loads was the focus of Chapters 5 and 6.

7.1 Summary of Research

Chapter 2: Synthetic Jet Actuator Design and Fabrication

Governed by the control strategy and the chosen platform, THUNDER, 32-mm diameter disc unimorphs were chosen as the primary driver of the actuators designed and manufactured in this research. The resonant frequency of these particular cylindrical THUNDER actuators was approximately 2200 Hz with maximum exhibited displacements of 0.13 mm at 150 volt peak to peak excitations. Due to the limited capabilities of the membrane and the project objectives, the overall thickness of the actuator did not exceed 10 mm.

As suspected, each new actuator design actuator had to be accurately characterized before it could be successfully applied to influence external flows. Data on similar devices did not exist in the literature, so to optimize their efficiency, investigations on some of their characteristics were conducted in this chapter. Synthetic jet actuator geometries were varied and tested over a range of frequencies.

Synthetic jet actuator systems were represented by a two-degree of freedom model to better understand the relationship between its two fundamental frequencies. The closer the two resonant peaks of the frequency response, the more efficient the actuator performance. Changes in the cavity or orifice parameters altered the acoustic characteristics of the device but inclusion of compressibility effects, viscous and orifice losses effects had to be properly accounted for as well. Viscous effects had the capability to suppress the effect of the Helmholtz resonance, deteriorating the overall performance. Orifice sizing was particularly important as viscous effects were most sensitive to orifice geometry parameter ratios. Comparison of various geometry parameter ratios alone was not sufficient to predict the jet velocity or its impact on the surrounding flow. The frequency response of the actuator, unsteadiness effects and viscous effects had to be understood and taken into consideration when stating facts about the performance and capabilities of any newly designed synthetic jet actuator.

Chapter 3: Synthetic Jet Analysis in Quiet Conditions

The velocity fields produced by a number of different synthetic jet actuator configurations in inert external conditions (i.e. no cross flows) were measured using a traversing constant temperature anemometer sensor. Non-dimensional formation parameters, like the Strouhal number and the Reynolds number, were used to explain the observed unsteadiness effects. For a given Reynolds number a distinct formation of a directed jet was observed for a range of Strouhal numbers below approximately two, while for large Strouhal number, of two and higher, the majority of the ejected fluid was drawn back into the cavity during the suction stroke. Barely any indications of the jet were noticed above the Strouhal number of four. For high Reynolds numbers and relatively higher Strouhal numbers occurrence of very incoherent structures was observed. Velocity decay rates as a function of different geometry parameters were investigated and recorded in velocity contours plots. Insights based on the actuation performance trends for these non-dimensional actuator parameters should be useful for future actuation design considerations.

Chapter 4: Synthetic Jet Analysis in Cross Flow Conditions

Individual actuators were placed in cross flows. Major non-dimensional operating parameters of interest were the jet-to-free stream velocity ratio and the jet diameter to boundary layer thickness ratio and their effect on the flow field structure. Synthetic jet actuators were studied in several different cross flows: 3, 6, 10, 15 and 20 m/s. The jet velocities tested ranged from 10 to 25 m/s. The orifice diameter of the actuator ranged

from 1 to 7.5 mm. As expected, in all cases, intense mixing between the jet and cross flow caused a very complicated flow interaction near the orifice and at distances downstream. More obvious intrusion of synthetic jets were seen at high velocity ratios (one and higher). At low velocity ratios (one and below), the flow inside the orifice was overpowered by the cross flow and the ejected jet didn't have enough momentum to escape the boundary layer. This caused almost an immediate deflection of the jet and less drastic disruption of the main flow field.

The thickness of the boundary layer and the size of the orifice were also seen as important contributors to the behavior of the synthetic jet in cross flows. A very small diameter was detrimental as it influenced the mass flow free passage and very large diameter on the other hand represented unacceptably large opening on the surface. The change of the diameter of the orifice also changed the Strouhal number magnitude so it was important to take this effect into consideration.

Lastly the effect of the jet-to-free stream velocity ratio on the jet's spreading rate and consequently the change in their circumference and area was assessed. Velocity flow fields of jet cross sections were measured at several locations downstream of the orifice for different velocity ratios. The jet shape changed from a circle to ellipse as it progressed downstream and as the velocity ratio decreased. The circle to ellipse transformation was more pronounced for lower velocity ratios.

Chapter 5: Modeling of Synthetic Jet in Cross Flow

A simplified model offering the ability to investigate the sensitivity of the character of the flow field produced by synthetic jets in cross flow to jet velocity, location and jet diameter was developed. A control volume concept and integral techniques were used to monitor the global quantities along the jet centerline. The model required assumptions to be made about the jet cross sectional shape, entrainment rate and surface forces coefficients. Jet velocity deficit prediction, jet growth and the trajectory were only accurately presented if both the effects of entrainment of the cross flow by the jet and the effects of the pressure exerted by the cross flow on the jet boundaries were included. The relative importance of the pressure drag and the entrainment rate were shown to be of the same order of magnitude.

Predictions of jet trajectory, velocity decay and area growth agreed well with experimental results. Model validation demonstrated the usefulness of the theory for estimating the location and size of the jet with respect to the orifice location but only for jet to free stream velocity ratios of ~2 and higher. Difficulties occurred in predicting flow fields responses to transverse synthetic jets at very low velocity ratios due to the different importance of the dominating mechanisms under these circumstances.

Chapter 6: Predicting the load distribution on a surface due to the synthetic jet actuation

Development of the models in Chapter 5 made it possible to work on development of a simplified mathematical model for capturing synthetic jet actuator effects on the global flow field properties and in particular on surface pressure distributions. A combination of doublets and sinks, representing the synthetic jet entrainment and blockage effect, were placed along the jet trajectory predicted using the Chapter 5 model in order to determine the velocity induced by these potential elements on a lifting surface. The Biot Savart Law was used to determine the total interference velocity. Downwash induced due to the presence of the jets was used as an effective measure of the virtual camber in the lifting surface integral and used to estimate the aerodynamic loads. A small percentage in the lift increase was demonstrated by using the simplified version of the lifting surface theory developed by Multhopp.

7.2. Major Contribution of this Research

Four major contributions of this research were found in:

(i) Adding to the synthetic jet experimental data base by designing and manufacturing high frequency synthetic jet actuators and characterizing them in quiet conditions. Detailed experimental and theoretical analysis of the frequency response functions of these actuators was provided and integrated with non-dimensional parameter

analysis. Viscous and compressibility effects associated with small scale-high frequency synthetic jet actuators were assessed and compared with the observations on larger scale, lower frequency devices.

(ii) Experimentally analyzing the effect of these synthetic jets on fully attached flows developed over a flat plate to investigate the authority potential needed by synthetic jet actuators for manipulating fully attached flows. Literature has speculated that the power needed by synthetic jets to successfully operate under these conditions was on a much higher level than investigated to date. This work provided more detailed information on the needed order of magnitude of such intensities with respect to the strength of the underlying boundary layer.

(iii) Developing a simplified model of transverse jet predictions to facilitate parameter sensitivity studies and advance optimization and real time feedback control aspects of synthetic jet actuation technology. Similar models of jet crossflow flow interactions have not been addressed in literature. The model developed in this dissertation established the analytical foundation for the development of mode complex models that can tackle issues such as simulations of multiple jet interaction.

(iv) Applying a lifting surface theory model to predict the load distribution on a given surface due to activation of a single synthetic jet actuator. Using potential flow elements to model the synthetic jet-cross flow interference and demonstrating the ability

to simulate aerodynamic loads due to synthetic jet actuation has, to the author's knowledge, been the first such attempt in estimating the authority of synthetic jets on this level. The utility of this approach lies in the flexibility of expanding this model to simulate symmetric and asymmetric loads and moments due to the presence of strategically positioned synthetic jet arrays.

7.3. Future Research Needs

1. Synthetic Jet Actuator Characterization Improvements- miniature high frequency synthetic jet actuators were characterized in this project using a constant temperature anemometer. Global, time averaged and phase averaged data was collected and presented as a function of various geometry and structural parameters. To obtain a better understanding of the transient behavior of these devices it would be more beneficial to obtain phase locked information of synthetic jets developed under these different conditions. Signal triggering, PIV methods or high speed camera flow visualization would all provide very interesting, detailed properties of these flow fields.

2. Synthetic Jet Actuator Interaction- if phase locked measurements were available a detailed analysis of mutual interaction of synthetic jets could be carried on, significantly augmenting our understanding of these actuators and the potential for active flow control application. Synthetic jets will be used in arrays, not as isolated synthetic jets. Of particular interest would be investigating the spacing

and relative angle of location of different synthetic jet actuators. It would be particularly interesting to find out if a combination of these actuators could be used to form the regions of recirculating flow talked about in this dissertation. For an example, it seems that one of the actuators could be used to separate the flow and the actuator placed behind it, operating out of phase, could be used to reattach the flow. The size of this region of flow between the two actuators could be changed depending on the spacing of the actuators. A vast combination of similar manipulations of location and phase angles is available and has yet to be investigated.

3. Improvements in the Transverse Synthetic Jet Modeling- frequency actuation needs to be more carefully considered and incorporated as part of this model, as does change in jet responses for differently shaped orifices. Another important challenge for future work is as a first step, in modeling two synthetic jets in cross flow as a function of orifice spacing and position. Entrainment functions of such flows would be very different than of the single jets and require significant considerations.

4. Expanded Lifting Surface Program- lifting surface theory applied in this work was extremely simplified and crudely approximated. One chordwise point was used applying information on the jet induced downwash at only that point on the surface. Several points along the chord have to be used to get a better estimate of the effect of these actuators on the overall load distribution. Only a single actuator

acting over the entire surface was considered in this model. This of course could be extended once the mutual interaction of synthetic jets is understood and the induced downwash due to the array of these jets is known. Asymmetric loading could then also be included in this analysis to determine the maximum moments induced on the lifting surface due to the sequence of synthetic jet actuation. Addition of another set of sinks to create an "afterbody" representing the wake region needs to be added for a better jet influence description.

5. Experimental Array Validation Studies- once the model has been extended to an array of actuators and operational configurations, experiments to validate these findings should be conducted. Confidence in the validity of the model would then allow us to identify the arrangement and operational mode of these arrays to achieve optimum aerodynamic loads and moments on the given lifting surface.

APPENDIX A

Geometry Effects of the Synthetic Jet Actuators on Synthetic Jet-Cross Flow Interactions

Detailed parametric study of synthetic jet actuators in quiet (zero cross flow) conditions was conducted and presented in Chapter 3. Chapter 4 focused on studying the flow topology of synthetic-jet cross flow interaction particularly highlighting the character of such mixing structures as a function of jet-to-free stream velocity ratio and boundary layer thickness-to-orifice diameter ratio. In addition detailed analysis was performed on studying the effects of the geometry parameters on the flow structure above the orifice when embedded in various strength cross flows. Due to the strong resemblance in trends that were observed for actuators this discussion is presented as an addendum to supplement the results presented in Chapter 4. Features associated with the development of synthetic jets in cross flows of 10, 15 and 20 m/s are presented in this Appendix as a function of various actuator orifice and cavity parameters.

A.1. Orifice Length Effects

The length of the orifice was varied from L/D = 0.16 to L/D = 0.48 while other geometric parameters were held fixed. Figure A.1 shows flow fields due to three different synthetic jets exhausting in 20 m/s cross flow next to the velocity contour plots of the same synthetic jet actuators in quiet conditions. As the length of the orifice increased so did the shear effect inside the orifice, increasing the boundary layer displacement thickness and restricting the synthetic jet mass flow. Larger orifice length for these designs did not influence the peak mean velocities as much as it influenced the penetration length of the synthetic jet. Quiet condition data also exhibited this effect displaying a synthetic jet restricted to a close wall region in the case of higher L/D. This effect was also manifested in the penetration capabilities of these actuators into the 20 m/s cross flow. For the smallest L/D case vortex breakdown occurred further downstream. The concentration of energy was spread out over a larger area above the orifice and the jet was then more susceptible to deflections in the presence of external cross flow. This trajectory had the lowest slope of all three cases, a sign of a weaker jet. As the length of the orifice increased, the energy of the synthetic jet was concentrated to a smaller region closer to the jet exit plane. The jet was able to significantly oppose the cross flow momentum which is reflected in the length of its strong vertical direction in the flow for the last two cases. The penetration length, however, was significantly reduced (by almost two times) for the largest L/D. The case with the length to diameter ratio of ~0.3 had the highest ability to force its way through non-zero cross flow conditions. Generally, in comparison to quiet conditions flow fields, presence of the cross flow reduces the penetration length of synthetic jets.

a)

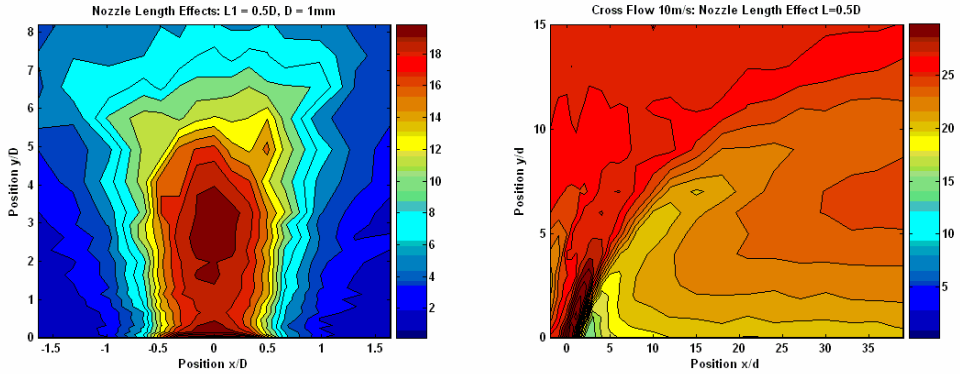

b)

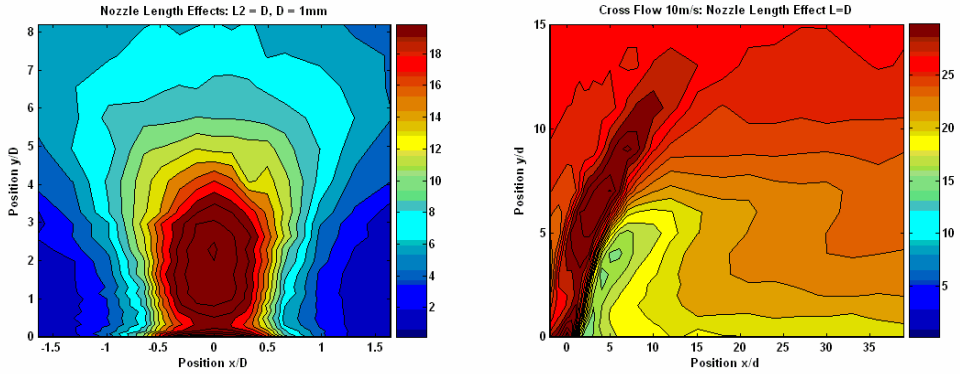

c)

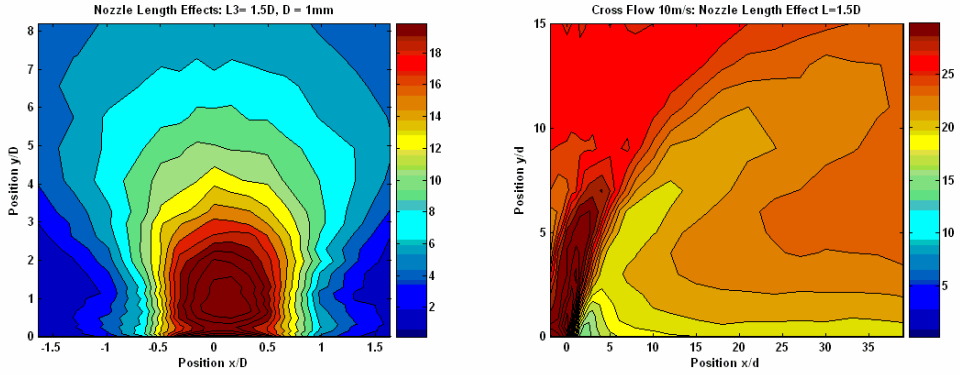

Figure A.1 Velocity contour plots of synthetic jets under quiet conditions (left column) and in 20 m/s cross flows (right column) at different actuator nozzle lengths. a) L/D=0.16, b) L/D=0.3, c) L/D=0.48.

A.2. Cavity Height Effects

Ingestion of higher momentum fluids by the synthetic jet (in the case of the external cross flow presence) could reduce the amount of any existing dead volume inside the cavity, improving the cavity's energy level and theoretically creating a stronger jet. The influence of the cavity height on synthetic jet trajectory wasn't observed in these experiments presumably, because the diaphragm amplitude-to-cavity height ratio was high enough to displace the entire volume of air without the need for extra momentum from the external cross flow. Velocity contours plots of cavity height effects on the non-zero ambient flow show the same trends as detected in zero external flow conditions in terms of the jet penetration capabilities. Same set of actuator configurations were tested at two different cross flow conditions: 10 and 20 m/s (Figure A.2). Trends for both scenarios were the same and were explained using the Helmholtz resonance effects (explained with more detail in Chapter 3, Section 3.3.3). As expected, when the synthetic jets acted on a lower Reynolds number flow they demonstrated greater influence on the flow which was clearly visible in a much higher penetration length of synthetic jets in the 10 m/s cases as compared to the 20 m/s cases.

a)

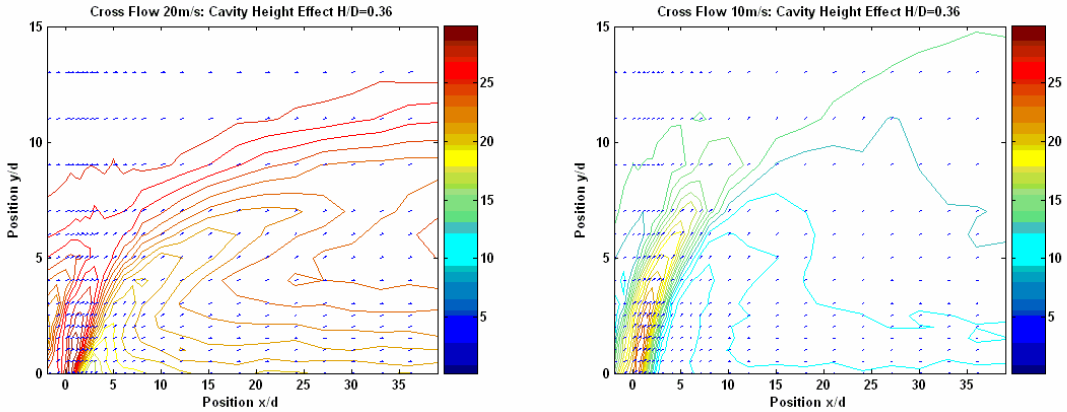

b)

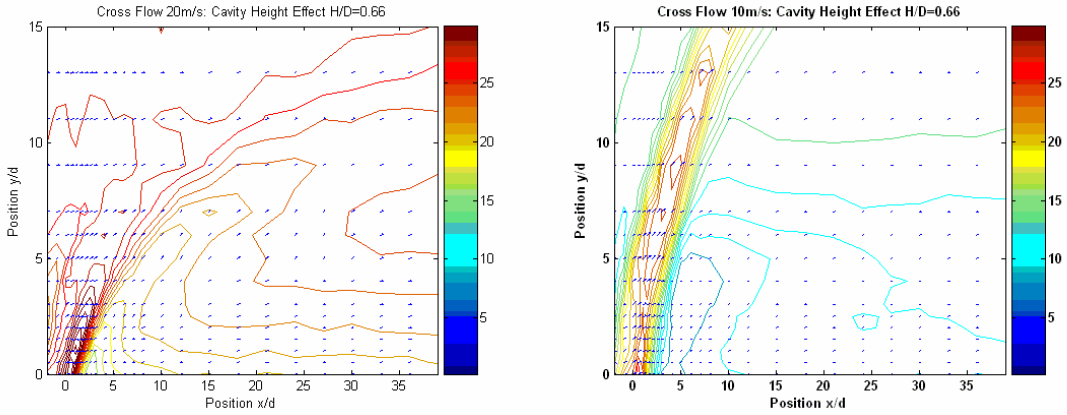

c)

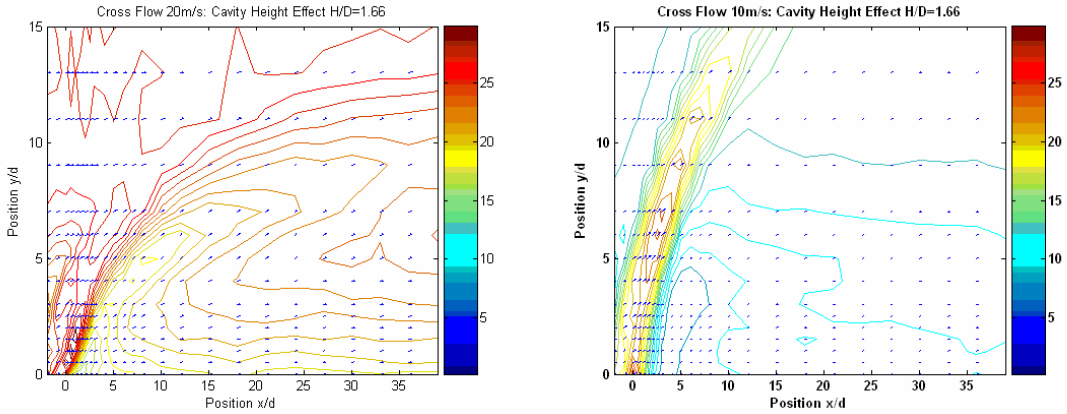

Figure A.2 Effects of the cavity height on the development of the synthetic jet in 20 m/s (left column) and 10 m/s cross flow (right column). a) H/D=0.36, b) H/D=0.6, **c)** H/D=1.66.

A.3. Orifice Diameter Effects

Figure A.3 presents the velocity contours of the effect of the synthetic jet actuator with various orifice diameters (1 mm to 3 mm) on a free-stream velocity of 15 m/s (white frames denote the same dimensional regions). The actuator with the 2 mm orifice diameter had a slightly higher impact on the flow and was able to penetrate the boundary layer more easily than the actuator with the orifice diameter of 1 mm. However, as the diameter was increased even further, to 3 mm, the combination of the Helmholtz resonance, Strouhal number effects (proportional to the orifice diameter) and the viscous-inviscid regime limitations caused the synthetic jet performance to reduce.

a)

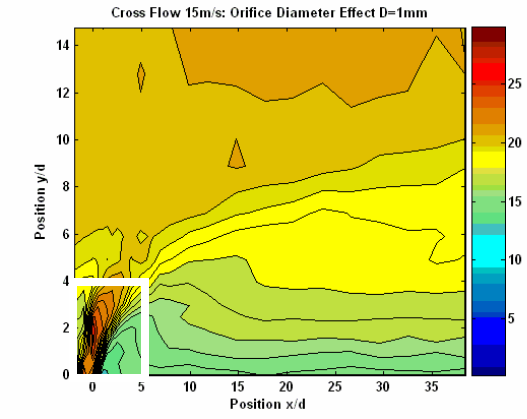

b)

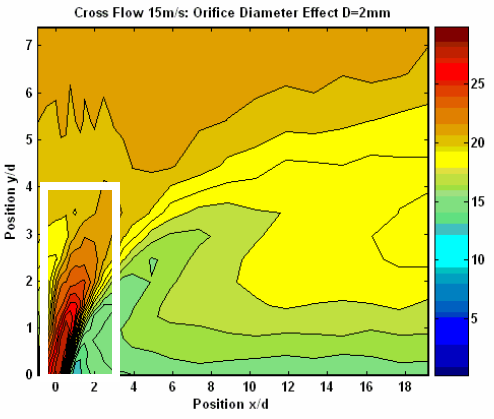

c)

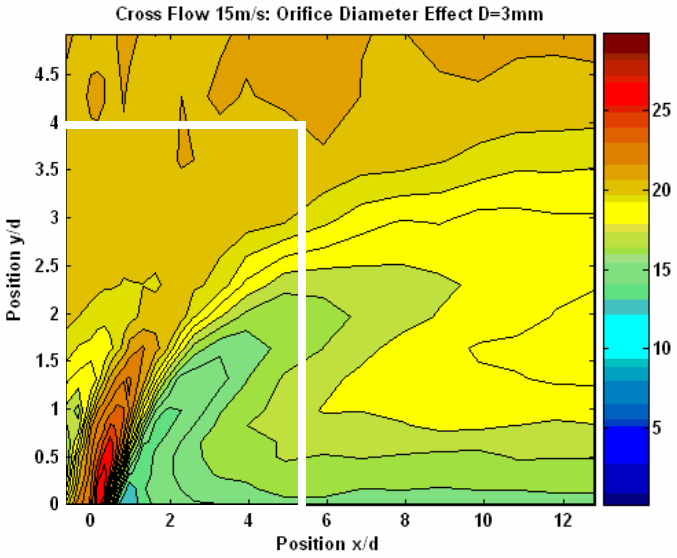

Figure A.3 Effects of the orifice diameter on the development of the synthetic jet in 15 m/s cross flow. a) D=1 mm, b) D=2D1, c) D=3D1.

APPENDIX B

Experimental Analysis of the Effect of a Synthetic Jet Actuator Array on a Flow over a NACA 0012 airfoil

Intelligent application of synthetic jet actuators requires advanced understanding of their mutual interaction and a detailed comprehension of their relationship with various external cross flows. There is a list of open ended questions on various aspects of this research that need to be addressed to achieve the objective of developing innovative high value control systems capable of significantly improving the flight envelope. Successful application of synthetic jet technology faces some unresolved issues: (i) how many actuators/arrays to use, (ii) how to distribute them on a lifting surface, (iii) is placing them on the upper lifting surface more advantageous than placing the on the lower side of the lifting surface, (iv) what type of flow benefits do we expect when placing them on the leading edge with respect to placing them in the trailing edge region, (v) what should the spacing between the discrete actuators be, (vi) do frequency and jet momentum coefficient govern the optimum spacing between the actuators, (vii) can we use actuation phase difference between the neighboring actuators to increase their benefits level (viii) does the size of the orifice significantly impact the flow above the lifting surface, (ix) can the same array of actuators be used for various flow control strategies (flow separation,

laminar flow control, dynamic virtual shaping), (x) should the actuators be operated at high Strouhal number and low Reynolds number or vice versa, (xi) what roles do the actuation frequency and the frequency of the flow play in optimum control application?

These are just a few parameters/issues that can significantly impact the load/moment distribution results. The list of variables is intimidating. It supports the need for a model capable of simplifying the experimental test matrix by studying the sensitivity of some of these parameters and their combination on the final result. Before having worked on such a model a set of experiments incorporating an array of synthetic jet actuators embedded in a NACA 0012 airfoil was conducted guided solely by the flow separation control results to place the actuation that might work to produce a noticeable change in lift. These experiments are presented as an addendum to this work. They emphasize the still immature level of this technology and to provide the data needed to validate a future version of the model founded and discussed in Chapter 6, i.e. one that can incorporate the effects of multiple actuators.

B.1. Experimental Set-Up

To study the potential of using synthetic jet actuators for inducing loads and moments on lifting surfaces at low angles of attack a test bed (a 3-inch chord, 12-inch span NACA 0012 airfoil) and an array of eight THUNDER based synthetic jet actuators (Figure B.1) was fabricated. The spacing between the actuator was arbitrary and was guided by the intention to evenly place them along the span of the airfoil. Orifices of each distributed

actuator were far enough apart not to influence each the performance of adjacent actuators. Each actuator was separately tested using the Polytec Laser Vibrometer and boundary conditions were tuned such that their resonance frequency was the same (relative maximum difference between some of the actuators was +/- 5 Hz). The velocity profile of each of the individual actuators was measured with the constant temperature anemometer to assure the uniformity of the output of the array (in the orifice region). The array was integrated into the test bed such that the orifices were positioned along the quarter chord line (Figure B.2). This location was selected based on previous investigations that tested synthetic jet actuator applications for flow separation control.

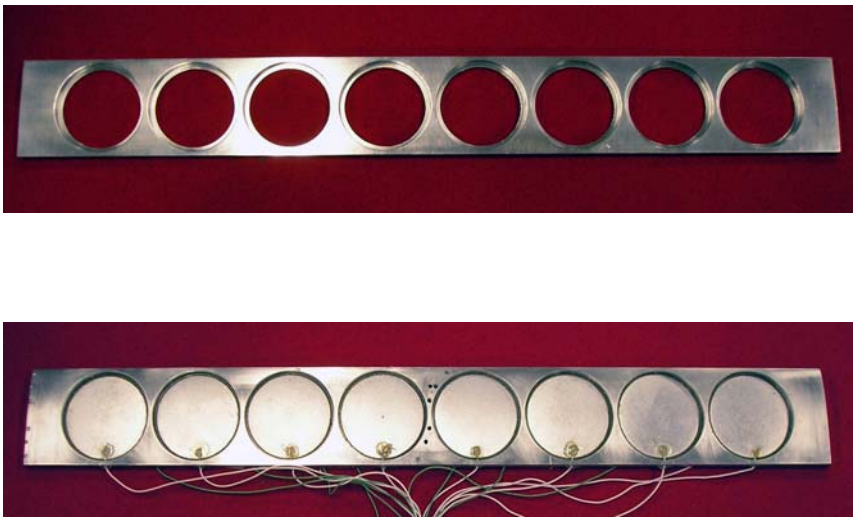

Figure B.1 An Array of eight THUNDER based synthetic jet actuators.

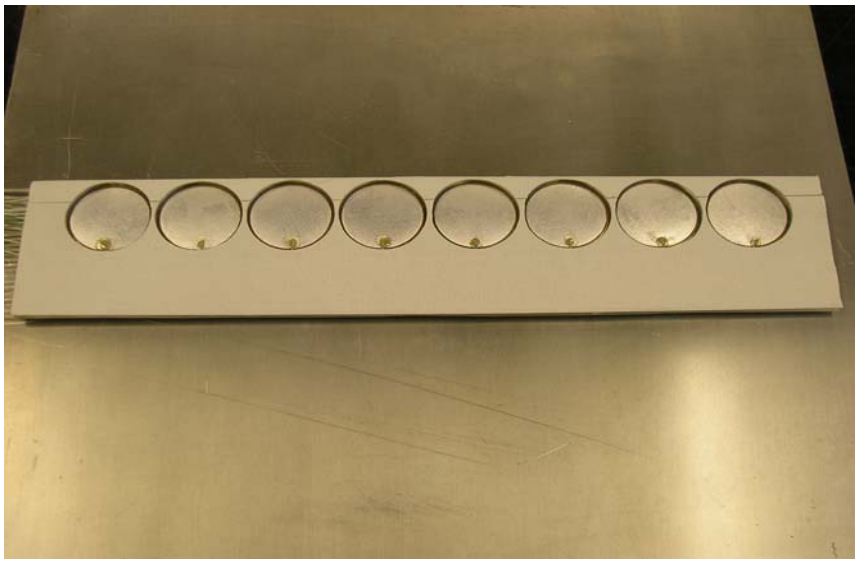

Figure B.2 NACA 0012 with THUNDER based synthetic jet actuator array.

The need for a detailed theoretical analysis was clear as several potentially critical design parameters had to be decided on and no design guidelines were available. The number of options for determining positions of the individual actuators in the array with respect to each other and with respect to the wing platform, in addition to the effects of the potential variety of velocity ratios and excitation frequencies was overwhelming.

To replicate some of the tests performed in the literature and to expand these results to low angles of attack, these tests included the investigation of only one location of jet arrays on a NACA 0012 wing operating in several flow regimes. The airfoil was mounted in the wind tunnel test section (Figure B.3) and lift curves were generated using a force balance. Resultant lift was measured with and without array actuation at four different Reynolds numbers (17500, 58000, 85000 and 117500). Only one actuation frequency and one jet velocity output were tested.

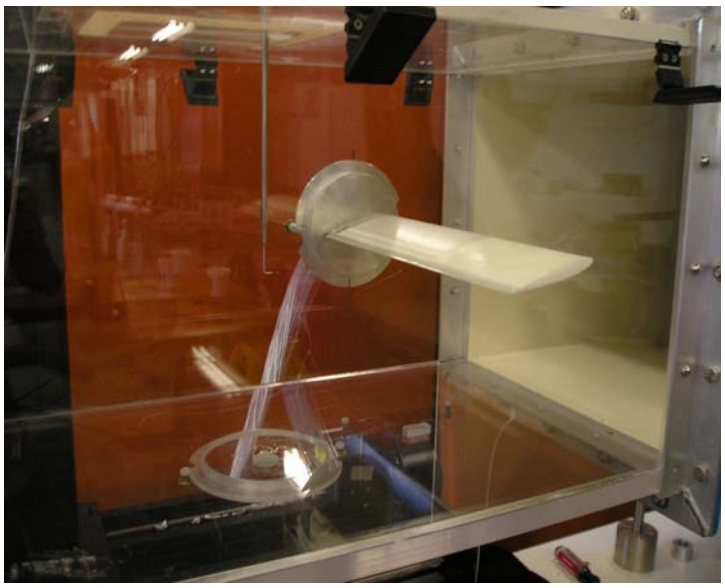

Figure B.3 NACA 0012 airfoil instrumented with synthetic jet actuator arrays mounted in the wind tunnel test section.

B.2. Results and Discussion

Resulting lift curves are shown in Figure B.4. They demonstrated distinct effects of the synthetic jet actuator in post stall regimes. For very low Reynolds number, where the flow is very receptive to flow separation, the actuators have shown effectiveness along the entire lifting curve. As the jet coefficient momentum was decreasing (at higher Reynolds number) so was the influence of the array on the lift curve. Difference between the lift curves of forced and unforced regimes was least significant at the highest Reynolds number tested (117,500). Unfortunately, equipment limitations did not allow for the drag forces to be observed.

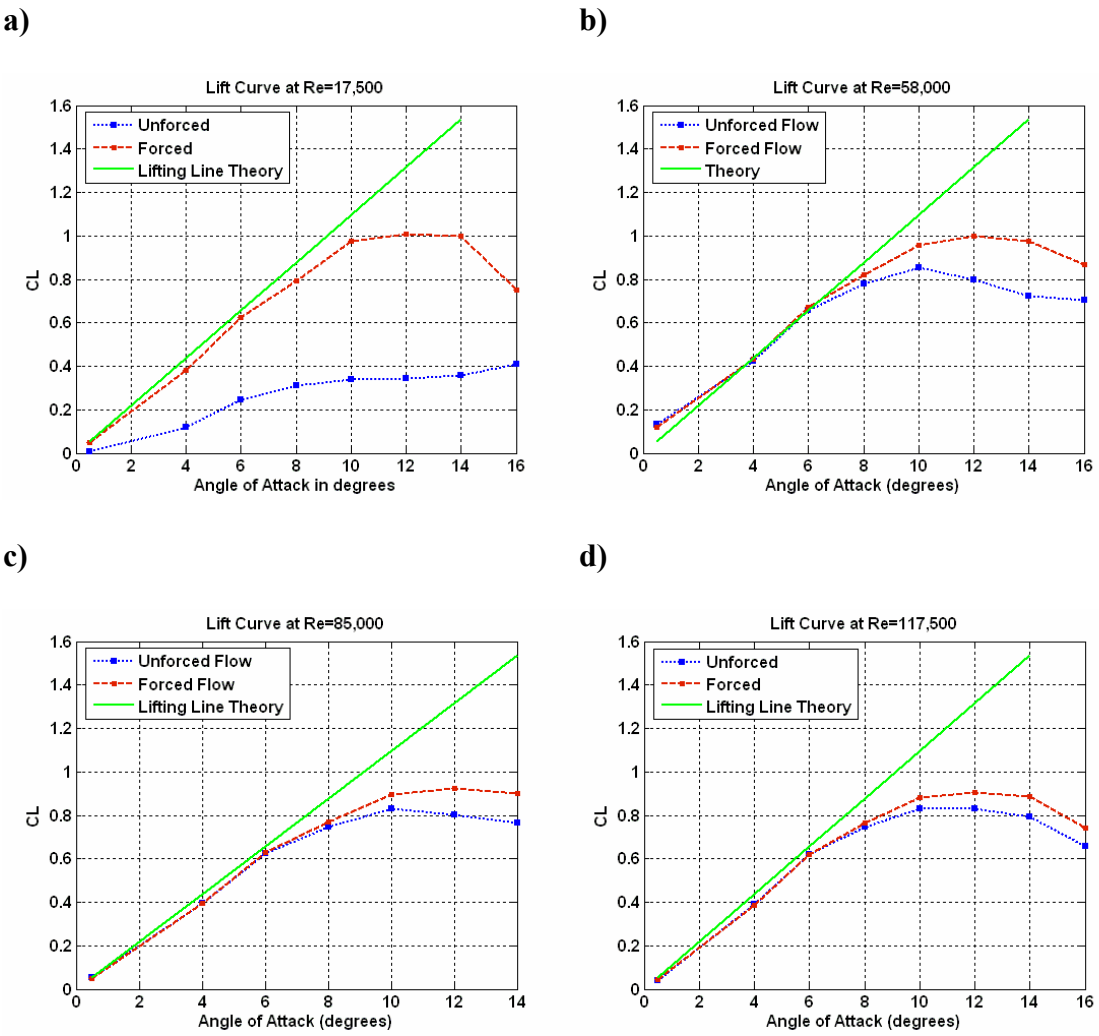

Figure B.4. Lift Distribution over a NACA 0012 at various Reynolds number with and without actuation: **a)** Re=17,500, **b)** Re=58,000, **c)** Re= 85,000, **d)** Re = 117, 500.

Boundary layer measurements have been added to this study in an attempt to better understand the effects of the jets in two different regimes (Reynolds numbers of 17500 and 117500). Hot wire measurements were collected at nine different locations along the chord of the airfoil section and were limited to the boundary layer region

(Figure B.5). Synthetic jet directly changed the velocity profile of the boundary layer and, as expected, was more influential at lower Reynolds number. This type of investigation would be more beneficial if transient measurements were possible. The effect of synthetic jet vortices on the flow field is of primary importance. When boundary layer control is the target application, such or similar measurements (i.e. flow visualization) would have been more informative. Figure B.6 and Figure B.7 show the velocity profiles of the boundary layer with and without actuation at the free stream velocity of 3 and 20 m/s, respectively.

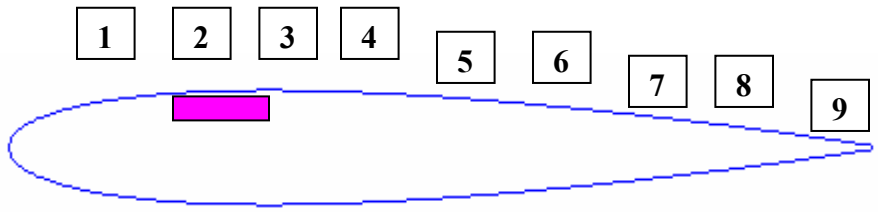

Figure B.5. NACA0012 airfoil with the actuator located at the quarter chord and labeled positions at which boundary layer measurements

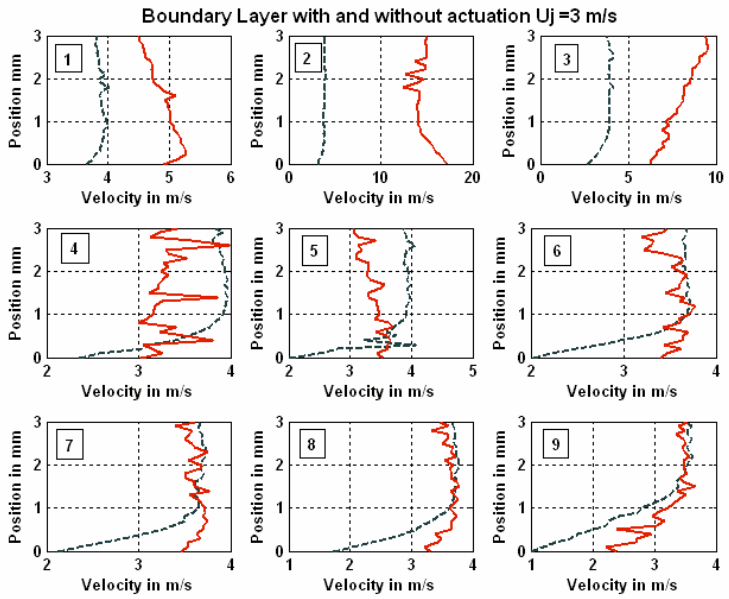

Figure B.6 Boundary layer measurements with (solid) and without (dashed line) actuation at the free stream velocity of 3 m/s.

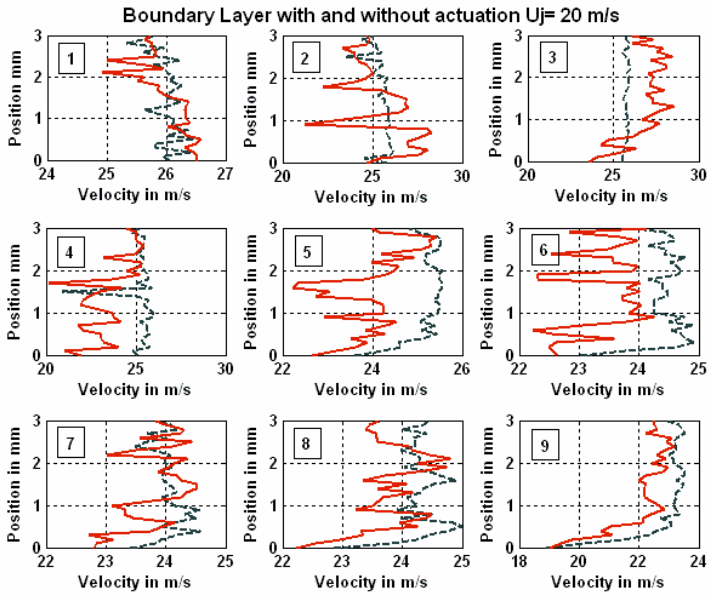

Figure B.7 Boundary layer measurements with (solid) and without (dashed line) actuation at the free stream velocity of 20 m/s.

These results were not conclusive enough to state that synthetic jet actuator technology can be used for inducing significant loads and moments at low angles of attack. Our theoretical approximation, however, has shown that lift increments would have been possible if the array was placed on the lower surface. More benefits, in terms of maneuverability authority, may have been achieved by placing the array closer to the trailing edge. No such conclusions can be stated with any type of certainty without sophisticating the model and validating those simulations. With the model foundation discussed in Chapter 5 and 6 and with the hardware built, tested and only briefly discussed in this Appendix, it is believed that this work has laid down a strong foundation to answer most if not all the questions posed at the beginning of this section.

Bibliography

[Abramovich1963] Abramovich G., "The Theory of Turbulent Jets", MIT Press, Cambridge, Mass., 1963.

[Adler1978] Adler D., Baron A., "Prediction of a Three Dimensional Circular Turbulent Jet in Crossflow", AIAA Journal Vol. 17, 1978.

[Amitay2000] Amitay M., Pitt D., Kibens V., Parekh D., Glezer A., "Control of Internal Flow Separation using Synthetic Jet Actuators", AIAA 2000-0903.

[Amitay, Smith2001] Amitay M., Smith D., "Aerodynamic Flow Control over an Unconventional Airfoil using Synthetic Jet Actuators", AIAA Journal, Vol. 39, No. 3, March 2001.

[Amitay2002] Amitay M., Glezer A., "Synthetic Jets", Annu. Rev. Fluid Mech. 2002.

[Amitay2003] Amitay M., Washburn A., Anders S., Parekh D., Glezer A., "Active Flow Control on the Stingray UAV: Transient Behavior", AIAA 2003- 4001.

[Bailo2000] Bailo K., Brei D., Calkins F., "Investigation of PVdf Active Diaphragm for Synthetic Jets", Proceedings SPIE Vol. 3991, pp. 220-231, 2000.

[Baker1987] Baker A., Snyder P., "Three Dimensional Nearfield Characterization of a VSTOL Jet in Turbulent Crossflow", AIAA Paper 87-0051.

[Blevins1979] Blevins R., "Formulas for Natural Frequencies and Mode Shape", New York: Van Nostrand Reinhold Co, 1979.

[Brei2003] http://www.icase.edu/series/Morphing/Brei

[Bruun1995] Bruun H., "Hot Wire Anemometry: Principles and Signals", Oxford University Press, New York, 1995.

[Campbell1972] Campbell J., Schetz J., "Flow Properties of Submerged Heated Effluents in a Waterway", AIAA Paper No. 72-79.

[Cater, Soria2002] Cater J., Soria J., "The Evolution of Round Zero Net Mass Flux Jets", J. Fluid Mech. (2002), vol. 472, pp 167-200.

[Chatlynne, Glezer2001] Chatlynne E., Rumighy N., Amitay M., Glezer A., "Virtual Aero- Shaping of a Clark-Y Airfoil using Synthetic Jet Actuators", AIAA Paper 2001-0732.

[Chen1999] Chen Y., Liang S., Glezer A., Jagoda J., "Enhanced Mixing in a Simulated Combustor Using Synthetic Jet Actuators", AIAA 99-0449.

[Chen, Bryant2000] Chen F., Beeler Y., Bryant R., "Development of Synthetic Jet Actuators for Active Flow Control at NASA Langley", AIAA 2000- 2405

[Chen2004] Yao C., Chen F., Neuhart D., Harris J., "Synthetic Jet Flow Field Database for CFD Validation", AIAA 2004- 2218.

[Coelho1989] Coelho S., Hunt J., "The Dynamics of the Near Field of Strong Jets in Crossflows", Journal of Fluid Mechanics, Vol. 200, pp. 96-120, 1989.

[Crook, Wood2001] Crook A., Wood N., "Measurements and Visualizations of Synthetic Jets", AIAA Paper 2001-0145.

[Crabb1981] Crabb D., Durao D., Whitelaw J., "A Round Jet Normal to a Crossflow", Journal of Fluid Engineering, Vol. 203, March 1981.

[Davis, Glezer2000] Davis S., Glezer A., "The Manipulation of Large and Small Scales in Coaxial Jets using Synthetic Jet Actuators", AIAA 2000-0403.

[Demuren1985] Demuren A., "Modeling Jets in Cross Flow", Department of Mechanical Engineering, Old Dominion University, Norfolk, VA 23529.

[Demuren 1992] Demuren A., "Multigrid Acceleration and Turbulence Models for Computations of 3D Turbulent Jets in Crossflow", International Journal of Heat and Mass Transfer", Vol. 35, No. 11, pp 2783-2794.

[Gad-el-Hak2000] Gad-el-Hak M., "Flow Control: passive, active and reactive flow management", Cambridge; New York: Cambridge University Press 2000.

[Gallas, Cattafesta2003] Gallas Q., Holman R, Nishida T., Carroll B., Cattafesta L., "Lumped Element Modeling of Piezoelectric Driven Synthetic Jet Actuators", AIAA Journal, Vol. 41, No. 2, February 2003.

[Gilarranz1998] Gilarranz J., Yue C, Redinioitis O., "PIV Measurements and Modeling of Synthetic Jet Actuators for Flow Control", ASME Fluids Engineering Divison Summer Meeting, June 1998.

[Gharib1998] Gharib M., Rambod E., Shariff K., "A Universal Time Scale for Vortex Ring Formation", J. Fluid Mech., 360, pp. 121-140, 1998.

[Gilarranz2001] Gilarranz J., Rediniotis O., "Compact, High- Power Synthetic Jet Actuators for Flow Separation Control", AIAA 2001-0737.

[Glezer1998] Glezer, et al., "Synthetic Jet Actuator and Application Thereof", United States Patent. 5,758,823.

[Gordon, Soria2002] Fordon M., Soria J., "PIV Measurements of a Zero-Net-Mass-Flux Jet in Cross Flow", Experiments in Fluids 33 (2002), 863-872.

[Gordon2004] Gordon M., Cater J., Soria J., "Investigation of the mean passive scalar field in zero-net-mass-flux jets in cross flow using planar-laser-induced fluorescence", Physics of Fluids, Vol. 16, No 3, 2004.

[Guy2001] Guy Y., McLaughlin T., Morrow J., "Velocity Measurements in a Synthetic Jet", AIAA 2001- 0118.

[Hassan2005] Hassan A., "On the Benefits of Active Flow Control (AFC) for Low Speed Unmanned Rotorcraft/Aircraft, AHS International Specialist's Meeting, January 2005.

[Hassan, Munts2000] Hassan A., Munts E., "Transverse and Near Tangent Synthetic Jets for Aerodynamic Flow Control, AIAA 2000- 4334.

[Holman, Utturkar2005] Holman R., Utturkar Y., Smith B., Cattafesta L., "Formation Criterion for Synthetic Jets", AIAA Journal, Vol. 43, No. 10, October 2005.

[Ingrad1950] Ingrad U., Labate S., "Acoustic Circulation Effects and Non-linear Impedance of the Orifices", Journal of the Acoustic Society of America, Vol. 22, No. 2, 1950, pp. 211-218.

[Jamesand 1996] Jamesand R., Jacobs J., "A Round Turbulent Jet Produced by an Oscillating Diaphragm", Physics of Fluids 8, (9), September 1996.

[Johari2002] Johari H., Rixon G., "Evolution of a Pulsed Vortex Generator Jet in a Turbulent Boundary Layer", AIAA 2002-2834.

[Keffer1962] Keffer J., Baines W., "The Round Turbulent Jet in a Cross Wind", The Journal of Fluid Mechanics, Vol .15, part 4, 1962

[Keffer1968] Keffer J., "The Physical Nature of the Subsonic Jet in a Cross-Stream", University of Toronto (Subsonic Jet in Cross Flow), 1968.

[Kral1997] Kral L., Donovan J., Cain A., Cary A., "Numerical Simulation of Synthetic Jet Actuators", AIAA 1997-1824.

[Kral2000] Kral L., Guo D., Cary A., "Numerical Simulation of the Interaction of Adjacent Synthetic Jet Actuators", AIAA Paper 2000-2565.

[Krieg2005] Krieg M., Pitty A., Salehi M., Mohseni K., "Optimal Thrust Characteristics of a Synthetic Jet Actuator for Application in Low Speed Maneuvering of Underwater Vehicles", OCEANS 2005, Vol. 3.

[Lachowicz1998] Lachowicz J., Yao C., Wlezien W., "Scaling of an Oscillatory Flow-Control Actuator", AIAA 98-0330.

[Lee, Goldstein2002] Lee C., Goldstein D., "Two-Dimensional Synthetic Jet Simulation", AIAA Journal Vol. 40, No.3, March 2002.

[Leissa1993] Leissa A., "Vibration of Plates", Acoustical Society of America, 1993.

[McCormick2000] McCormick D., "Boundary Layer Separation Control with Directed Synthetic Jets", AIAA Paper 2000-0519.

[McMahon1968] McMahon H., Mosher D., "Experimental Investigation of Pressures Induced on a Flat Plate by a Jet Issuing into a Subsonic Crosswind", Georgia Institute of Technology, (Subsonic Jet in Cross Flow Volume), 1968.

[Merovitch2001] Meirovitch L., "Fundamentals of Vibration", McGraw Hill Companies, 2001.

[Milanovoic2003] Milanovoc I., Zaman K., "Synthetic Jets in Cross Flow. Part II: Jets from Orifices of Different Geometry", AIAA 2003-3715.

[Milanovic2004] Milanovic I., Zaman K., "Fluid Dynamics of Highly Pitched and Yawed Jets in Crossflow", AIAA Journal, Vol. 42, No. 5, May 2004.

[Mittal2001] Mittal R., Rampunggoon P. "Interaction of a Synthetic Jet with a Flat Plate Boundary Layer", AIAA Paper 2001-2773.

[Moussa1977] Moussa Z., Trischka J., Eskinazi S., "The Near Field in the Mixing of a Round Jet with a Cross-stream", Journal of Fluid Mechanics, Vol. 80, part 1, pp. 49-80, 1977.

[Mungal, Smith1998] Smith S., Mungal M., "Mixing, structure and scaling of the jet in cross flow", Journal of Fluid Mechanics, (1998), Volume 357, pp.83-122.

[Muppidi2006] Muppidi S., Mahesh K., "Passive Scalar Mixing in Jets in Cross Flow", AIAA 2006-1098.

[Nae1998] Nae C., "Synthetic Jet Influence on NACA 0012 Airfoil at High Angles of Attack", AIAA 98-4523.

[Needham1988] Needham D., "A Jet in Crossflow", Journal of Fluid Mechanics, Vol. 188, pp. 159-184.

[Parekh2000] Parekh D., Glezer A., "AVIA: Adaptive Virtual Aerosurface", AIAA 2000- 2474

[Parekh2003] Parekh D., Williams S., Amitay M., Glezer A., Washburn A., Gregory I., Scott R., "Active Flow Control on the Stingray UAV: Aerodynamic Forces and Moments", AIAA 2003- 4002.

[Perkins, Hazen1953] Perkins C., Hazen D., "Some Recent Advances in Boundary Layer and Circulation Control", Fourth Anglo- American Aeronautical Conference, 1953.

[Pratte1967] Pratte B., Baines D., "Profiles of the Round Turbulent Jet in a Cross Flow", Journal of the Hydraulics Division, November, 1967.

[Rajaratnam1976] Rajaratnam N., "Developments in Water Science, Turbulent Jets", Elsevier, New York 1976.

[Rathnasingham 1996] Rathnasingham R., Breuer K., "Characteristics of Resonant Actuators for Flow Control", AIAA Paper 96-0311, January 1996.

[Rediniotis1999] Rediniotis O., Ko J., Yue K., "Synthetic Jets, their Reduced Order Modeling and Application to Flow Control", AIAA 1999-1000.

[Ricou1960] Ricou F., Spalding B., "Measurement of entrainment by axisymmetrical turbulent jets", Journal of Fluid Mechanics, 1960 pp 21-32.

[Ritchie2000] Ritchie B., Mujumdar D., Seitzman J., "Mixing in Coaxial Jets Using Synthetic Jet Actuators", AIAA 2000- 0404.

[Rizzetta1999] Rizzetta D., Visbal M., Stanek M., "Numerical Investigation of Synthetic Jet Flowfields", AIAA Journal Vol 37, No. 8, August 1999.

[Sauerwein 1999] Sauerwein S., Vakili A., "An Experimental Study of Zero-Mass Jets in Crossflow", AIAA 99-0668.

[Scaeffler2003] Schaeffler N., "The Interaction of a Synthetic Jet and a Turbulent Boundary Layer", AIAA 2003-643.

[Schetz1980] Schetz J., "Injection and Mixing in Turbulent Flow", AIAA, New York, 1980.

[Schlichting 1968] Schlichting H., "Boundary Layer Theory", McGraw Hill Series, 7th Edition, 1968.

[Schober2006] Schober S, Marzocca P., "Reduced Order Models for Synthetic Jet Actuators on a Lifting Surface for Optimization and Control", AIAA 2006-1906.

[Seifert, Wygnansky1996] Seifert A., Wygnanski I., "On the Delay of Airfoil Stall by Periodic Excitation", Journal of Aircraft, Vol. 33, No. 4, 1996, pp. 691-699.

[Seifert, Pack1999] Seifert A., Pack L., "Oscillatory Flow of Separation at High Reynolds Numbers", AIAA Journal, Vol. 37, No. 9, September 1999.

[Sharma2006] Sharma R., "An Analytical Model for Synthetic Jet Actuation", AIAA 2006-3035.

[Shaw2006] Shaw L., Smith B., Saddoughi S., "Full Scale Flight Demonstration of Active Flow Control of a Pod Wake", 2006-3183.

[Shuster2005] Shuster J., Oink R., McEligot D., Smith D., "The Interaction of a Circular Synthetic Jet with a Cross-flow Boundary Layer", AIAA 2005-4749.

[Smith1998] Smith B.,Glezer A., "The Formation and Evolution of Synthetic Jets", Physics of Fludis, Vol. 10, No. 9, 1998.

[Smith, Amitay1998] Smith D., Amitay M., Glezer A., "Modification of Lifting Body Aerodynamics using Synthetic Jet Actuators", AIAA98-0209.

[Smith, Glezer1997] Smith B., Glezer A., "Vectoring and Small Scale Motions Effected in Free Shear Flows Using Synthetic Jet Actuators", AIAA Paper 97-0213.

[Smith, Glezer1998] Smith B. Glezer A., "The Formation and Evolution of Synthetic Jets", Physics of Fludis, Vol. 10, No. 9, 1998.

[Smith, Trautman, Glezer1999] Smith B., Trautman M., Glezer A., "Controlled Interactions of Adjacent Synthetic Jets", AIAA99-0669.

[Smith, Swift2003] Swift B., Swift G., "A Comparison between Synthetic Jet and Continuous Jets", Experiment in Fluids, 34 (2003), 467-472.

[Tang, Zhong2005] Tang H., Zhong S., "Modelling of Characteristics of Synthetic Jet Actuators", AIAA 2005-4748.

[Tang, Zhong2006] Tang H., Zhong S., "Lumped Element Modeling of Synthetic Jet Actuators", AIAA 2006-3696.

[Smith, Amitay1998] Smith D., Amitay M., Glezer A., "Modification of Lifting Body Aerodynamics using Synthetic Jet Actuators", AIAA98-0209.

[Smith, Amitay1999] Smith B., Trautman M., Glezer A., "Controlled Interactions of Adjacent Synthetic Jets", AIAA99-0669.

[Shuster2004] Shuster J., Smith D., "A Study of the Formation and Scaling of a Synthetic Jet", AIAA 2004-90.

[Ugrina, Flatau2003] Ugrina S., Flatau A., "Investigation of Synthetic Jet Actuators Parameters", 11th SPIE International Symposium.

[Ugrina, Flatau2004] Ugrina S., Flatau A., "Experimental and Analytical Investigation of Different Synthetic Jet Actuator Configurations", 2004 ASME International Mechanical Engineering Congress and Exposition

[Utturkar2002] Utturkar R., Mittal R., Rampunggoon R., Cattafesta L., "Sensitivity of synthetic jets to the design of the jet cavity", AIAA 2002-0124.

[Utturkar2003] Utturkar R., Holman R., Sheplak M., Cattafesta L., "A Jet Formation Criterion for Synthetic Jet Actuators", AIAA 2003-0636.

[Washburn2004] Washburn A., Amitay M., "Active Flow Control on the Stingray UAV: Physical Mechanisms", AIAA 2004- 0745.

[Whitehead2003] Whitehead J., Gursul I., "Aerodynamics and Propulsion of Synthetic Jet Based Micro Air Vehicles", AIAA 2003-4004.

[Wooler1967] Wooler P., Burghart G., Gallagher J., "Pressure Distribution on a Rectangular Wing with a Jet Exhausting Normally into an Airstream", J. Aircraft Vol. 4, Nov.-Dec., 1967.

[Wu, Breuer2003] Wu K., Breuer K., "Dynamics of Synthetic Jet Actuator Arrays for Flow Control", AIAA Paper 2003-4257

[Yao, Chen2004] Yao C., Chen F., Neuhart D., Harris J., "Synthetic Jet Flow Field Database for CFD Validation", AIAA 2004- 2218.

[Yuan1998] Yuan L., Street R., "Trajectory and Entrainment of a Round Jet in Cross Flow", Physics of Fluids, VOl. 10, No. 9, 1998.